NUREG/CR--3091-Vol.6

TI85 017037

NUREG/CR-3091
BNL-NUREG-51630
Vol. 6

REVIEW OF WASTE PACKAGE VERIFICATION TESTS
SEMIANNUAL REPORT COVERING THE PERIOD OCTOBER 1984 - MARCH 1985

P. Soo, Editor

CONTRIBUTORS

C. Anderson
C. Brewster
M. S. Davis
E. P. Gause
H. Jain
C. Pescatore
C. Sastre
P. Soo
T. Sullivan

DISCLAIMER

This report was prepared as an account of work sponsored by an agency of the United States Government. Neither the United States Government nor any agency thereof, nor any of their employees, makes any warranty, express or implied, or assumes any legal liability or responsibility for the accuracy, completeness, or usefulness of any information, apparatus, product, or process disclosed, or represents that its use would not infringe privately owned rights. Reference herein to any specific commercial product, process, or service by trade name, trademark, manufacturer, or otherwise does not necessarily constitute or imply its endorsement, recommendation, or favoring by the United States Government or any agency thereof. The views and opinions of authors expressed herein do not necessarily state or reflect those of the United States Government or any agency thereof.

Manuscript Completed: March 1985
Date Published: July 1985

Prepared by
Brookhaven National Laboratory
Upton, New York 11973

Prepared for
Division of Waste Management
Office of Nuclear Material Safety and Safeguards
U.S. Nuclear Regulatory Commission
Washington, D.C. 20555
FIN A3167

DISTRIBUTION OF THIS DOCUMENT IS UNLIMITED

DISCLAIMER

Portions of this document may be illegible in electronic image products. Images are produced from the best available original document.

NOTICE

This report was prepared as an account of work sponsored by an agency of the United States Government. Neither the United States Government nor any agency thereof, or any of their employees, makes any warranty, expressed or implied, or assumes any legal liability of responsibility for any third party's use, or the results of such use, of any information, apparatus, product or process disclosed in this report, or represents that its use by such third party would not infringe privately owned rights.

NOTICE

Availability of Reference Materials Cited in NRC Publications

Most documents cited in NRC publications will be available from one of the following sources:

1. The NRC Public Document Room, 1717 H Street, N.W.
   Washington, DC 20555
2. The NRC/GPO Sales Program, U.S. Nuclear Regulatory Commission,
   Washington, DC 20555
3. The National Technical Information Service, Springfield, VA 22161

Although the listing that follows represents the majority of documents cited in NRC publications, it is not intended to be exhaustive.

Referenced documents available for inspection and copying for a fee from the NRC Public Document Room include NRC correspondence and internal NRC memoranda; NRC Office of Inspection and Enforcement bulletins, circulars, information notices, inspection and investigation notices; Licensee Event Reports; vendor reports and correspondence; Commission papers; and applicant and licensee documents and correspondence.

The following documents in the NUREG series are available for purchase from the NRC/GPO Sales Program: formal NRC staff and contractor reports, NRC-sponsored conference proceedings, and NRC booklets and brochures. Also available are Regulatory Guides, NRC regulations in the *Code of Federal Regulations*, and *Nuclear Regulatory Commission Issuances*.

Documents available from the National Technical Information Service include NUREG series reports and technical reports prepared by other federal agencies and reports prepared by the Atomic Energy Commission, forerunner agency to the Nuclear Regulatory Commission.

Documents available from public and special technical libraries include all open literature items, such as books, journal and periodical articles, and transactions. *Federal Register* notices, federal and state legislation, and congressional reports can usually be obtained from these libraries.

Documents such as theses, dissertations, foreign reports and translations, and non-NRC conference proceedings are available for purchase from the organization sponsoring the publication cited.

Single copies of NRC draft reports are available free, to the extent of supply, upon written request to the Division of Technical Information and Document Control, U.S. Nuclear Regulatory Commission, Washington, DC 20555.

Copies of industry codes and standards used in a substantive manner in the NRC regulatory process are maintained at the NRC Library, 7920 Norfolk Avenue, Bethesda, Maryland, and are available there for reference use by the public. Codes and standards are usually copyrighted and may be purchased from the originating organization or, if they are American National Standards, from the American National Standards Institute, 1430 Broadway, New York, NY 10018.

ABSTRACT

The potential of WAPPA, a second-generation waste package system code, to meet the needs of the regulatory community are analyzed. The analysis is based on the contents of the code manual, a letter-form update of the code and, to a lesser extent, on the source program. The analysis includes an in-depth review of WAPPA's individual process models and a review of WAPPA's operation. The analysis lists and discusses potential problems in the use of WAPPA. It is concluded that the code is of limited use to the NRC in the present form. Recommendations for future improvement, usage, and implementation of the code are given.

This report also describes the results of a testing program undertaken to determine the chemical environment that will be present near a high level waste package emplaced in a basalt repository. For this purpose, low carbon 1020 steel (a current BWIP reference container material), synthetic basaltic groundwater and a mixture of bentonite and basalt were exposed, in an autoclave, to expected conditions some period after repository sealing (150°C, ≈10.4 MPa). The experimental program consisted of three phases. The Phase I test involved a two-month gamma irradiation test in an inert argon environment. The Phase II test involved an irradiation test in a methane-containing environment also for a period of two months. These two experiments were followed by a Phase III study which was conducted in the absence of radiation in a methane environment. Parameters measured include changes in gas pressure with time and gas composition, variation in dissolved oxygen (DO), pH and certain ionic concentrations of water in the packing material across an imposed thermal gradient, mineralogic alteration of the basalt/bentonite mixture, and carbon steel corrosion behavior.

A second testing program was initiated to check the likelihood of stress corrosion cracking of austenitic stainless steels and Incoloy 825 which are being considered for use as waste container materials in the tuff repository program. The issue arose because data in the literature showed that one of the candidate steels (Type 304L) cracked in boiling water containing air and low chloride levels in the presence of gamma irradiation. Preliminary data from three-month tests are given.

CONTENTS

ABSTRACT iii
FIGURES x
TABLES xv
ACKNOWLEDGMENTS xvii
EXECUTIVE SUMMARY

1. INTRODUCTION (M. S. Davis, P. Soo) 5

2. REVIEW OF WAPPA (C. Pescatore, T. Sullivan, C. Sastre) 11

2.1 Introduction 11

2.1.1 Background Information 11
2.1.2 The Code WAPPA 12
2.1.3 Objectives and Organization of this Report 12

2.2 Review of WAPPA's Process Models 14

2.2.1 WAPPA's Radiation Model (RMODEL) 14

2.2.1.1 Review of Modeling Approach 14

2.2.1.1.1 Source Term Submodel 14
2.2.1.1.2 Attenuation Submodel 15
2.2.1.1.3 Radiolysis Submodel 15
2.2.1.1.4 Damage Submodel 15

2.2.1.2 Discussion 15

2.2.1.2.1 Source Term Submodel 16
2.2.1.2.2 Attenuation Submodel 16
2.2.1.2.3 Radiolysis Submodel 18
2.2.1.2.4 Damage Submodel 19

2.2.1.3 Conclusions 19

2.2.2 WAPPA's Thermal Model (TMODEL) 20

2.2.2.1 Review of Modeling Approach 20
2.2.2.2 Discussion 21
2.2.2.3 Conclusions 22

2.2.3 WAPPA's Mechanical Model (FMODEL) 22

2.2.3.1 Review of Modeling Approach 23

CONTENTS (Continued)

2.2.3.1.1 Canister Fracture Submodel 23
2.2.3.1.2 Waste Form Fracture Submodel 23
2.2.3.1.3 Stress Analysis Submodel 23

2.2.3.2 Discussion 24

2.2.3.2.1 Limitations of the Modeling Approach 24
2.2.3.2.2 Adequacy of the Modeling Approach . . 25

2.2.3.3 Conclusions 25

2.2.4 WAPPA's Corrosion Model (CMODEL) 25

2.2.4.1 Review of Modeling Approach 27

2.2.4.1.1 Dry Corrosion 27
2.2.4.1.2 Wet Corrosion 27

2.2.4.2 Discussion 27
2.2.4.3 Conclusions 30

2.2.5 WAPPA's Leach-and-Transport Model (WMODEL) 30

2.2.5.1 Review of Modeling Approach 30

2.2.5.1.1 Leach Submodel 30
2.2.5.1.2 Transport Submodel 32

2.2.5.2 Discussion 33

2.2.5.2.1 Leach Submodel 33
2.2.5.2.2 Transport Submodel 36

2.2.5.3 Conclusions 38

2.2.6 Conclusions 38

2.3 Review of WAPPA's Operation 40

2.3.1 Initial Specifications 40

2.3.1.1 Geometrical Configuration and Materials Specification 40
2.3.1.2 Calculation Times and Error Control 42

CONTENTS (Continued)

2.3.1.3 Nuclides Requested 43
2.3.1.4 Repository Boundary Conditions 43
2.3.1.5 Data Base 44
2.3.1.6 Radionuclide, Gamma Alpha, and Thermal Power Source Terms 44

2.3.2 Output Specifications 45
2.3.3 Conclusions 45

2.4 Conclusions and Recommendations 45

2.4.1 Conclusions 45
2.4.2 Recommendations 47

2.5 References 49

3. DETERMINATION OF LOCAL CORROSION CONDITIONS FOR LOW-CARBON STEEL HIGH LEVEL WASTE CONTAINERS IN A BASALT REPOSITORY (E. Gause, C. Brewster, P. Soo) 51

3.1 Introduction 51
3.2 Materials 52
3.3 Autoclave System Design 56
3.4 Experimental Procedures 58

3.4.1 Slurry Preparation 58
3.4.2 Autoclave Pressurization 60
3.4.3 Irradiation Procedure 61
3.4.4 Post-Test Procedures 61

3.5 Results and Discussion 62

3.5.1 Pressure Measurements 62
3.5.2 Pressure Changes Due to Radiolysis 63

3.5.2.1 Radiolysis of Water in a Closed System 63
3.5.2.2 Radiolysis of Methane in Aqueous Solution and in the Gaseous Phase 65

3.5.3 Gas Analyses Results 70

3.5.3.1 Phase I Test Gas Analysis Results 70
3.5.3.2 Phase II Test Gas Analysis Results 70
3.5.3.3 Phase III Test Gas Analysis Results 71
3.5.3.4 Comparison of Gas Analyses Results 71

3.5.4 Measurement of pH and DO and Calculation of Eh 72

CONTENTS (Continued)

3.5.4.1 Measurement of pH and Dissolved Oxygen of Unreacted Packing Material Slurry 72
3.5.4.2 Measurement of pH and Dissolved Oxygen of Reacted Packing Material Slurry 73

3.5.4.2.1 Measurement of Phase I Test pH and Dissolved Oxygen and Calculation of Eh 73
3.5.4.2.2 Measurement of Phase II Test pH and Dissolved Oxygen and Calculation of Eh 74
3.5.4.2.3 Measurement of Phase III Test pH and Dissolved Oxygen and Calculation of Eh 75

3.5.4.3 Comparison of pH and DO Measurements and Eh Calculations for All Tests 75

3.5.5 Measurement of Ionic Concentrations in Slurry Water . . . 76

3.5.5.1 Measurement of Ionic Concentrations in Phase I Test 78
3.5.5.2 Measurement of Ionic Concentrations in Phase II Test 78
3.5.5.3 Measurement of Ionic Concentrations in Phase III Test 78
3.5.5.4 Comparison of Measured Ionic Concentrations For All Tests 79

3.5.6 SEM-EDX Analysis of Colloidal Material 80

3.5.6.1 SEM-EDX Analysis of Colloidal Material Removed From Phase I Test Solution 80
3.5.6.2 SEM-EDX Analysis of Colloidal Material Removed From Phase II Test Solution 81
3.5.6.3 SEM-EDX Analysis of Colloidal Material Removed From Phase III Test Solution 81
3.5.6.4 Comparison of SEM-EDX Analyses of Colloidal Materials 81

3.5.7 Analysis of Unreacted Bentonite and Reacted Bentonite Portion of Slurry 89

3.5.7.1 Analysis of Bentonite 89
3.5.7.2 Analysis of Montmorillonite Portion of Bentonite 89

CONTENTS (Continued)

3.5.7.2.1 Montmorillonite XRD Phase I Test . . 89
3.5.7.2.2 Montmorillonite XRD Phase II Test . . 98
3.5.7.2.3 Montmorillonite XRD Phase III Test . 100
3.5.7.2.4 Comparison of Montmorillonite XRD Studies For All Tests 101

3.5.8 Analysis of Reacted Basalt 102

3.5.8.1 Comparison of XRD Patterns of Pulverized Basalt 102
3.5.8.2 Comparison of Micrographs of Polished Basalt Thin Sections 105

3.5.9 Metallography of Carbon Steel Sleeve and Identification of Surface Products 105

3.5.9.1 Metallography of Phase I Test Sleeve 108
3.5.9.2 Metallography of Phase II Test Sleeve 112
3.5.9.3 Metallography of Phase III Test Sleeve 117
3.5.9.4 Comparison of Pitting Corrosion For All Tests . 119

3.6 Summary 119

3.7 Recommendations for Future Work 123

3.8 References 123

4. TESTING FOR STRESS CORROSION CRACKING OF HIGH LEVEL WASTE CONTAINER MATERIALS IN TUFF REPOSITORY ENVIRONMENTS (H. Jain, C. Brewster, C. Anderson, P. Soo) 127

4.1 Introduction 127
4.2 Survey of Stress-Corrosion Behavior of Austenitic Stainless Steels in Relatively Pure Steam/Water/Air Environments 127
4.3 Test Plan 133
4.4 Materials and Specimens 134
4.5 Apparatus 139
4.6 Test Procedure 140
4.7 Results to Date 144
4.8 References 152

FIGURES

2.1. Schematic representation of how WAPPA operates within each time step 13

2.2. Geometrical representation of the waste form as a line source surrounded by the engineered barriers of the waste package 17

2.3. Typical waste form and canister design 26

2.4. Schematic representation of oxide thickness versus time. WAPPA considers thickness as a function of temperature and time 29

2.5. Improved oxide thickness calculation considers thickness as a function of temperature and previous history 29

2.6. Geometry of waste package 31

2.7. Initial configuration of the waste package in WAPPA's complex verification test case.

3.1. Generalized stratigraphy of the Columbia River Basalt Group, Yakima Basalt Subgroup, and intercalated and suprabasalt sediments within the Pasco Basin 53

3.2. Autoclave system being leak checked 57

3.3. Cross section through autoclave 58

3.4. Lengthwise section through autoclave 59

3.5. Pressure changes with time and temperature in the autoclave system for the three phases of the experiment: Phase I (absence of methane and presence of radiation), Phase II (presence of methane and radiation), Phase III (presence of methane and absence of radiation.) 64

3.6. Effect of dose rate on H_2 equilibrium pressures for concrete (neat), concrete containing Fe_2O_3, and concrete containing MnO_2 66

3.7. Solubility of methane in water at high temperatures and pressures . 67

3.8. Solubilities of O_2, N_2, and H_2 in water as a function of temperature 72

3.9. Micrograph of colloidal material recovered from the Phase I test (800X) 82

3.10. EDX analysis of colloidal material recovered from the Phase I test 82

FIGURES (Continued)

3.11. EDX analysis of rod in colloidal material recovered from the Phase I test 83

3.12. EDX analysis of crystal in colloidal material recovered from the Phase I test 83

3.13. Micrograph of protuberances appearing in colloidal material recovered from the Phase I test after bombardment with 17-kV electrons (1000X) 84

3.14. Micrograph of colloidal material recovered from the Phase II test heater region (1000X) 84

3.15. Micrograph of colloidal material recovered from the Phase II test wall region (1000X) 85

3.16. Micrograph of colloidal material recovered from the Phase II test heater region (300X) 85

3.17. Micrograph of the colloidal material recovered from the Phase III test heater region (100X) 86

3.18. Micrograph of the colloidal material recovered from the Phase III test wall region (100X) 86

3.19. EDX analysis of colloidal material recovered from the Phase III test heater region 87

3.20. EDX analysis of colloidal material recovered from the Phase III test wall region 87

3.21. EDX(TEM) analysis of colloidal material recovered from the Phase III test wall region 88

3.22. Micrograph of unreacted bentonite clay (100X) 88

3.23. Comparison of X-ray diffraction patterns of reacted and unreacted bentonite present in the Phase I test centrifuged packing material slurry samples prepared as oriented clay mounts by evaporation of slurry on glass slides. [Range of scan: $2\theta = 3-37°$ (d = 2.43-29.4 Å).] 90

3.24. Comparison of X-ray diffraction patterns of reacted and unreacted bentonite present in the Phase II test centrifuged packing material slurry samples prepared as oriented clay mounts by evaporation of slurry on glass slides. [Range of scan: $2\theta = 3-37°$ (d = 2.43-2.94 Å)] 43

FIGURES (Continued)

3.25. Comparison of X-ray diffraction patterns of reacted and unreacted bentonite present in the Phase III test centrifuged packing material slurry samples prepared as oriented clay mounts by evaporation of slurry on glass slides. [Range of scan: 2θ = 3-37° (d = 2.43-29.4 Å)] 44

3.26. Appearance of Phase I centrifuged packing material slurries before and after reaction 45

3.27. Comparison of X-ray diffraction patterns of Phase I test reacted and unreacted montmorillonite present in the centrifuged packing material slurry samples prepared as oriented clay mounts by evaporation of slurry on glass slides; treatment by glycolation, followed by heating to 300°C for one hour. [Range of scan: 2θ = 3-9.5° (d = 9.30-29.4 Å)] 48

3.28. Comparison of X-ray diffraction patterns of Phase II test reacted and unreacted montmorillonite present in the centrifuged packing material slurry samples prepared as oriented clay mounts by evaporation of slurry on glass slides; heat-treated at 300°C for 18 hours, followed by glycolation at 60°C. [Range of scan: 2θ = 3-9.5° (d = 9.30-29.4 Å)] 97

3.29. Comparison of X-ray diffraction patterns of Phase III test reacted and unreacted montmorillonite present in the centrifuged packing material slurry samples prepared as oriented clay mounts by evaporation of slurry on glass slides; heat-treated at 150°C, followed by glycolation at 60°C, followed by heat-treatment at 300°C, followed by glycolation at 60°C. [Range of scan: 2θ = 3-9.5° (d = 9.30-29.4 Å)] 99

3.30. Comparison of X-ray diffraction patterns for reacted and unreacted basalt, prepared as unoriented mounts of pulverized basalt. [Range of scan: 2θ = 3-65° (d = 1.43-29.4 Å)] 103

3.31. Minerals in unreacted basalt as determined with a polarizing microscope under crossed polars (100X) 106

3.32. Minerals in Phase I test reacted basalt sampled from the heater region as determined with a polarizing microscope under crossed polars (100X) 106

3.33. Minerals in Phase I test reacted basalt sampled from the wall region as determined with a polarizing microscope under crossed polars (100X) 107

3.34. Minerals in the Phase III test reacted basalt sampled from the wall region as determined with a polarizing microscope under crossed polars (100X) 107

3.35. Appearance of carbon steel sleeve prior to reaction (left) and subsequent to Phase I test reaction (right) 109

3.36. Micrograph of outside diameter of carbon steel sleeve subsequent to Phase I test rection showing metal oxide and thin clay deposition layer (marked by arrow) (250X) 110

3.37. Micrograph of outside diameter of carbon steel sleeve subsequent to Phase I test reaction showing metal oxide and thick clay deposition layer between arrows (250X) 110

3.38. SEM-EDX micrograph of iron-rich layered material in Phase I test carbon steel surface product (1000X) 111

3.39. Micrograph of outside diameter of carbon steel sleeve prior to Phase I test reaction (250X) 111

3.40. Micrograph of weld metal in carbon steel sleeve subsequent to Phase I test reaction (250X) 113

3.41. Micrograph of outside diameter of carbon steel sleeve subsequent to Phase II test reaction showing metal oxide and thin clay deposition layer (marked by arrows) (250X) 113

3.42. Micrograph (SEM) of orange-brown sleeve surface product from Phase II test (100X) 114

3.43. Micrograph (SEM) of magnetic green-yellow sleeve surface product from Phase II test (100X) 114

3.44. Point plot of EELS spectrum of orangish-brown sleeve surface product from the Phase II test showing well-defined crystalline material containing iron and oxygen 115

3.45. Debye-Scherrer powder pattern for orange-brown sleeve surface product from Phase III test 116

3.46. Debye-Scherrer powder pattern for green-yellow sleeve surface product from Phase II test 116

3.47. Micrograph of outside diameter of carbon steel sleeve subsequent to Phase III test showing pitting, and a thin detached oxide layer (250X) 118

3.48. Micrograph of Phase III test green carbon steel surface product (100X) 120

3.49. EDX of Phase III test green carbon steel surface product 120

FIGURES (Continued)

3.50. Micrograph of Phase III test orange-brown carbon steel surface product (100X) 121

3.51. EDX of Phase III test orange-brown carbon steel surface product . . 121

4.1. Proposed relationship between chloride and oxygen content of alkaline phosphate treated boiler water and susceptibility to stress corrosion cracking of austenitic stainless steel exposed to the steam phase with intermittent wetting 128

4.2. The relationship between original strain in bent-beam specimen and time-to-crack for (a) Type 321 stainless steel at 300°C and (b) Type 304 stainless steel at 200°C 129

4.3. Effect of chloride added as NaCl on cracking of Type 304 stainless steel at 100°C. Solution transported by porous material to specimen 130

4.4. (a) Schematic diagram of double U-bend type specimen. (b) Schematic diagram of γ-ray irradiation 131

4.5. C-ring specimen design 135

4.6. C-ring stress corrosion cracking test apparatus 140

4.7. Load vs deflection of Type 304L stainless steel sensitized C-ring test specimen under compression 141

4.8. Schematic of the specimen arrangement in a test vessel 143

4.9. Load vs in situ strain at the apex of a Type 316L stainless steel C-ring specimen 145

4.10. Microstructure of Type 304L stainless steel. (a) As-received, etched in glyceregia. (b) Sensitized at 600°C for 100 hours, etched in oxalic acid 146

4.11. pH of the six test solutions at 101°C as a function of time. Each symbol represents the solution in one test vessel 147

4.12. C-ring specimens of Type 321 sensitized stainless steel after three-month test in "synthetic J-13 water" 149

TABLES

1.1. List of estimated spent fuel waste package conditions for a salt repository 7

1.2. List of estimated spent fuel waste package conditions for a basalt repository 8

1.3. List of estimated spent fuel waste package conditions for a tuff repository 9

2.1. Significant limitations of WAPPA's modeling 39

3.1. Compositions of Middle Sentinel Bluffs Flow basalt and reference Wyoming bentonite 54

3.2. Petrographic characteristics of primary and secondary phases reported as present in Grande Ronde basalt. 55

3.3. Composition of synthetic Grande Ronde groundwaters 56

3.4. Comparison of composition of gases sampled after reaction as determined by mass spectrometry 69

3.5. pH and DO as measured for packing material slurry and Eh as calculated for all tests 76

3.6. Comparison of ionic concentrations of reacted Grande Ronde GR-3 groundwater 77

3.7. Comparison of (00ℓ) d-spacings based on X-ray diffractometer studies of reacted and unreacted bentonite portions of centrifuged packing material slurries prepared as oriented clay mounts by evaporation of centrifuged slurry on glass slides. [Intensities not specified. Range of scan: $2\theta = 3\text{-}37°$ (d = 2.43-29.4 Å).] 94

3.8. Comparison of (00ℓ) d-spacings based on X-ray diffractometer studies of Phase I test reacted and unreacted montmorillonite, prepared as oriented clay mounts by evaporation of centrifuged packing material slurry on glass slides; treatment by glycolation at 60°C, followed by heating to 300°C for one hour. [Intensities not specified. Range of scan: $2\theta = 3\text{-}9.5°$ (d = 9.30-29.4 Å).] 95

3.9. Comparison of (00ℓ) d-spacings based on X-ray diffractometer studies of Phase II reacted and unreacted montmorillonite, prepared as oriented clay mounts by evaporation of centrifuged packing material slurry on glass slides; treatment by heating to 300°C for 18 hours, followed by glycolation at 60°C. [Intensities not specified. Range of scan: $2\theta = 3\text{-}9.5°$ (d = 9.30-29.4 Å).] 98

TABLES (Continued)

3.10. Comparison of (00ℓ) d-spacings based on X-ray diffractometer studies of Phase III reacted and unreacted montmorillonite, prepared as oriented clay mounts by evaporation of centrifuged packing material slurry on glass slides; heat-treatment at 150°C, followed by glycolation at 60°C, followed by heat-treatment at 300°C, followed by glycolation at 60°C. [Intensities not specified. Range of scan: 2θ = 3-9.5° (d = 9.30-29.4 Å).] 101

3.11. Comparison of (hkℓ) d-spacings based on X-ray diffractometer studies of reacted and unreacted basalt, prepared as unoriented mounts of pulverized basalt. [Intensities not specified. Range of scan: 2θ = 3-65° (d = 1.43-29.4 Å).] 104

3.12. Calculated d-spacings of Phase II test sleeve surface product based on measured Debye-Scherrer electron diffraction powder patterns . . . 117

4.1. SCC test in boiling deionized water 132

4.2. Test matrix for stress corrosion of candidate stainless steels and Incoloy-825 133

4.3. Vendor supplied chemical analysis of test alloys (weight percent) . 134

4.4. Mechanical properties of as-received test alloys (vendor supplied data) 134

4.5. Geochemical analysis of Topopah Spring tuff 137

4.6. Reference groundwater composition for tuff repositories (based on composition of Jackass Flats Well J-13 at the Nevada Test Site) . . 138

4.7. Amount of chemical compounds used in preparing 20 liters of synthetic J-13 water 139

4.8. Stress-strain properties of eight alloys as obtained from Instron machine tests on smooth C-ring specimens 142

4.9. pH of test solutions at the end of the three-month tests 148

4.10. Chemical composition of test solutions obtained at the end of three-month tests 150

4.11. Room temperature chemical composition of filtered solutions obtained from the reaction of distilled water with crushed tuff. Composition of reference J-13 groundwater is included for the purpose of comparison 151

ACKNOWLEDGMENTS

In the testing program the authors would especially like to thank Dr. Ramesh Dayal for his review of the manuscript. They are also grateful to Dr. Harpal Arora for his helpful discussions regarding the use of the X-ray diffractometer and mineralogical identification. Appreciation is also extended to Robert Sabatini and Johan Tafto for performing the SEM-EDX analyses and for their efforts in attempting to identify the composition of the carbon steel surface products. They would also like to thank Eugene Ferreri, Mary Kinsley, Andrew Cendrowski, Sue Oakley, Robert Wilson and John Warren for ion chromatography results, atomic absorption results, metallographic results, silica content determinations, gas analyses and SEM-EDX analysis of the colloidal material, respectively. The authors would also like to express their gratitude to Ms. G. Searles and Ms. A. Spira for their patience and skill in the typing and preparation of this report.

EXEGUTIVE SUMMARY

This Biannual Report describes two aspects of an ongoing program concerned with high level waste package evaluation. The first deals with a review of selected codes and models being developed by DOE to predict package performance, and the second is to perform verification tests to provide information on critical issues related to package behavior. Specifically, the potential of the WAPPA code (Waste Package Performance Assessment Code) to meet the needs as a licensing tool have been analyzed. This analysis is based on the contents of the code manual, an update of the code and the source program. The latter part of this report describes testing programs conducted by BNL to determine the chemical environment of a high level waste package in a basalt repository and to assess the potential of stainless steel containers to fail by stress corrosion cracking in a tuff repository system.

The WAPPA code in its present form is of limited use to the NRC. This code implements a modeling approach that is mostly empirical in nature. In practice, it operates as a data base manager that simply selects which correlation and which data are applicable to each particular situation. Because of the large amount of data the user has to supply for the empirical models and the number of situations for which they may have to be specified, data gathering, interpretation, and validation will require a significant effort by personnel who are thoroughly familiar with the assumptions that went into the code. The difficulty of preparing the data files will be compounded by the scarcity of adequate data in the literature and by ambiguities the required data may entail, e.g., data are needed which require a priori estimate of future waste package performance; and data are needed for correlations which factor in only a few of the several variables on which a particular process may depend. Furthermore, since most of the models are empirical, their applicability must be proven. This will require a suite of auxiliary codes representing state-of-the-art modeling of the actual processes considered.

While the use of WAPPA as a licensing tool requires extensive data and model validation, one may relax these requirements for use as a site screening tool or as a tool for preliminary design analysis. It will be necessary, however, to remove first some of the major inconsistencies identified in the modeling, e.g., the leach-and-transport model needs to be modified to conserve mass, etc. WAPPA is hardly amenable to probabilistic reliability analysis because of the large number of parameters to be sampled, and the need to re-run the code a number of times to demonstrate that the lack of error control and automatic time step selection logic has not produced a solution that depends on the user-defined time steps. That is, it must be shown that the solution converges to a value independent of the time step. The last difficulty may be hard to remove even if sensitivity analysis is performed first.

The objective of the first testing program was to determine the chemical environment that will be present within high level nuclear waste packages emplaced in a basalt repository. For this purpose, low carbon 1020 steel (a current BWIP reference container material), synthetic basaltic groundwater and a mixture of bentonite and basalt were exposed in an autoclave to expected repository conditions shortly after repository sealing (150°C, 10.4 MPa). The

experimental program consisted of three phases. Phase I involved a two-month irradiation test $(3.8 \pm 0.5) \times 10^4$ rad/h in an argon environment. The Phase II test was similar but was conducted in a methane environment. These two tests were followed by a Phase III control test which was similar to the Phase II study but it was performed in the absence of radiation.

All of these studies concentrated on changes in gas pressure and composition; on the differences in pH, dissolved oxygen (DO), calculated Eh and the concentration of those ions, which have been implicated in the corrosion of carbon steel, as sampled across a thermal gradient; on alterations of the packing material as determined by X-ray diffraction (XRD); and on the determination of localized and uniform corrosion of the carbon steel sleeve.

Trends in gas pressure were similar in each of the three tests. Over the two-month test periods, the gas pressure in the autoclave ranged from 9.3-9.7 MPa (1357 psi to 1404 psi) in the Phase I test, from 11.1-13.2 MPa (1612 psi to 1919 psi) in the Phase II test and from 9.8-11.7 MPa (1416 psi to 1702 psi) in the Phase III test. There was an early trend to decreasing pressures followed by a trend to pressures approaching or slightly exceeding the initial values. This indicates that pressure in a sealed repository environment may initially decrease and be followed by a slow increase. Overall, in all three tests, hydrogen was produced and oxygen was consumed, as determined by gas analyses and dissolved oxygen measurements. More hydrogen was produced in the Phase II test than in the Phase I and III tests due to the radiolysis of methane. Similar amounts of hydrogen were produced in the irradiated Phase I test and in the non-irradiated Phase III test. These results indicate that, in a repository, hydrogen will be produced and oxygen will be consumed but that some residual oxygen may be present, at least in the short term. Carbon-containing gases were produced in the Phase I test (CO_2 and CH_4) and in the Phase II test (CO_2 and C_2H_6) and possibly in the Phase III test.

There were different thermal gradients established across the packing material in each test. For Phase I, II, and III tests, these were, respectively, 1.0, 0.6, and 2°C/mm. After cooling the autoclave over a period of 25 minutes, the pH of the water in the basalt/bentonite packing material measured at room temperature was nearly neutral. There did not appear to be a significant change in pH across the thermal gradient in the packing material in any of the three tests. There did not appear to be a significant change in DO across the thermal gradient of the packing material in any of the tests. The calculated Eh values indicate that an oxidizing environment existed after quenching the contents of the autoclave. Reducing environments were not achieved under the current test conditions.

The concentrations of Cl^- and SO_4^{2-} measured at room temperature were greater near the cooler end of the thermal gradient in the tests. Changes in ionic concentrations occur across the thermal gradients but bulk changes in ionic concentrations, relative to the groundwater composition, may be more significant in terms of corrosive environments. The bulk of the Fe and Si content of the liquid system is present as colloidal material that is filterable. Colloids are formed in the absence of radiation but their production seems to be enhanced if radiation is present.

Hydrothermal conditions cause some change in the bentonite component of the packing material as determined by X-ray diffraction (XRD). The expandability of the bentonite portion of the wet packing material may be affected by periods of heating and simultaneous dehydration. Radiation may enhance expandability. Optical and XRD studies indicate that some changes occur in the mineralogical content of basalt during hydrothermal testing. The alteration of the pyroxenes in the basalt is one mineralogical change that was observed. Other alteration also occurs in the presence or absence of radiation as evidenced by changes in XRD patterns.

Adherent surface products removed from the carbon steel sleeve in the Phase I test contained mainly montmorillonite clay. Scanning electron microscope (SEM-EDX) analysis indicated the presence of other materials containing more Fe than that found in montmorillonite. Surface products removed from the carbon steel sleeve in the Phase II test were analyzed by SEM-EDX and electron diffraction but were not readily identifiable. (An orange-brown product contained large amounts of Si, Fe, and Al, while the green-yellow product was largely composed of Fe and Si.) Identification was also not possible for the Phase III surface products, which were analyzed by SEM-EDX and XRD. (Both Phase III surface products contained large amounts of Si and Fe, with the green phase also containing a large amount of Ca.)

There was no pitting on the carbon steel sleeve or the steel weldment in the Phase I test. There were hemispherically-shaped pits approximately 12 microns in depth in the Phase II test, and shallower (approximately 8 microns in depth) and more closely-spaced pits were formed in Phase III. At this time it is not clear whether surface polishing of the Phase II and Phase III steel sleeves prior to testing, or the presence of methane, encourages pitting. Under the conditions of these tests, the maximum predicted pit depth in 300 years is estimated to be <2.2 cm.

A literature survey of the pertinent stress corrosion data on stainless steels suggested that this mode of failure can occur in some of the materials under consideration by the tuff repository program for HLW containers. Therefore, a testing program was initiated to evaluate the stress corrosion cracking (SCC) susceptibility of the candidate alloys viz. Types 304L, 316L and 321 stainless steels, and Incoloy 825 in a simulated tuff repository environment. The notched C-ring test method has been adopted in which each specimen is stressed to 90% of the elastic limit calculated for the unnotched condition. Stressed specimens are being exposed at ≈100°C to the liquid as well as the steam phase over synthetic J-13 groundwater and ten-times concentrated J-13 groundwater both in equilibrium with crushed Topopah Spring tuff for a duration of 3, 6 and 12 months. The use of concentrated water simulates the situation when salts precipitated after initial evaporation of groundwater are redissolved in water subsequently percolating towards the repository horizon.

The three-month tests have been completed recently. Preliminary examination of the specimens shows that macroscopic stress corrosion cracks are absent. Examinations to detect microcracks are in progress. Chemical analysis shows that the concentrations of several ionic species increases during testing. This increase in concentration presumably results from the dissolution of salts in the crushed tuff. More results will be obtained upon completion of the six- and 12-month tests.

1. INTRODUCTION

The NRC Rule for the Disposal of High Level Waste in Geologic Repositories (10 CFR 60) dated June 1983, specifies two main performance objectives for the engineered barrier system:

> Containment of HLW within the waste packages will be substantially complete for a period to be determined by the Commission taking into account the factors specified in subsection 60.113(b) (of 10 CFR 60) provided, that such period shall be not less than 300 years nor more than 1,000 years after permanent closure of the geologic repository; and
>
> The release rate of any radionuclide from the engineered barrier system following the containment period shall not exceed one part in 100,000 per year of the inventory of that radionuclide calculated to be present at 1,000 years following permanent closure, or such other fraction of the inventory as may be approved or specified by the Commission; provided, that this requirement does not apply to any radionuclide which is released at a rate less than 0.1% of the calculated total release rate limit. The calculated total release rate limit shall be taken to be one part in 100,000 per year of the inventory of radioactive waste, originally emplaced in the underground facility, that remains after 1,000 years of radioactive decay.

In order to show compliance with these performance objectives the license applicant will need to provide a data base and analyses to quantify anticipated behavior of the waste package/repository system after permanent closure. This will necessarily involve research and testing programs to evaluate the likely modes by which engineered system components will degrade or fail by chemical or mechanical means. Knowledge of the ways in which the engineered barriers fail will permit estimates to be made regarding the containment capability of the waste package and the radionuclide release rate from the engineered system. A sequence of events leading to loss of containment and the release of radionuclides would include:

a. Groundwater entering the engineered barrier system
b. Groundwater penetrating the geologic packing material
c. Groundwater penetrating the container/overpack system
d. Groundwater leaching radionuclides from the waste form
e. Radionuclides transported through the failed container/overpack system, packing material and disturbed host rock to the near field environment.

For these scenarios, in which the individual engineered barriers are breached, probable chemical (corrosion) failure/degradation modes and mechanical failure/degradation modes need to be identified and quantified. These will depend on the specific design of the engineered system including selection of materials, local temperatures, local repository water conditions, radiation effects, water flow rates, and lithostatic/hydrostatic pressures, etc.

Estimates are given in Tables 1.1 through 1.3 of the potential range of conditions around a waste package in salt, basalt and tuff (NUREG/CR-2482, Vol. 7, 1984). These will of course be strongly dependent on final package geometries, designs and material selection. It is the interaction of the package with its environment that must be evaluated in order to predict with reasonable assurance that applicable regulatory criteria are met. The licensee will need to supply an appropriate data base and analysis, based on adequate test methods to support the projected performance of engineered barrier systems under anticipated repository conditions.

This report details two aspects of Brookhaven's program of reviewing DOE activities in the area of waste package performance verification testing. The first part of this report is a review of the Waste Package Performance Assessment Code (WAPPA). This code was designed as a tool to aid in waste package design, repository design, site selection and characterization and system assessment. The objective of this evaluation is to examine the adequacy of the modeling in WAPPA and to determine its potential use as a licensing tool.

The remainder of this report describes two test programs conducted by BNL. One was to determine the local corrosion conditions pertinent to a high level waste container in a basalt repository and the other was to check the possibility of stress corrosion cracking effects in stainless steel containers being considered for use in a tuff repository.

In the first test, low carbon steel (a current Basalt Waste Isolation Project, BWIP, reference container material), a basalt/bentonite packing material, and synthetic Grande Ronde basaltic water were reacted in an autoclave at 150°C and ≈10.4 MPa (1500 psi) pressure. The tests lasted for two-month periods and the gamma irradiation flux, when used, was $(3.8 \pm 0.5) \times 10^4$ rad/h. The Phase I irradiation test used an inert argon environment and Phase II involved a similar set of experimental conditions but used a methane cover gas. This was performed because high methane concentrations have been detected in basaltic water samples taken from Borehole RRL-2 in the Grande Ronde formation. The Phase III control test was also conducted in a methane environment, but in the absence of irradiation.

Measurements on the packing material slurry at the conclusion of the tests included pH and dissolved oxygen (DO) determination. The concentrations of Cl^-, total Fe (measured as Fe^{2+}), and SO_4^{2-} ions in the filtrate were also measured, since these ions are associated with the corrosion of carbon steel. Gases generated during the irradiation period may include H_2, O_2, N_2 and CO_2. Since several of these gases could have a deleterious effect on the waste container, gas analyses were made at the conclusion of the test period. The carbon steel sleeves were metallurgically evaluated for uniform and pitting corrosion. Hydrothermal alteration of the rock and clay constituents of the packing material was also investigated.

The stress corrosion cracking program was initiated because of concern that some reference container materials being considered for a tuff repository (Type 304L, 316L, 321 stainless steels and Incoloy-825) were susceptible to stress corrosion cracking. The issue arose because of data in the literature that show that stressed C-ring samples of Type 304L cracked in boiling water

containing small quantities of air and chloride ion in the presence of gamma radiation. The tests carried out in the current program involved the testing of stressed, V-notched C-rings in boiling water in the presence of crushed tuff.

References

Code of Federal Regulations, "Final Rule for the Disposal of High Level Waste In Geologic Repositories," 10 CFR Part 60, June 1983.

NUREG/CR-2482, Vol. 7, BNL-NUREG-51494, "Review of DOE Waste Package Program - Subtask 1.1 National Waste Package Program, Biannual Report," E. Gause and P. Soo, Brookhaven National Laboratory, September 1984.

Table 1.1. List of estimated spent fuel waste package conditions for a salt repository.

Parameter	Estimated Value			
	Operations Period	Thermal Period (0-300 yr)	Transition Period (300-1000 yr)	Geologic Control (>1000 yr)
Temperature at Centerline (Thermal Loading 12.4 W/m^2)		375°C max.	Approximately 150-110°C	<110°C
Total Gamma Dose (rad)		10^9-10^{10}	Little additional irradiation.	Little additional irradiation.
Brine Flow Rate		Total of about 7 liters per borehole for 24.7 W/m^2 thermal loading.	Little additional brine inflow	Little additional brine inflow
Brine Chemistry	Brine A or Brine B chemistries depending on repository location.	Brine A or Brine B with significant NaOH levels.	Brine A or Brine B with NaOH present.	
pH (measured at 25°C)	Steam/air plus small amounts of $HCl/SO_2/CO_2/H_2S$.	Initially acidic brine (pH ≈3.5) due to dissolution of acid gases. Changing to alkaline brine because of dissolution of colloidal sodium by brine inclusions. pH could rise to 9.5 based on experiments with irradiated salt and deionized water.	Probably alkaline.	Probably alkaline.
pH (at high temperature)		Lower than values measured at 25°C but no reliable values can be specified because of complex hydrothermal reactions and irradiation effects.		
Redox Conditions	Oxic	Probably oxic due to brine radiolysis.	Approaching Anoxic	Probably anoxic.
Stress (MPa)	0.1	Initially 0.1 MPa, rising to lithostatic stress of 16.2 MPa as host rock settles.		

Table 1.2. List of estimated spent fuel waste package conditions for a basalt repository.

Parameter	Estimated Value			
	Operations Period	Thermal Period (0-300 yr)	Transition Period (300-1000 yr)	Geologic Control (>1000 yr)
Temperature at Centerline (Thermal Loading 13.0 W/m^2)	250°C	265°C max. after ≈35 yr.	140-125°C	<125°C
Total Gamma Dose (rad)		10^7-10^8	Little additional irradiation.	No additional irradiation.
Vertical Hydraulic Conductivity (m/sec.)		Unknown, but likely to be much greater than that for horizontal flow because of buoyancy effects.		
Water Chemistry	Steam/air.	Significant increases in K^+, Ca^{2+}, Fe, Si, and SO_4^{-2} in the packing material water at higher temperatures. F^- is reduced in concentration.		Not known, but there should be a tendency to return to original Grande Ronde water chemistry.
pH (measured at 25°C)		Initially 8.0 in packing material water, decreasing to 6.5-7.5.	Increasing to approximately 9.0.	
pH (at high temperatures)		Lower than values measured at 25°C but no reliable values can be specified because of complex hydrothermal reactions and irradiation effects.		
Redox Conditions	Oxic.	Probably oxic due to water radiolysis.	Approaching anoxic.	Probably anoxic.
Stress (MPa)	0.1	Initially 0.1 MPa, rising to a value between hydrostatic and lithostatic stresses (11 to 33 MPa).		

Table 1.3. List of estimated spent fuel waste package conditions for a tuff repository.

Parameter	Estimated Value			
	Operations Period	Thermal Period (0-300 yr)	Transition Period (300-1000 yr)	Geologic Control (>1000 yr)
Temperature at Centerline* (Thermal Loading 12.4 W/m^2)		330°C max. to 100°C	100-60°C	<60°C
Total Gamma Dose (rad)		$\approx 10^{10}$	Little additional irradiation.	No additional irradiation.
Water Flow Rate	Steam/air conditions.	Steam/air for first several hundred years followed by liquid water flowing at about 8 mm/yr.	About 8 mm/yr.	About 8 mm/yr.
Water Chemistry	Steam/air conditions.	Probably similar to J-13 well water after steam conditions subside. May be more concentrated than J-13 water if precipitated salts redissolve.	Probably similar to J-13 well water but could be more concentrated if precipitated salts redissolve.	
pH (Measured at 25°C)		7.1 for J-13 well water. May be acidic because of radiolysis of $N_2/O_2/H_2O$ mixtures.	≈7.1	≈7.1
Redox Conditions	Oxic	Oxic	Oxic	Oxic
Stress (MPa)	0.1	Initially 0.1 MPa, rising to the lithostatic stress of 8.6 MPa as host rock settles.		

*Calculations were made for waste package without packing material.

2. REVIEW OF WAPPA

2.1 Introduction

2.1.1 Background Information

The Code of Federal Regulations 10 CFR Part 60, §60.113 (June 1983) requires that the applicant for a license to operate a nuclear waste repository demonstrate compliance of the proposed design with the following performance criteria of individual barriers after permanent closure:

1. Containment of HLW within the waste packages should be substantially complete for a period to be determined by the Nuclear Regulatory Commission. Such a period shall be not less than 300 years nor more than 1000 years after permanent closure of the repository.

2. The release rate of any radionuclide from the engineered barrier system following the containment period should not exceed one part in 100,000 per year of the inventory of that radionuclide calculated to be present at 1,000 years. Exception to this rule is allowed for radionuclides whose release rate is less than 0.1% of the calculated total release rate limit, which is taken to be 1 part in 100,000 per year of the (total) inventory of radioactive waste that remains after 1,000 years of radioactive decay.

3. Pre-waste-emplacement groundwater travel time along the fastest path of likely radionuclide travel from the disturbed zone to the accessible environment should be at least 1,000 years or such other travel time as may be approved or specified by the Nuclear Regulatory Commission.

Although the controlled release requirement is on the engineered barrier system (the waste package and the underground facility), it is expected that the applicant will rely primarily on the waste package. Thus, waste package performance is the direct concern of two out of three NRC individual-barrier performance criteria.

Two waste-package system performance codes have been developed: BARIER and WAPPA. Both codes were developed for the salt program (ONWI-302, 1981; ONWI-452, 1982), but were kept general enough to be applied to hard rock repositories. At present, development of the code BARIER has been discontinued, and WAPPA is the only code used by the salt and tuff programs for integrated waste package performance. In particular, the tuff program is modifying WAPPA to allow its use for nonsaturated conditions. The basalt program does not have a waste-package system code.

This document presents a review of the code WAPPA as it is presented in the code manual ONWI-452 of April 1983 and in a subsequent, letter-form update of December 1983 by the code custodian[1]. For clarity, the code WAPPA is briefly introduced in Section 2.1.2. This document's objectives and organization are presented in Section 2.1.3.

[1]Private communication from Leslie A. Scott to Claudio Pescatore, December 14, 1983.

2.1.2 The Code WAPPA

The Waste Package Performance Assessment Code WAPPA was constructed for general applicability to all candidate geologic media, to any waste type, and to conventional waste package designs and geometries. The code was designed to serve as a tool in all of the following major areas: waste package design, repository design, site selection and characterization, and system assessment.

WAPPA consists of about 13,000 source program statements representing five physical process models and a system drive model. With reference to Figure 2.1, the five process models include a radiation model, a thermal model, a mechanical model, a corrosion model, and a leach-and-transport model. These models are sequentially activated in the above order within each time step by the system drive model. Each process model applies to all waste package barriers at the same time. For instance the radiation model would determine the radiation field throughout the waste package as well as corrosion and leaching enhancement factors for wetted barriers. Thus, the implemented approach is termed "barrier-integrated and process-sequential." The code uses one-dimensional, radial axisymmetric geometry with correction factors for finite length effects.

The modeling approach implemented in WAPPA is more empirical than mechanistic. Thus a most significant but little emphasized task in the operation of WAPPA is the preparation of a data base encompassing all empirical parameters for the problem at hand. The task can be overwhelming due to the recognized lack of pertinent data in the literature and to the large variation of problems one may have to solve.

2.1.3 Objectives and Organization of this Report

The present review of WAPPA has been prompted by the importance of this code within the DOE community which regards it as the preferred code for integrated waste package analysis.

The objective of this report is to examine the code's level of modeling in order to determine its potential uses for the regulatory community, i.e., whether the code could be used for licensing, reliability analysis, screening of various waste package designs, etc. Furthermore, we have also examined the possibility of adapting parts of WAPPA into existing codes at BNL.

Chronologically, we have first run the code at BNL and examined the Complex Verification Test Case provided by the code developer. This indicated some potential problems in the code modeling and its structure. We then examined each process model following the code manual and, to some extent, the source program. This effort also resulted in re-writing part of the Leach-and-Transport model. Our findings were documented in a series of memos-to-file which were made available to the NRC and its contractors (BNL, MF 125, 126, 127, 132, 135, 141, 142, 149, 151, 1983 through 1984).

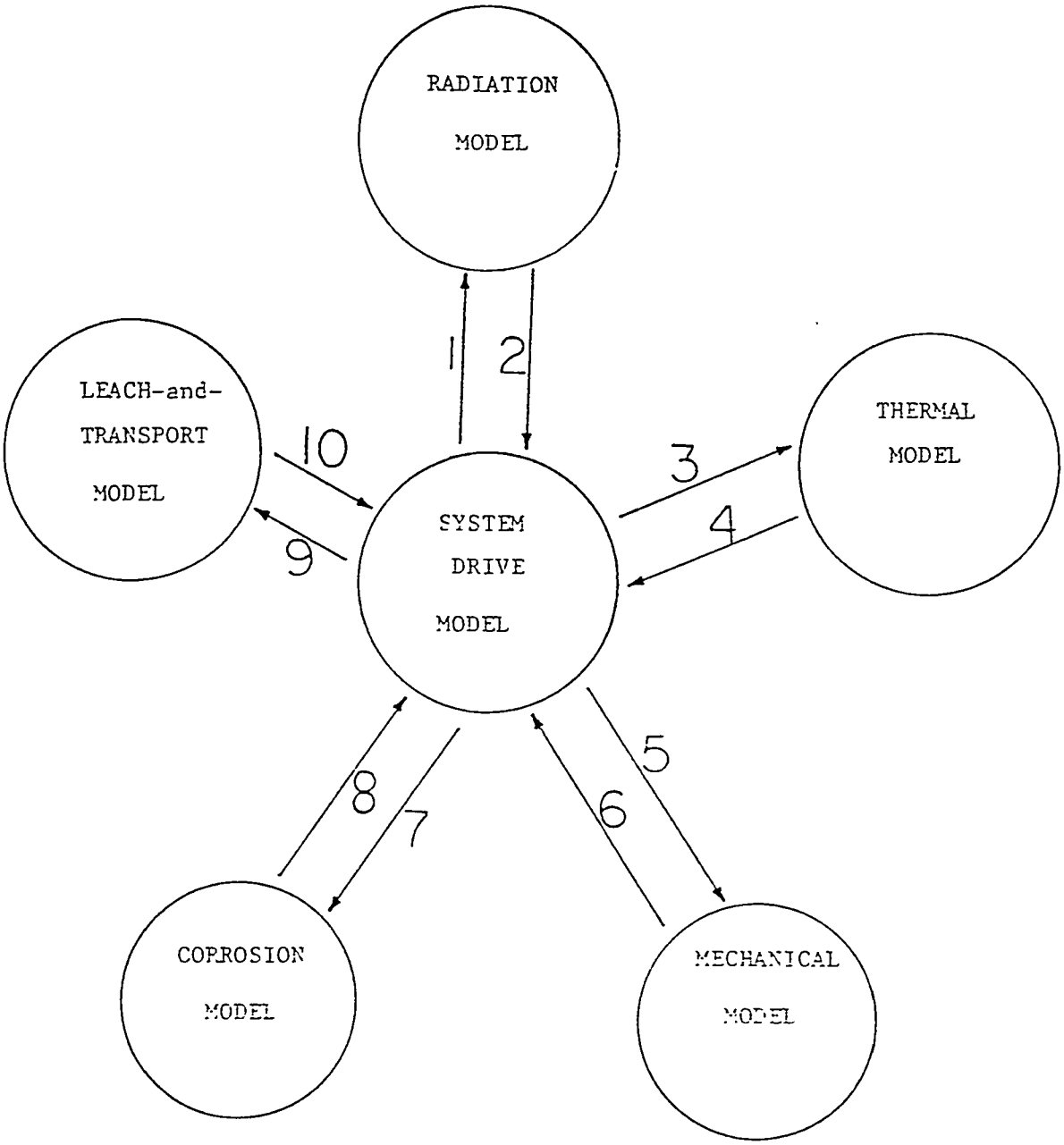

Figure 2.1 Schematic representation of how WAPPA operates within each time step.

The present report draws on the material of our original memoranda. With minor changes they constitute Section 2.2 and 2.3 of the document, and deal with each process model and WAPPA's operation, respectively. Conclusions are drawn in Section 2.4, which also gives our final recommendations.

2.2 Review of WAPPA's Process Models

As indicated earlier, the code WAPPA was constructed for general applicability to all candidate geologic media, to any waste type, and to conventional waste package designs.

The code uses one-dimensional, radial axisymmetric geometry with correction factors for finite length effects, where applicable. System performance is determined through sequential use of five main process models a radiation model, thermal model, mechanical model, corrosion model, and leach-and-transport model. With reference to Figure 2.1, sequential coupling in the above order is operated by a system drive model. Thus, within each time step, results from the Radiation Model can be used in the four remaining process models, results from the Thermal Model can be used in the three remaining models, and so on. Each model is reviewed separately in Sections 2.2.1 through 2.2.5. General conclusions about WAPPA's level of modeling are drawn in Section 2.2.6.

2.2.1 WAPPA's Radiation Model (RMODEL)

The primary function of the radiation model is to calculate radiation induced effects that are required as input to other WAPPA process models. Thus, the radiation model obtains the decay heat rate which is used by the thermal model, the alpha damage to the waste form to be used in the mechanical model, and corrosion and leaching enhancement factors due to radiolysis to be used in the corrosion and leach-and-transport models, respectively. These quantities are calculated through four distinct submodels: (a) Source Term, (b) Attenuation, (c) Radiolysis, and (d) Damage. These are reviewed in the following section.

2.2.1.1 Review of Modeling Approach

2.2.1.1.1 Source Term Submodel

The first function of this submodel is to obtain the decay heat rate, gamma ray and alpha particle emission rate, and radionuclide mass inventory within the waste form at any given time. The basis of the calculation is a logarithmic interpolation procedure using a user supplied time-dependent data base. Presently, this data base is prepared by using the isotope buildup and decay code ORIGEN2 (ORNL-5621).

The second function of this submodel is to calculate the gamma dose and the alpha particle displacement dose at the waste form periphery. The alpha particle displacement dose is used by the Damage submodel to calculate degradation of waste form properties. The gamma dose is used by the Radiolysis

submodel to calculate enhancement of corrosion and leaching caused by gamma radiolysis. It should be emphasized that this gamma dose is at the periphery of the waste form and not in the groundwater where the radiolysis occurs.

2.2.1.1.2 Attenuation Submodel

This submodel calculates the attenuation of gamma rays as they travel from the waste form to the repository. This is accomplished by calculating the gamma flux as a product of the source in the waste form, a buildup factor, and an attenuation factor. The empirical buildup factor simulates the effect of scattered radiation. The attenuation factor is a function of the thickness and type of barriers in the waste package.

2.2.1.1.3 Radiolysis Submodel

WAPPA assumes that the influence of gamma radiolysis on corrosion and leaching can be modeled through empirically determined enhancement factors. These are multiplicative factors defined so that multiplication of the leach or corrosion rate by the enhancement factor gives the enhanced rate due to radiolysis. The radiolysis submodel determines these enhancement factors, as function of the gamma flux, dose rate and cumulative dose at the edge of the waste form, through a logarithmic interpolation of user supplied data.

2.2.1.1.4 Damage Submodel

This submodel calculates changes in the thermal conductivity, fracture strength, thermal expansion coefficient and density of the waste form due to alpha-induced damage. These properties remain unchanged until the alpha displacement dose reaches a user defined critical value. After reaching this value, the material property under consideration is degraded according to a saturating exponential which depends on the cumulative dose and empirically determined coefficients.

2.2.1.2 Discussion

The primary method used in WAPPA's radiation submodels for calculating a desired quantity involves reading a data base. This causes two problems. First, the input required for the data base may not be readily available. If this is the situation, the required information could be obtained through ad hoc experiments or through use of more advanced computer simulations. For example, assuming that the buildup factor in basalt is unknown, a detailed photon transport calculation could be performed and the buildup factor chosen such that the flux as calculated by the transport code matched the flux calculated by WAPPA's attenuation submodel. The second problem is that each user must construct his own data base. WAPPA does not supply the data. It does not even supply a list of references where the appropriate data can be found. This makes the calculation subject to the user's ability to obtain the proper data. Because of the paucity of present data, and the uncertainty in some of the data, it is unlikely that any two users will create the same data base.

2.2.1.2.1 Source Term Submodel

The Source Term submodel's major function involves reading waste-form inventory information from a data base. The modeling it implements does have two conservative approximations: (1) it does not account for redistribution of nuclides due to leaching; therefore it overpredicts the radiation source within the waste form; and (2) it uses the gamma flux and total dose at the waste form periphery for determining enhancement of leaching and corrosion, which overpredicts the effects of radiolysis. Indeed, during the containment period the flux at the waste form periphery will be much greater than in the groundwater. Thus, the calculated total dose to the groundwater will exceed the actual dose. Since the enhancement is a function of both dose and flux, radiolysis effects are overpredicted.

2.2.1.2.2 Attenuation Submodel

The attenuation submodel serves no obvious purpose. Currently, the only use for the gamma flux is to determine the amount of radiolysis that occurs in the groundwater. However, since WAPPA uses the gamma flux at the waste form boundary, as determined by the Source Term submodel, calculations of the flux in the remainder of the waste package are superfluous.

Assuming that future revisions of the code do use the gamma flux within the waste package, the following comments become relevant.

The documentation for this submodel lacks detail and justifies this shortcoming on the claim that the model uses standard expressions from the Reactor Shielding Design Manual (Rockwell, T.; 1956). However, the equations are applied incorrectly in WAPPA. The error involves improper definition of the buildup factors. Before explaining this error, a description of buildup factors and their properties is presented.

Buildup Factors

WAPPA assumes that the effects of scattered radiation can be accounted for through a buildup factor. This prevents the need for a detailed transport calculation. However, it requires the use of an empirically determined buildup factor, defined as the ratio of the total flux to the uncollided flux. As the distance travelled by the gamma rays increases, the proportion of scattered flux to the total flux increases. Therefore, the buildup factor increases with distance. This does not imply the total flux increases with distance, in fact it decreases with distance as the total flux is the product of a buildup factor and an attenuation factor which decreases faster than the buildup factor increases.

Error in the Buildup Factor

Viewing Figure 2.2, and noting that WAPPA approximates the gamma radiation from the cylindrical waste form as originating from an infinite line source, the error made in WAPPA can be explained. For a gamma ray originating within the line segment $d\ell$, it must travel a distance R to reach point P.

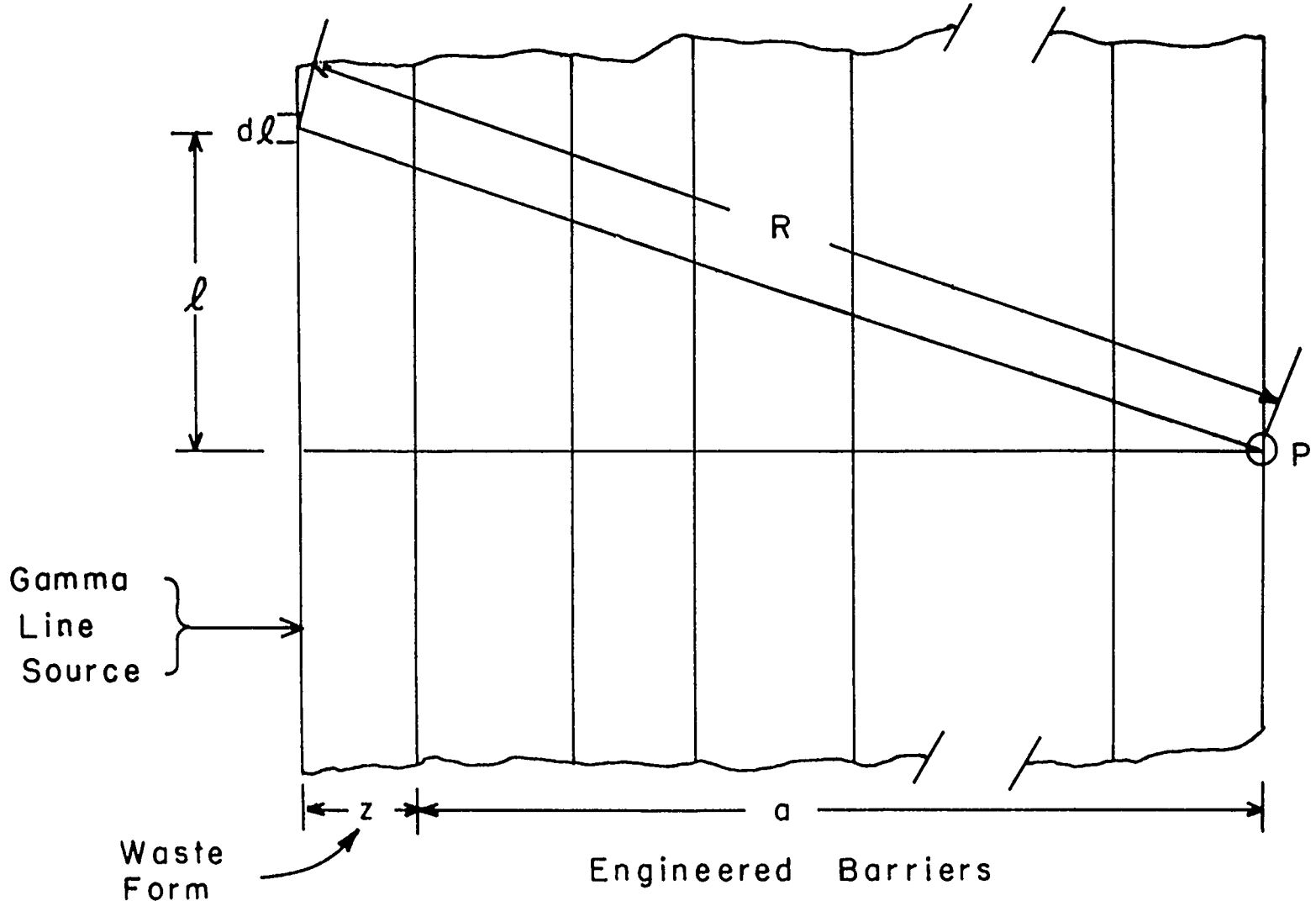

Figure 2.2 Geometrical representation of the waste form as a line source surrounded by the engineered barriers of the waste package.

However, WAPPA calculates the buildup factor based on the normal distance between the line source and point P, the distance a+z in Figure 2.2. Because (a+z) < R and the buildup factors increase with distance, this assumption is non-conservative. Heuristic arguments (Sullivan, T., MF-142, 1984), indicate that the calculated flux will be within a factor of 10 of the flux obtained using the distance R in calculating the buildup factor. Considering the uncertainties in the entire calculation and the fact that corrosion or leaching are expected to be enhanced by less than 20 percent for an order of magnitude increase in gamma dose, this error may not be significant, but it should be addressed in the code manual.

Empirical Coefficients in Buildup Factor Expression

Although WAPPA claims to use standard formulae, the expression for the buildup factor uses slightly different definitions for the empirical coefficients when compared to the definitions found in the Reactor Shielding Design Manual (Rockwell, T., 1956), the reference for buildup factors cited by WAPPA.

WAPPA defines the buildup factor B_i for material "i" as:

$$B_i = A_{1i}e^{-\alpha_{1i}t_i} + A_{2i}e^{-\alpha_{2i}t_i} \qquad (2.1)$$

where A_{1i}, A_{2i}, α_{1i}, and α_{2i} are material dependent empirical coefficients and t_i is the thickness of material "i" normal to the line source. In contrast, the Reactor Shielding Design Manual defines the buildup factor as:

$$B_i = A_{1i}e^{-k_{1i}\mu_i T_i} + A_{2i}e^{-k_{2i}\mu_i T_i} \qquad (2.2)$$

where A_{1i}, A_{2i}, k_{1i}, and k_{2i} are material dependent empirical coefficients and μ_i is the adsorption coefficient of the medium, and T_i is the thickness of medium that the gamma ray passes through.

From these two expressions it is clear that

$$a_{ji} = k_{ji}\mu_i \qquad j = 1,2 \qquad (2.3)$$

and the equations are similar. However, this discrepancy is not pointed out in the manual.

2.2.1.2.3 Radiolysis Submodel

WAPPA calculates only one leach enchancement factor. This assumes that radiolysis has the same effect on all waste form constituents. However, radiolysis changes the number and types of molecular and radical species present in the groundwater. This in turn influences the solubilities of the different species in the groundwater and alters the leach rates from the waste form. Each species will react differently to these radiation induced changes.

WAPPA does not model alpha radiolysis nor does it attempt to account for the gamma flux in the groundwater that arises from particles leached from the waste form. Once leaching begins, alpha and gamma emitting species enter the groundwater. Alpha particles do not interact with the groundwater in the same manner as gamma rays (PNL-4452, 1983). Therefore, the water chemistry is different and leaching from the waste form will respond accordingly. This effect may be negligible because the amount of alpha and gamma emitting nuclides in the groundwater should be small.

The WAPPA manual does not mention the possibility of chemical changes due to gamma irradiation in salt repositories (BNL-NUREG-33658, 1983). In principle, this could be handled through leach and corrosion enhancement factors as currently done in WAPPA.

Lack of a detailed water chemistry model in WAPPA limits any attempt at modeling radiolysis effects to be heuristic and prone to be at most qualitatively correct. The accuracy of the radiolysis model is totally dependent on external justification.

2.2.1.2.4 Damage Submodel

Although the idea that alpha damage can be represented as a saturating exponential function of the total dose is not new, the data base to support this is limited. This may be a particular problem for glass. The reference cited in WAPPA (Weber, W. J., 1980) that proposes the saturating exponential correlation bases its model on experimental results on radiation effects in crystalline ceramic materials. The other radiation damage reference (Weber, W. J., 1979) does consider glass, however the data reported is for one glass composition and does not provide data for all of the radiation-induced property changes used in WAPPA.

The damage submodel does not attempt to calculate a leach enhancement factor due to alpha damage of the waste form. Apparently this was considered at one time by the developers of WAPPA because the empirical coefficients for the saturating exponential correlation are requested as input. However, these coefficients are unused. The manual does not justify neglecting this effect.

2.2.1.3 Conclusions

All of the submodels used to evaluate radiation-induced phenomena are structured to rely heavily on a user supplied data base. Assuming the data are available, the radiation model might provide a conservative estimate of the processes it models. Use of a data base approach allows the models to be simple and the computational times short. However, it also places a large burden on the user. Furthermore, because of the large quantity of data requested, coupled with the uncertainty in some data, it is unlikely any two users will develop the same data base.

2.2.2 WAPPA's Thermal Model (TMODEL)

WAPPA's Thermal Model computes the temperature profile within the waste package and feeds it to the System Drive Model for updating temperature dependent parameters in the Mechanical, Corrosion, and Leach-and-Transport models. Following a description of the modeling approach in Section 2.2.2.1, Section 2.2.2.2 discusses the limitations of the implemented submodels. Conclusions are drawn in Section 2.2.2.3.

2.2.2.1 Review of Modeling Approach

WAPPA's thermal modeling approach rests on the assumption that the heat capacity of waste package barriers is negligible and that the temperature distribution is a function only of radial distance from the waste form centerline. In the waste form it is assumed that the heat source is uniform. Solution of the resulting steady-state heat conduction equation yields a parabolic temperature distribution (Perry, R. H. and C. H. Chilton; 1973). In the cylindrical annulus representing the various waste package barriers it is assumed that there is no generation of heat. Solution of the heat conduction equation in this region without a source results then in a logarithmic profile (Perry, R. H. and C. H. Chilton; 1973). In terms of the temperatures at the waste form centerline and at the interfaces between adjoining barriers, the waste package temperature profile is expressed as follows:

$$T_o = T_1 + \frac{q'(t) r_1^2}{4\ k_0(T_1)} \tag{2.4}$$

$$T_i = T_{i+1} + \frac{Q_i(t)}{2\pi H\ k_i(T_{i+1})}\ \ln\ (r_{i+1}/r_i), \quad i=1,2,\ldots,N \tag{2.5}$$

where T_o is the centerline temperature; T_1 is the temperature at the waste form periphery; r_i is the distance of the i-th interface from the waste form centerline; $T_i = T(r_i,t)$; $q'(t)$ is the volumetric heat generation rate in the waste form; H is the height of the waste package; $k_0(T_1)$ is the effective thermal conductivity of the waste form; $k_i(T_{i+1})$ is the effective thermal conductivity of the i-th barrier based on the temperature at the outer edge of the barrier; $Q_i(t)$ is the effective, total conductive heat flux out of the i-th interface.

Heat transfer by convection is considered important in liquid or gas filled annuli when the Grashof number exceeds 20,000. The Grashof number is a dimensionless parameter defined as:

$$N_{GR} = \frac{X^3\ \rho^2\ g\ \beta_f\ \Delta T}{\mu^2} \tag{2.6}$$

where X is the gap width; ρ is the density of the fluid; g is the acceleration due to gravity; β_f is the volumetric expansion coefficient; ΔT is the

temperature difference across the gap; and μ is the fluid viscosity. When convection is important, the parameter k_i in Equation (2.5) is the familiar thermal conductivity corrected through an equivalent conduction enhancement factor which is a function of the Grashof number.

Heat transfer by radiation is considered for gas filled annuli and is modeled through modification of the conductive heat flux. Thus, for gas gaps, the quantity $Q_i(t)$ used in Equation (2.5) is the total heat flux minus the total radiative heat flux, $q_i(t)$, which is defined as follows:

$$q_i = A_i F_{i,i+1} \sigma (T_i^4 - T_{i+1}^4), \tag{2.7}$$

where:

A_i - area of i-th interface

$F_{i,i+1}$ - view factor from i-th to (i+1)-th interface

σ - Stefan-Boltzmann constant.

Radiation heat transport will be most important during the first few years after burial when the heat source and temperature gradients through the waste package are largest.

Equations (2.4) and (2.5) can be solved sequentially once either the temperature at the waste form centerline or the temperature at the waste package-host rock interface is specified as function of time. The Thermal Model adopts the second one as the reference temperature. The waste package-host rock interface temperature is provided in the code as a user supplied table of temperature data versus time.

The above formulation is abandoned when the total heat generation rate becomes less than 1 watt. At that time, a few hundred years, all temperatures within the waste package are set equal to the user-provided, reference repository temperature.

2.2.2.2 Discussion

WAPPA's assumed parabolic-logarithmic temperature profile within the waste package is the profile that would exist in the system if this had had infinite time to equilibrate thermally with its surroundings while the heat generation rates were kept constant. As such, it would certainly yield a conservative estimate of waste package temperatures if, at any time t, the user-supplied boundary temperature were the thermally equilibrated value. Engineering judgement, however, suggests that, after the first few months during which heat storage effects in the waste package are important, Equations (2.4) and (2.5) closely represent the shape of the waste package temperature profile. Therefore, the accuracy of WAPPA's temperature estimates within the waste package after the first few months rests on the accuracy of

the user supplied boundary temperature data. If these data are in error by X degrees, the calculated temperature profile is displaced by the same number of degrees in the waste package.

Since the waste package-repository boundary temperature depends on waste package dimensions and heat generation rates as well as on repository properties, such as rock thermal properties, waste package arrangement, area thermal load, etc., the present Thermal Model logic would call for a large data base of boundary temperature values versus time. In analogous situations, other researchers have preferred to couple the waste package thermal model, Equations (2.4) and (2.5), with a thermal code for the repository. Both options would require substantial improvement of WAPPA.

WAPPA is inadequate for reliable temperature prediction during the first few months after burial as the Thermal Model formulation breaks down in the limit when heat storage effects in the the waste package are important. However, the model would still provide reasonable estimates of internal waste package temperatures provided an "appropriate" set of boundary temperature data is supplied by the user.

2.2.2.3 Conclusions

The usefulness of WAPPA's thermal model usefulness for short-term temperature prediction,i.e., during the first few months after burial, is limited to providing conservative estimates of waste package temperatures by selecting "appropriate" values for the user-supplied boundary temperature. Reliable, short-term temperature prediction would require adding a temperature submodel to the code which includes heat storage effects.

WAPPA's thermal model may provide reliable estimates of waste package temperatures a few months after burial provided the user-supplied data base of boundary temperatures is shown to be accurate. This may require a separate run of a repository thermal code which takes into account waste package heat generation rates and dimensions as well as waste package arrangement, rock thermal properties, etc.

2.2.3 WAPPA's Mechanical Model (FMODEL)

In WAPPA's modeling approach three types of stress-assisted breaching of waste package barriers can occur: 1. stress corrosion cracking of metallic barriers, 2. fracture of metallic barriers at pre-existing cracks, and 3. brittle fracture of the waste form.

The purpose of FMODEL is to predict the magnitude of local stresses (stress intensity factors) at pre-existing flaws on metal surfaces, and to determine the extent to which the waste form fractures due to the applied stress. These tasks are accomplished by coupling a Canister Fracture (CF) Submodel and a Waste Form fracture (WF) Submodel to a Stress Analysis (SA) Submodel. These submodels are introduced next. A discussion follows in Section 2.2.3.2. Conclusions are drawn in Section 2.2.3.3.

2.2.3.1 Review of Modeling Approach

2.2.3.1.1 Canister Fracture Submodel

Given the calculated stress level from the SA submodel and the user-specified length of pre-existing cracks on metallic barriers, the CF submodel computes empirical, elastic stress intensity factors.

If the metal has not yielded plastically, the stress intensity factor is compared with the metal's critical value of fracture toughness. Breaching occurs when the stress intensity factor exceeds the fracture toughness.

If the metal has already yielded plastically, a new effective crack length is calculated. The stress intensity factor is then recomputed and compared with the fracture toughness of the material.

The equations used in this submodel are empirical in nature. Therefore one must make sure they apply to the materials, loading pattern, and geometry at hand. To that effect, the CF submodel write-up does not give useful references, therefore these equations must be accepted with reservations.

2.2.3.1.2 Waste Form Fracture Submodel

From the various components of the stress as calculated by the SA submodel, the WF submodel checks for regions where tensile stresses exceed the fracture strength of the material. Since the problem is regarded as axisymmetric, this defines an outer annulus where the waste form is fractured. The volume of the fractured region is then multiplied by an empirical coefficient to determine an equivalent surface-area increase to be used later by the Leach-and-Transport Model.

2.2.3.1.3 Stress Analysis Submodel

While the CF and WF submodels are empirical in nature, the SA submodel is based on classical theories of materials strength and stress analysis.

For a strength analysis, the FMODEL considers five types of materials whose properties are modeled as follows:

1. The <u>waste form</u> is modeled as an elastic/brittle material which undergoes fracture in the region where tensile stresses exceed the waste form fracture strength.

2. <u>Metallic barriers</u> are modeled as elastic/plastic materials. These materials yield plastically in regions where the TRESCA criterion is satisfied. Namely, when

$$\text{Max}\left(\left|\sigma_r-\sigma_\theta\right|,\ \left|\sigma_\theta-\sigma_z\right|,\ \left|\sigma_r-\sigma_z\right|\right) \geq \sigma_{yield}$$

3. <u>Packing materials</u> are modeled as compressible elastic elements. They yield, i.e., they are extruded, when the Von Mises maximum stress exceeds the yield stress. That is when:

$$\sigma_{max} = \frac{3}{2} \sqrt{(\sigma_r - \sigma_H)^2 + (\sigma_\theta - \sigma_H)^2 + (\sigma_z - \sigma_H)^2} > \sigma_{yield},$$

σ_H - the hydrostatic pressure.

4. Gas gaps are modeled as having zero pressure and no stress transfer capability.

5. Liquid gaps are modeled as incompressible elements. Also, all "failed" portions of the barriers, i.e., the fractured waste form region, the plastically yielded portion of metallic barriers, and all corrosion layers are treated as incompressible elements.

From a stress analysis point of view, the modeling approach regards the waste package as a series of concentric cylindrical annuli encircling a solid core. The length of the waste package is infinite and loading compressive in both the horizontal and vertical directions. Horizontal loading is due to the repository confining horizontal pressure, to thermal expansion, and to initial residual stresses at the canister/waste form interface. Vertical loading is due to the repository vertical confining pressure. No shear, torsion, or bending is accounted for, nor are gravity loading and friction between components. As a result, all deformations take place horizontally in the radial direction. Stress enhancement due to the finite length of the waste package is handled through an empirical factor which multiplies the calculated stress.

2.2.3.2 Discussion

2.2.3.2.1 Limitations of the Modeling Approach

Any model appearing in a general purpose code like WAPPA can only be expected to handle a few important effects and failure modes. In the case of the FMODEL, the modelers have identified brittle fracture of the waste form and cracking of the metal barriers at pre-existing flaws as the main mechanical failure modes of the waste package. To that end they disregard bending, torsion, gravity loading, friction effects, creep, buckling, etc., which is likely to be an acceptable approach but it is not justified in the document. Also, the expressions used for calculating empirical stress intensity factors at pre-existing cracks are not properly referenced and justified.

The implemented modeling approach does present some desirable features, i.e., it accounts for degradation of mechanical properties due to radiation (empirical factors and data have to be used) and for the influence of temperature on the stress. The model also accounts for initial, residual processing stresses.

The most important limitations are that materials strength, as measured by yield stress and tensile strength, is not modeled as a function of temperature, and that the volumetric expansion of the corrosion products is not addressed. Corrosion products are known to exert very large pressures in constricted regions, e.g., the phenomenon of denting in nuclear steam generators and the wedging action of corrosion products (Pickering, H. W.; 1962).

2.2.3.2.2 Adequacy of the Modeling Approach

Two relevant waste package failure modes are not given sufficient attention in the implemented modeling approach. These are, 1.) failure of the waste package ends and, 2.) buckling of metal barriers beyond their elastic stability region.

With reference to Figure 2.3, which reports a typical waste package design for high-level waste (AESD-TME-3131, 1982), it appears that a weak area in the canister structure is the neck area. In that area the metal is not supported by the waste form and the neck shape favors concentration of stresses. Thus, crushing of the air gap appears to be an important failure mode which ought to be addressed. Stresses may also concentrate at the bottom of the canister at the welds between the base and the rest of the metal, thus causing the base to detach. This failure mode should also be addressed.

Furthermore, it should be noted that as the unfailed part of metal barriers becomes progressively thinner due to corrosion and plastic yielding, it may be subject, at one point, to elastic instability, i.e., under sufficiently high stress the cylindrical metal annulus may buckle into an "eight" shape. This may be an important failure mode for waste package performance.

FMODEL uses a number of empirical correlations to represent mechanical behavior of the waste package. For this reason, the ability of FMODEL to provide a conservative estimate of waste form fracture and canister failure can not be guaranteed unless the data used by the correlations can be shown to be conservative.

2.2.3.3 Conclusions

The FMODEL cannot be used by itself in a predictive mode. It relies heavily on user-supplied data which may not be obtained from the literature and for which the user may have to make ad hoc experiments. This is the case for important quantities related to failure mode analysis, such as (a) the empirical coefficient to convert waste form fractured volume to an increase in waste form surface area, (b) the empirical formulae used to calculate stress intensity factors, and (c) the empirical coefficient to deal with end effects. The FMODEL does not factor in the volumetric expansion of corrosion products which, depending on the degree of fracturing of the host rock, may result in additional confining pressures. Furthermore, the model does not take into account failure of both canister ends nor does it account for the elastic stability of the metal barriers.

2.2.4 WAPPA's Corrosion Model (CMODEL)

The corrosion model calculates the degradation of each metallic barrier in the waste package due to the following processes:

(1) Dry oxidation;
(2) General corrosion;
(3) Galvanic corrosion;
(4) Localized corrosion, including pitting and crevice corrosion; and
(5) Stress corrosion cracking, including hydrogen embrittlement and active path stress corrosion cracking.

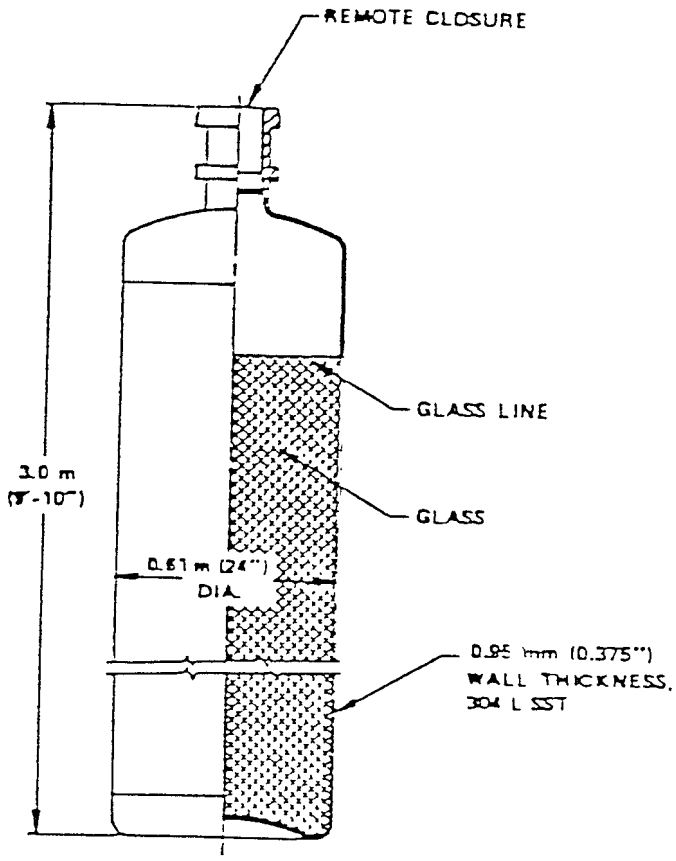

Figure 2.3 Typical waste form and canister design (adapted from AESD-TME-3131, 1982).

Along with barrier degradation, CMODEL tracks the penetration of water into the waste package as the barriers fail. Following a description of the submodels, Section 2.2.4.2 discusses the limitations of CMODEL and conclusions are drawn in Section 2.2.4.3.

2.2.4.1 Review of Modeling Approach

2.2.4.1.1 Dry Corrosion

Before a barrier is contacted by water, CMODEL considers the spatially uniform one-dimensional thinning of barriers due to oxidation. Oxide growth is calculated by one of three empirical growth laws: logarithmic, parabolic, or a power relation in time. The coefficients required in these laws are defined as a function of temperature through user supplied input tables.

2.2.4.1.2 Wet Corrosion

Upon wetting of a barrier, wet corrosion models are activated. A distinction is made between mechanisms that cause a uniform degradation of the entire barrier versus mechanisms that cause local barrier degradation. Uniform corrosion submodels consider galvanic and general corrosion. Local corrosion includes stress corrosion cracking, pitting, and crevice corrosion.

The submodel for galvanic corrosion determines whether water (an electrolyte) is in contact with two adjacent barriers thereby allowing a galvanic cell to form. (This situation can only occur if local corrosion has caused a breach in an outer barrier.) Based on input data, the barrier that acts as the anode is determined and the thickness of this barrier is reduced linearly with time. The rate of degradation is a function of temperature and is increased through the effects of radiolysis. The model does not give credit for cathodic protection.

The model for general corrosion provides a spatially uniform thinning of the barrier. The rate of degradation is determined from an input table, for each barrier, of corrosion rate versus temperature. The effects of radiolysis are incorporated by multiplying the corrosion rate by an enhancement factor which is a function of the gamma dose and flux. The net rate of corroson is a linear function of time.

Local corrosion events are considered "catastrophic". That is, if the conditions required to initiate one of these processes arise, the barrier is considered breached instantaneously at the beginning of the current time step. Given user supplied empirical data for pitting/crevice/crack size and density, the total "breached" area is calculated. Simultaneous with the breach of the barrier, groundwater flows to contact the next barrier.

2.2.4.2 Discussion

WAPPA's corrosion model was developed with the intention of providing a calculation of the maximum rate of barrier degradation, i.e., a conservative estimate. However, before conservatism can be assured, the following points concerning the data and numerical modeling must be considered.

First, and most important, it is emphasized that all of the corrosion submodels are empirical and extremely data intensive. Corrosion is a complex phenomena that is not understood well from a quantitative, fundamental viewpoint. For this reason, CMODEL uses empirical correlations to supply all the information on corrosion rates for each of the various models and for each barrier. The coefficients used in each correlation are supplied by the code user as a function of temperature. No attempt is made at modeling the influence of solution chemistry on corrosion rate. The effect of solution chemistry is assumed to be incorporated in the empirical input supplied by the user. Before CMODEL can be considered conservative, the data used in the empirical correlations must be shown to be conservative over the entire range of potential repository conditions.

Second, the numerical strategy used in CMODEL contains two flaws. The first error involves solution for the amount of dry oxidation, general and/or galvanic corrosion. The solution strategy in WAPPA is process sequential, that is, WAPPA looks at radiation, thermal, mechanical, corrosion, and leaching processes as occurring sequentially in a given time step. In particular, the temperature distribution is calculated before CMODEL calculates the temperature dependent corrosion rate. If the temperature is decreasing with time, this is the expected condition after the first few hundred years, the corrosion rate is calculated based on a lower temperature and therefore the calculation is non-conservative. This could be corrected through use of the temperature at the previous time step to calculate the amount of corrosion when the temperature is decreasing.

The other error involves solution of the dry oxidation corrosion model. The empirical laws used in calculating oxide thickness are, in general, developed from non-linear, integral-type relationships based on isothermal experimental data. For this non-isothermal system, care must be taken to account for the influence of temperature variations on oxide growth.

The method of solution used in WAPPA for calculating oxide thickness is most easily understood while viewing Figure 2.4, a plot of oxide thickness versus time for two temperatures. For the initial time step, time zero to time t_1, the system is at temperature T_1 and the oxide grows to a depth, d_1. In the subsequent time step, time t_1 to time t_2, the system temperature has been updated and is T_2. WAPPA calculates the incremental oxide growth, Δd_2, as the amount of growth that would have occurred over the time interval t_2-t_1 provided the system had been held at temperature T_2 for the entire calculation time. This growth is represented by the curve through points b and c on the graph. The total oxide thickness is obtained by summation of d_1, the oxide thickness and Δd_2, the incremental growth. Viewing each time step as a new initial value problem, it is seen that the WAPPA code changes the "initial condition" for oxide thickness at each time step. Since growth rate is a function of thickness, this procedure is incorrect.

A better solution procedure is schematically represented in Figure 2.5. Here, after the oxide has grown to a depth d_1 at temperature T_1, time is advanced to the next time step and the temperature is updated and is T_2. In this case, growth of the oxide is calculated starting from a depth d_1 on the isothermal curve for temperature T_2. This is point b in Figure 2.5. Growth

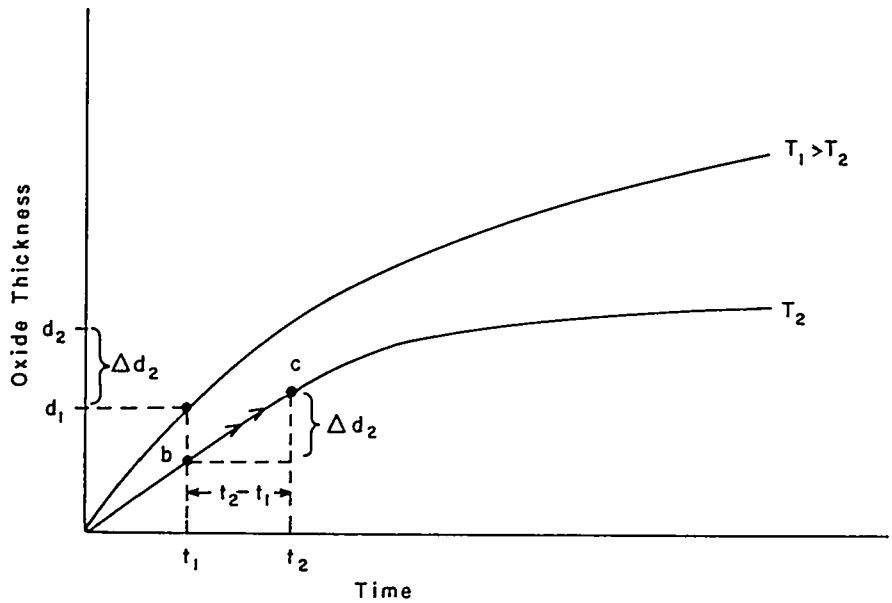

Figure 2.4 Schematic representation of oxide thickness versus time. WAPPA considers thickness as a function of temperature and time.

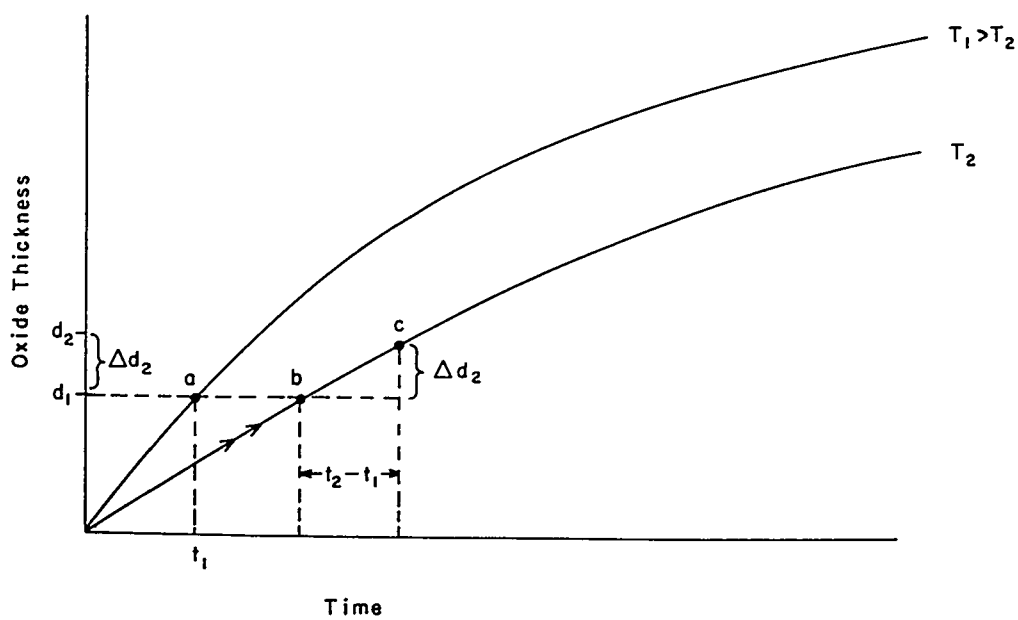

Figure 2.5 Improved oxide thickness calculation considers thickness as a function of temperature and previous history.

progresses along this isothermal curve for a time period corresponding to the length of the time step, $t_2 - t_1$. This is represented by the path between points b and c. The new oxide thickness is the sum of d_1, the initial thickness, and Δd_2, the incremental growth. This model takes the viewpoint that corrosion rate is a function of temperature and oxide thickness whereas the WAPPA model views the corrosion rate as a function of temperature and time.

Provided the temperature is monotonically decreasing with time and neglecting the "improper" use of the temperature at the end of the time step to calculate oxide growth as previously mentioned, the solution procedure currently used by WAPPA for dry oxidation will overpredict the amount of corrosion. Although this approach is inconsistent from a physical viewpoint, it will be conservative.

2.2.4.3 Conclusions

The corrosion models used in WAPPA are intended to provide a conservative framework for estimating the degradation of the metallic barriers in the waste package. The modeling approach relies exclusively on user supplied empirical corrosion rates for each type of corroson process. These corrosion rates are generally supplied as a function of temperature only. The influence of other environmental parameters such as solution composition are not accounted for explicitly. Assurance that WAPPA's corrosion models are conservative requires that the input data can be shown to be conservative under any conditions expected in the repository during the containment period and the numerical solution procedure improved to calculate corrosion based on the maximum temperature during the time step.

2.2.5 WAPPA's Leach-and-Transport Model (WMODEL)

With reference to Figure 2.6, the Leach-and-Transport Model is activated when all barriers have failed through one or more degradation mechanisms and the waste form is exposed to direct attack from the fluid flooding the breached barriers.

The purpose of WMODEL is to calculate the release of radionuclides from the waste form, their transport out of the waste package, and the accumulated mass of each radionuclide delivered to the host rock. To that effect, the WMODEL relies on a leach submodel and on a transport submodel.

A description of the modeling approach is provided in Section 2.2.5.1. A discussion follows in Section 2.2.5.2 and conclusions are drawn in Section 2.2.5.3.

2.2.5.1 Review of Modeling Approach

2.2.5.1.1 Leach Submodel

The leaching submodel is a leach rate expression which includes both dissolution and diffusion from the waste form and is modified by empirical correlations to account for the effects of temperature, radiation, solution saturation, and waste form fracturing. The implemented expression is:

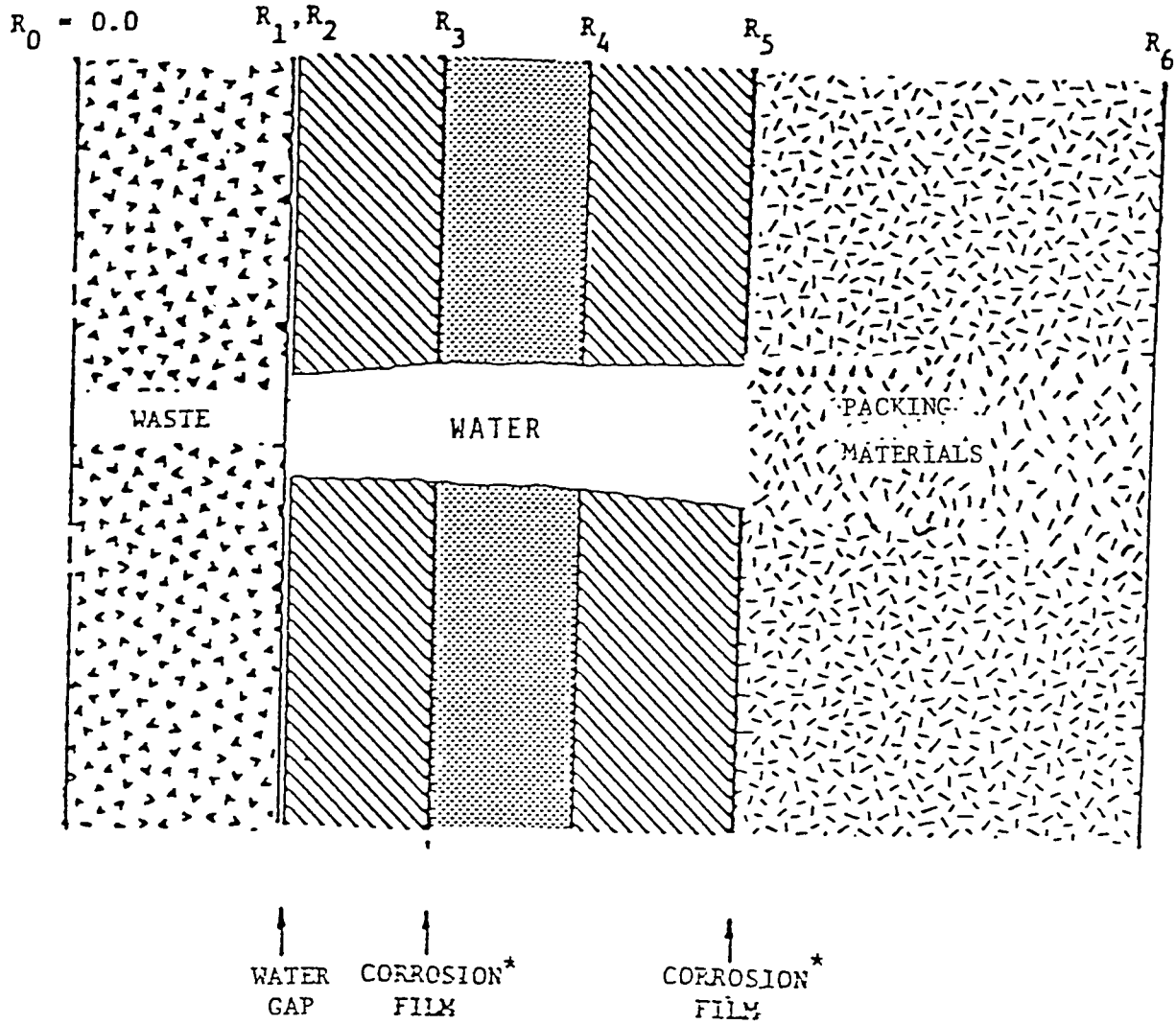

*Corrosion layer placed on the outer radius of the metal

Figure 2.6 Geometry of waste package (adapted from ONWI-452, 1982).

$$Q_L = \left(\frac{1}{2}\ k_{dif} t^{-1/2} + k_{dis}\right) \cdot A_{FW} \cdot LEF \cdot SDENSF \left(1 - \frac{C_{WM}}{C_{sat}}\right) \exp \frac{E(T-T_o)}{RTT_o} \quad (2.8)$$

where:

Q_L	= mass leach rate from waste form to solution (g/s);
k_{dif}	= leach rate coefficient for diffusion ($g/m^2\text{-}s^{1/2}$);
k_{dis}	= leach rate coefficient for dissolution ($g/m^2\text{-}s$);
A_{FW}	= total surface area of the waste form, including geometric and fractured areas (m^2);
LEF	= combined leach enhancement factor, the product of leach enhancement factors for alpha damage and γ-radiolysis as obtained in RMODEL (dimensionless);
SDENSF	= density degradation factor due to alpha damage as obtained in RMODEL (dimensionless);
C_{WM}	= concentration of the solute in the fluid at the waste form/canister boundary (g/m^3);
C_{sat}	= saturation concentration of the solute (g/m^3);
T_o	= reference temperature for k_{dif} and k_{dis} (°K)
E	= activation energy (kcal/g-mole);
R	= gas constant (kcal/g-mole-°K);
T	= temperature of the waste form (°K).

The release rate depends on which species is being modeled as the two leach rate coefficients and the saturation concentration vary for each nuclide under consideration.

2.2.5.1.2 Transport Submodel

For modeling purposes and with reference to Figure 2.6, the WMODEL subdivides the cylindrical layered medium representing the waste package into three distinct regions: the waste form plus the fluid filled region extending to the first metal barrier, the flooded barriers, and the packing materials. The model further assumes that each species under consideration behaves independently from other species. Thus, given a particular species, one is left in general with solving a system of three coupled equations in terms of the concentration of the given species in the leachant next to the waste form, in the leachant within the flooded barriers, and in the pore fluid of the packing materials. In practice, however, the WMODEL solves a system of four equations which could be shown to reduce to one nonlinear ordinary differential equation. Proceeding from the waste form radially outwards, the reference equations of the WMODEL are as follows:

(a) The first equation describes the rate at which any selected species is transferred from the waste form to the contacting aqueous solution. This is Equation (2.8). It is the same for all species and it is the classical, diffusion and network-dissolution expression for the leach rate modified by a concentration-dependent, solubility limited factor and by further leach enhancement factors due to

cracking of the waste form surface, α-damage to the waste form structure, and γ-radiolysis of the water. The dependence on temperature is handled through an Arrhenius expression. In particular, the concentration profile within the water gap between the waste form and the canister is assumed to be uniform and to be controlled by diffusion processes taking place within the flooded barriers.

(b) The second equation couples the concentration of any given species in the water gap next to the waste form to the concentration of the same species at the interface between the flooded barriers and the packing materials. The concentration profile in this region is assumed to respond instantly to concentration variations at its boundaries and corresponds to a steady-state diffusion profile. Taking into account the layered, cylindrical geometry of the system, solution of the diffusion equation yields a concentration profile which drops logarithmically across the flooded barriers.

(c) The third equation computes a time-dependent, space-averaged concentration of a given species within the packing materials. This is accomplished by treating the packing materials as a mixing cell, i.e., the entering fluid is instantaneously mixed in the volume of the packing materials, and the concentration varies as function of time only. Any directionality of the flow field is lost in this approach, and convection in and out of the packing materials is handled through a leachant renewal frequency term. Diffusion in and out of the packing materials is difficult to justify in this approach. Nevertheless, a diffusion term, which has some directional information, appears in the equation. In particular, diffusion out of the system is assumed to take place through a concentration gradient operating from the location of the log mean radius of the packing materials to their boundary with the host rock where the concentration of all species is assumed to be zero. Sorption on the packing materials is modeled through a constant retardation coefficient which slows transport out of the region.

(d) By continuity, the above space-averaged concentration of any species in the packing materials could be set equal to the concentration at the interface with the outer metal. This is not deemed, or recognized to be acceptable. Thus the fourth equation in the WMODEL relates the two concentrations through a proportionality constant defined as the ratio between the thickness from the log mean radius to the outer radius of the packing materials and the total thickness of the packing materials.

2.2.5.2 Discussion

2.2.5.2.1 Leach Submodel

Three major limitations have been found in the leach submodel. They are:

(1) The leach rate expression is not coupled with the radionuclide inventory in the waste form.

(2) The leach rate expression does not account for increasing radionuclide inventory under certain conditions.

(3) There is an inconsistency in the calculated mass released to the repository when the waste form is depleted.

Limitation(1)

The first limitation can be found through examination of the leach rate expression, Equation (2.8), which states that the rate of mass transfer from the waste form into solution is independent of the concentration in the waste form. According to this expression, the leach rate depends heavily on the diffusion and dissolution coefficients, k_{dif} and k_{dis}, which are to be determined empirically from experimental results and are specified in the code as input parameters that are constant with time. However, it can be shown theoretically (Pescatore, C., 1983) that both k_{dif} and k_{dis} are the product of the nuclide concentration in the waste form times a physical parameter that is process specific. For example, the leach rate dissolution coefficient is the product of surface concentration, C(t), times the waste form dissolution velocity, u(t):

$$k_{dis} = u \cdot C(t). \tag{2.9}$$

Since the waste form concentration is a function of time due to leaching and radioactive decay, k_{dis}, as expressed in Equation 2.9, is also a function of time even if the dissolution velocity were constant.

To make the release rate a function of waste form concentration, k_{dis} and k_{dif} would have to be expressed as explicit functions of waste form concentration. However, WAPPA does not make any attempt to calculate waste form concentration. Thus, if the WAPPA model is to be retained, k_{dis} would have to be input as a time dependent function which reflects the changes in waste form concentration. This implies that the user would need to estimate the waste form concentration as a function of time before performing the calculation. Similar remarks apply to k_{dif}.

The release rates of Cm-244 and Cm-245, as obtained from WAPPA's complex verification test case (Pescatore, C. and Sullivan, T., MF-127, 1983; Sullivan, T., MF-135, 1984) provide an example of the problems that can arise by not coupling the leach rate to the mass inventory in the waste form. Since Cm-244 and Cm-245 are isotopes of the same element, they were given identical leach rate coefficients in the test problem. Therefore both nuclides were calculated to be released from the waste form at the same rate, despite a 14-orders-of-magnitude mismatch in their initial inventories. In fact, WAPPA predicted all of the Cm-244 to be released from the waste form within the first second of leaching.

Furthermore, the nuclide concentration within the breached engineered barriers and the packing materials is a function of the nuclide release rate

from the waste form. Thus, a consequence of unreasonably high leach rates is that calculated concentrations throughout the waste package are much too large and mass is not conserved. That is, the mass of a given nuclide in the entire waste package system exceeds the total inventory of that nuclide.

For example, at 5600 years, which is the end of the first computational time step since the beginning of leaching, WAPPA calculates the average Cm-244 concentration as $5x10^{-3}g/m^3$. However, the total inventory a supplied by the data base is $6x10^{-16}g$. WAPPA does check whether the total mass released to the repository exceeds the current inventory in the waste form and it does prevent spurious mass from entering the repository. Nevertheless, it is wrong and misleading to calculate the concentration within the waste package as being so large that mass is not conserved.

Limitation (2)

The second situation in which WAPPA does not conserve mass occurs when the inventory of a given nuclide is increasing in time due to decay of other nuclides in the waste form. WAPPA calculates the release of each species until the mass released at a given time step equals the total mass found in the waste package. After this time, WAPPA assumes this species is completely and permanently removed from the waste form. WAPPA neglects to check for production of the species due to decay of other nuclides after the nuclide under study has been removed from the waste form. This approach is non-conservative and can underpredict the release of a nuclide to the repository. To clarify this point, the complex verification test case was run and the results for Th-229 (which does have an inventory that increases in time) mass release to the repository was examined (Sullivan, T., MF-135, 1984). WAPPA predicted that $2.6x10^{-3}g$ of the Th-229 was released to the repository over the first time step since the onset of leaching. At this time, this was the entire Th-229 inventory. Therefore, WAPPA stopped calculating release of Th-229 and $2.6x10^{-3}g$ remained as the total release to the repository. However, the inventory of Th-229 continued to increase reaching a value of 2.1g at the end of the calculation. Thus, there is a non-conservative discrepancy between the amount of mass in the system and the amount of mass in the repository.

Limitation (3)

The third problem occurs because WAPPA takes an inconsistent approach to mass conservation within the repository. In most cases, radioactive decay within the repository is not taken into account. The output data for Tc-99 provides an example: after 10^6 years WAPPA predicts there are 435 grams of Tc-99 in the repository. However, part of the data base required to run WAPPA is the mass inventory that would exist if the waste form had been left undisturbed. In this test problem, the mass inventory supplied from the ORIGEN2 computer code for Tc-99 at 10^6 years is only 16.8 grams. The cause of this discrepancy is that WAPPA does not account for radioactive decay once a nuclide has left the waste form. Thus, the Tc-99 which leaves the waste form when the inventory is high enters the repository and remains there. Neglecting radioactive decay provides a conservative estimate of the mass in the repository.

However, there is one exception when radioactive decay in the repository is taken into account. This occurs when the waste form concentration is depleted by leaching during a time step. In this case, WAPPA sets the amount of mass in the repository to the total available for leaching. This approach has the effect of accounting for radioactive decay in the repository and can lead to a decrease in the amount of mass in the repository. Pu-239 exhibits the results of this logic. After 10^5 years, the calculated release to the repository is 34.4 grams. At $2x10^5$ years, the end of the next computational time step, the ORIGEN2 inventory of Pu-239 is 8.6 grams and it is all released to the repository. Instead of adding the 8.6 grams to the amount in the repository and thereby neglecting decay, the mass in the repository is set to the ORIGEN2 inventory of 8.6 grams. Provided the mass inventory is decreasing, accounting for decay in this manner will still be conservative. However, it is inconsistent.

In addition to the logic flaw identified above, the expression for the leach rate itself appears to be unrealistic, or very conservative, for species which exhibit large solubility in water, e.g., the alkalis. Indeed, the model predicts for these species an initial inverse-square-root-of-time law for the release rate followed by a constant release rate at longer times, which is contrary to experience at low flow rates. This however does not constitute a serious error unless alkali leach rates are used in the future for helping predict the groundwater chemistry.

Another error in the leach submodel occurs when there are isotopes of a chemical element. In this case, saturation of the solution with respect to the element should be calculated based on all of the isotopes. This would require the saturation limiting term in the leach rate, Eqn (2.8), be changed from:

$$1 - C_{WM}/C_{sat};$$

to:

$$1 - \sum C_{WM,i}/C_{sat};$$

where the summation on i represents the addition of all isotopes. This change would also require a new concentration boundary condition as the current model assumes that saturation exists at the waste form boundary for all species.

2.2.5.2.2 Transport Submodel

Despite claims to the contrary, the WMODEL does not give "realistic" credit to partially breached barriers for retardation of radionuclide transport. Indeed, as soon as the breach occurs, the waste form is assumed to become totally wetted and to release directly into the packing materials. The only attenuation of the leach rate comes from adjusting its concentration dependent term to reflect a logarithmic concentration profile across the flooded barriers. Since this correction is very small, the barriers do not play any meaningful retarding role. Thus, under the logic of the WMODEL, a marked decrease in leach rates occurs only when solution saturation limits, with a value typical of waste form/canister interface fluid, are approached in the packing materials. This conservativeness is probably unnecessary.

The treatment of radionuclide transport in the packing materials is also unrealistic. The mixing-cell approach applies best to situations where flow is not laminar, and it breaks down when diffusion becomes the predominant transport mechanism. Since the case has often been made for the packing materials to reduce convection and to make diffusion dominant mode of transport, a space- and time-dependent equation for the concentration of any given species in the packing materials would be more adequate. This would also eliminate the problem of extrapolating a space-dependent concentration from a space-averaged one, as is presently being done. Nevertheless, the approach implemented in the WMODEL is conservative providing accurate parameters are fed into the model.

Another potential problem with the transport submodel involves retardation of solute transport in the packing materials which is handled by a constant retardation coefficient. As the groundwater percolates through the packing materials some of the nuclides become sorbed on the solid thereby slowing their transport. In dilute solutions, experiments indicate the distribution between the solid and liquid phases is constant and therefore retardation is constant. However, as the solution concentration increases this is often no longer true (RHO-BWI-LD-48, 1981) and retardation decreases. Therefore, since the solution will be near the solubility limits around the waste package, a constant retardation coefficient may not be justified everywhere in the packing materials.

Furthermore, the retardation coefficient is expressed in terms of an experimentally determined distribution coefficients K_d and before the retardation coefficient can be useful for WAPPA it must be shown that the K_d's used are relevant to the situation. In particular, current K_d measurements are obtained from single component tests. For example, the distribution of plutonium between the solid and liquid phases is measured in an experiment which has only plutonium in solution. In general, sorption is a complex phenomenon which depends strongly on solution chemistry. Therefore, single component tests may not be applicable to repository conditions which will contain all of the nuclides released from the waste form. A more detailed examination of the potential problems with using a constant K_d (and therefore constant retardation coefficient) coefficient have been enumerated (Sullivan, T., MF-150, 1984).

The numerical strategy implemented in the WMODEL appears to be too crude and error prone. In practice, the WMODEL solves a non-linear differential equation of the type:

$$\frac{dC_B}{dt} = f(t,C_B) \tag{2.10}$$

in terms of the space-averaged concentration of radionuclides in the packing materials, $C_B(t)$, during a time step (t_i, t_{i+1}), where $f(t,C_B)$ is a nonlinear function of time. The quantity $C_B(t)$ is related to the concentration at the outer surface of the metal, C_n, through a practically constant factor, b, comprised between 1 and 2 (Section 2.2.5.1.2):

$$C_n(t) = b\ C_B(t) \tag{2.11}$$

The concentration at the waste form-metal barriers interface, C_1, is related to C_B through the following relationship:

$$\begin{aligned} C_1(t) &= C_n(t) + d \cdot (k_1 t^{-1/2} + k_2)\ (1 - \frac{C_1}{C_{sat}}) \\ &= b \cdot C_B(t) + d \cdot (k_1 t^{-1/2} + k_2)\ (1 - \frac{C_1}{C_{sat}}) \end{aligned} \tag{2.12}$$

where d is nearly constant, and k_1, k_2 and C_{sat} are constants. The WMODEL solves the above problem by taking t in the RHS of Equation (2.9) and $t^{-1/2}$ in Equation (2.11) as constant over the time step, which is obviously a poor approximation if the time step is large. Thus, even if, with adequate data, the logic of the WMODEL would insure conservatism, one can not guarantee it until a numerical error analysis is made.

2.2.5.3 Conclusions

WAPPA's Leach-and-Transport Model is inadequate in that it does not conserve mass, does not couple the leach rate of a nuclide to the concentration within the waste form, does not even calculate the waste form concentration, and at times is inconsistent with its own assumptions. To properly repair the WAPPA model would require expansion of the current scheme of calculating four primary variables: leach rate, and concentrations in the packing materials, at the edge of the packing materials, and in solution at the surface of the waste form; to include a fifth variable: concentration within the waste form. Also, a global mass balance should be performed to insure that mass is conserved and that the total mass in the waste package/repository system is equal to the mass inventory supplied as input. To accomplish this would require that a substantial part of WAPPA's leach-and-transport model be rewritten.

As currently implemented in WAPPA, the Leach-and-Transport model will provide a conservative estimate of the release of any species from the waste package through the engineered barriers to the repository only if the mass inventory of a given species decreases with time and the accuracy or conservativeness of the input parameters and numerical solution can be assured. This cannot be done easily.

2.2.6 Conclusions

A common aspect to all of WAPPA's process models is that they involve an empirical approach to modeling the physico-chemical behavior of the waste package under expected repository conditions. A list of specific limitations of the modeling work in general and of the individual process models in particular is presented in Table 2.1.

Table 2.1 Significant limitations of WAPPA's modeling.

Model		Limitations
General	1)	Most models are empirical and extremely data intensive.
	2)	No explicit groundwater chemistry model.
	3)	Groundwater flow treated as a boundary condition.
	4)	No internal time step selection and error control.
Radiation	1)	Data requested for radiation damage models may be unavailable.
	2)	Radiolysis effects are independent of temperature, groundwater chemistry, and nuclide under consideration.
Thermal	1)	Temperature at the waste package/repository boundary is required as input.
Mechanical	1)	Materials strength is independent of temperature.
	2)	Expansion of corrosion products is neglected.
	3)	Failure of the waste package ends is neglected.
	4)	Data for empirical formulae may not be available.
Corrosion	1)	All corrosion processes depend only on temperature.
	2)	Data for pitting, crevice, and/or crack size and density may not be available.
Leach-and-Transport	1)	No global mass balance.
	2)	Leach rate independent of mass in the waste form.
	3)	Leach rate does not consider radionuclide inventory increasing due to decay of other nuclides.
	4)	Inconsistent approach in calculating mass released to the repository.
	5)	Leaching and transport retardation are independent of solution chemistry.
	6)	Data may be unavailable or difficult to obtain.

The main shortcoming of this modeling approach is that the process models are not self-standing, i.e., they imply a large number of assumptions and rely heavily on user-supplied inputs. For practical applications and acceptability of the results, it will behoove any potential user of WAPPA to make sure that all assumptions that went into the modeling are indeed warranted and that the data used are indeed relevant for each problem. Both tasks are significant as they may require comparison with more detailed analyses and initial information that is difficult to obtain from or may not even exist in the literature. In particular, because of the recognized lack of pertinent data in the literature and the uncertainty associated with some of the data, it is unlikely that any two users will create the same data base.

An additional complication of the implemented modeling approach is that it requires a priori knowledge of the coupling between repository and waste package performance as temperature, pressure, and groundwater flow rate at the waste package-host rock interface as a function of time do depend on waste package feedback effects. At present it is not clear how this inconsistency can be solved.

A major omission in WAPPA's modeling approach is a groundwater chemistry model. The influence of groundwater chemistry on corrosion, leaching, and nuclide transport is assumed to be incorporated into the user supplied input. There is no provision for modeling the coupling between these processes and changes in groundwater chemistry. This places on the user the extra burden of showing that the selected data is indeed conservative under all expected groundwater compositions.

2.3 Review of WAPPA's Operation

WAPPA's modeling approach is more empirical than mechanistic, which places the task of preparing extensive data files to run the code for each problem at hand on the user.

In order to make clearer how the code operates, user's input specifications to WAPPA are reviewed in Section 2.3.1. Output specifications are briefly touched upon in Section 2.3.2. Conclusions are drawn in Section 2.3.3.

The analysis presented is based on the code manual and the complex verification test case which accompanies the code. The test case will be referred to as "the test listing".

2.3.1 Initial Specifications

2.3.1.1 Geometrical Configuration and Materials Specification

With reference to Figure 2.7 which shows the initial configuration of the waste package in WAPPA's Complex Verification Test Case, the waste package is always approximated by a cylindrical, axisymmetric set of concentric barriers. This permits a one-dimensional radial formulation with empirical corrections for end effects.

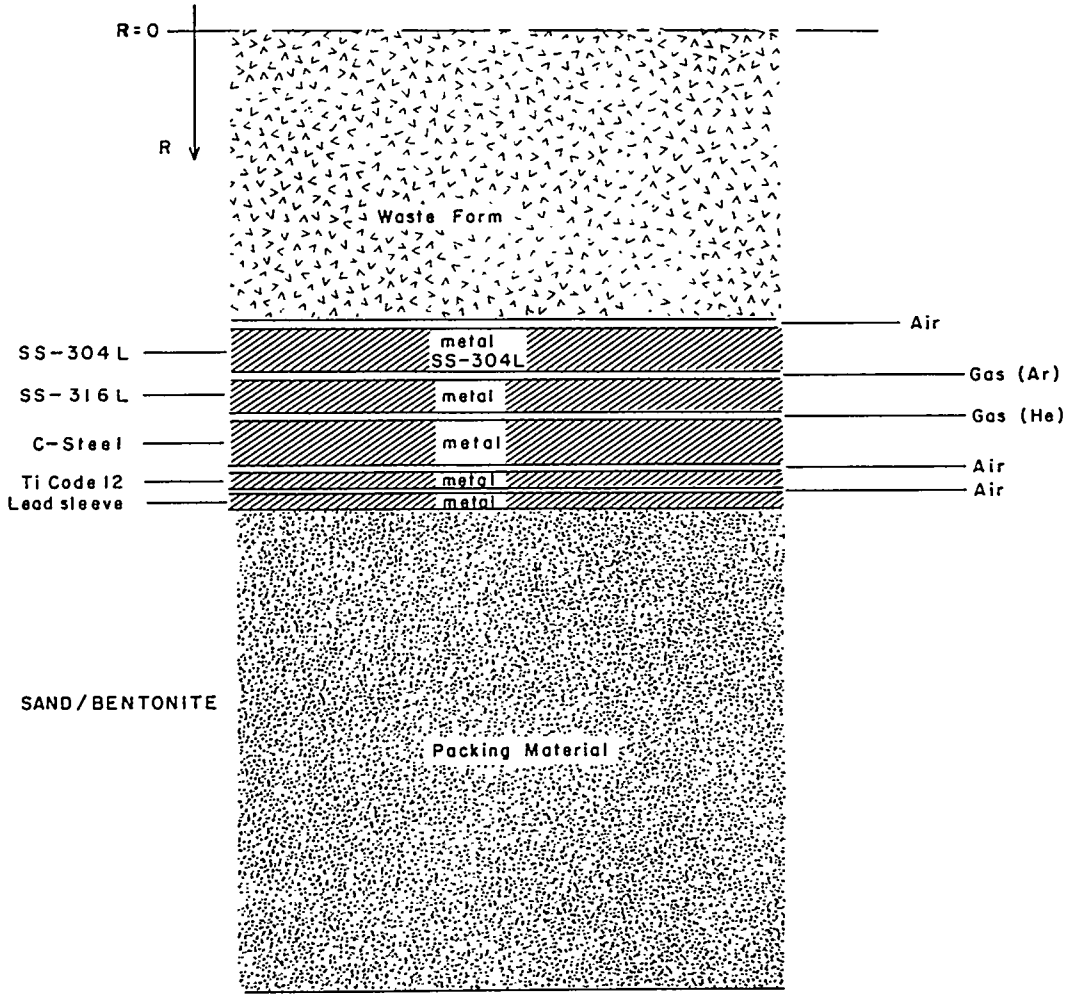

Figure 2.7 Initial configuration of the waste package in WAPPA's complex verification test case.

Proceeding from the inside of the waste package outwards, materials specifications are indicated by entering the material identifier and its outer radius. Materials identifiers are 3-digit numbers. They are used to locate the material properties in the data base for each barrier material.

Allowable barriers are waste forms, metals, corrosion films, gases and packing materials. There can be 17 barriers at most; one waste form, one packing material, and five each of the other barrier materials. The materials reported in Figure 2.1 were inferred from Chapter 2 in the code manual. As a general comment, the test listing does not provide a key to the identification of each particular material constituting the waste package barriers. For instance the listing leaves one uncertain as to whether the waste form is glass or spent fuel.

Initially there will be no corrosion layer. Thus, WAPPA automatically assigns a zero thickness corrosion layer on the outside of each metal barrier. As a minor point, however, since WAPPA accounts for dry oxidation of metals, it would seem more consistent if, when applicable, corrosion layers were placed on both sides of metal barriers.

The above information is complemented by inputting the waste package length, the volume fraction of the waste form which is waste, the density of the waste form matrix without the waste, the density of the waste, and the mass ratio of reprocessed waste-to-original fuel fed in the reactor. In particular, the listing does not mention the age of the waste. That has to be inferred by examining the power source decay rate.

2.3.1.2 Calculation Times and Error Control

In the preparation of the input to the code, the user must define the time span to be investigated along with a set of up to 400 time steps into which the analysis should be subdivided. A restart option also exists which allows restarting the program at any specified time point and continuing the analysis with a newly defined time-step vector.

In any numerical simulation of a time-dependent problem, the solution accuracy can be enhanced, while retaining efficiency, by selecting a time step that is small when changes are most rapid and increasing the time step when the rate of change decreases. In modeling waste package performance, the time when changes are going to be most rapid are initially when the heat source decreases most rapidly due to the decay of short-lived radionuclides, and, at later times, when breaching of a barrier occurs allowing the groundwater to contact the next barrier. Since the user specifies the time step through an input table containing all of the time steps, WAPPA does not determine the time step consistent with the physical processes that occur. This can lead to large, although conservative, errors in the calculated times of breaching and onset of leaching. For example, if the calculation showed the barrier adjacent to the waste form will breach between the requested computational times of 1000 and 1500 years, leaching would be assumed to begin at 1000 years.

To define the temporal location of barrier failures more precisely, the calculation must be repeated with a finer subdivision of computational times. WAPPA can facilitate this process through the restart option. Using the previous example, to determine the onset of leaching within a 50 year period, the calculation could be restarted at 1,000 years requesting a computation every 50 years between 1,000 and 1,500 years. This procedure is a cumbersome burden to the user which could have been avoided by incorporating some time step selection logic into the computer code.

Furthermore, the lack of error control during the calculation prompts the question of how accurate is the solution. The only method the user has to determine if the solution has converged is to rerun the code several times using a finer time step for each new run and comparing the results. Again, this is a burden to the user which could be resolved by proper checks within the computer code.

2.3.1.3 Nuclides Requested

The user is required to specify as input the radionuclides to be tracked during a particular computation. Each radionuclide is identified by a five digit number representing the radionuclide's atomic number and its atomic mass. Thus, 43099 is Tc-99 and 93237 is Np-237. As an added feature each nuclide is also reported in the test listing using the element symbol and its atomic mass.

2.3.1.4 Repository Boundary Conditions

In order to account for waste package interaction with the near field of the repository the user must supply WAPPA with the temperature, fluid flux, vertical stress, and radial stress at the waste package-host rock interface as function of time. The user must also specify packing materials resaturation time.

Singling out the waste package-host rock temperature, one must reason that it depends, as a function of time, both on repository properties such as rock thermal properties, area thermal load, waste package arrangement, etc. and on intrinsic waste package properties such as waste package dimensions and heat generation rates. Thus, in order to specify the problem, it would seem that one needs to have solved it before hand. The same is true for packing materials resaturation time, fluid flux, and, to a lesser extent, for the repository confining pressures.

Boundary conditions specification is one of the most limiting problems in the use of WAPPA, as the above quantities do depend on waste package feedback effects. The problem might be solved by attempting to develop simplified near- and far-field models and interface them with WAPPA.

2.3.1.5 Data Base

WAPPA's basic modeling approach is empirical in nature and therefore extemely data intensive.

Data needed in order to operate the code include radiation decay properties, radiation shielding properties, empirical data for radiation damage, thermal properties, mechanical properties, empirical data for end effects on stress analysis, empirical data for corrosion, empirical data for leaching. Some of these data need to be supplied as a function of waste package system variables like temperature, pH, etc.

The task of assembling such a large data base can be overwhelming for several reasons. First, the user must be thoroughly acquainted with the limitations and the range of applicability of the models. He should also be able to judge whether the data exist in the literature. If the data are not available, ad hoc experiments and/or extensive calculations are needed. Because of the paucity of the data and uncertainty in some of the data, it is unlikely that any two users will create the same data base. The second problem is that the range of experimental data to be inserted in the data base should cover the entire history of the waste package under expected repository conditions. The waste package environment and physical barriers can vary so extensively during the time span of a repository that it is hardly conceivable that an adequate data base where all synergistic effects are accounted for can be produced. For instance, the Corrosion Model uses empirical correlations to supply all information regarding corrosion rates for each of the various models and barriers. The coefficients used in each correlation are supplied by the code user as a function of temperature alone. One would expect corrosion to depend also on pH, Eh, salts content of the groundwater, etc. which readily increases the complexity of the problem of obtaining adequate experimental data. It is forseeable that the user of WAPPA shall not model all synergisms and will refer to single or few-component test data. In that case, the user will have to show that these data are conservative.

2.3.1.6 Radionuclide, Gamma, Alpha, and Thermal Power Source Terms

At each new time step WAPPA updates the radionuclide inventory and the thermal-power, gamma-photon, and alpha-particle densities in the waste form through use of user-provided input tables. These tables are prepared by first running an isotope inventory code like ORIGEN2.

The task of preparing the above inputs is not onerous to the user as it requests that only the age and type of waste be known. Barring numerical errors due to WAPPA's lack of internal time step and numerical errors controls, this approach is conservative, as the source term code would not account for radionuclide depletion with time from the waste form due to leaching and transport.

2.3.2 Output Specifications

WAPPA allows many options to control the amount of data to be printed. Options exist for echo prints of the input a well as the output of results generated during execution. Always provided are the total radial heat flow leaving the waste package, the cumulative γ-radiation dose, nuclide fluxes at the waste package boundary, total nuclide mass outflow through the waste package boundary, radial nuclide concentration, profiles of the waste package, barrier wetting times, and barrier failure times.

The output of the code reads well. It requires however some familiarity with the code structure and how it operates. As a general comment we would suggest that the output be improved to show 1) The name of each material being considered rather than only a numerical identifier, 2) The mode by which a barrier may have failed, and 3) Whether mass is conserved or not in the system. Additional minor points are the following: 1) the leach rate diffusion and dissolution coefficient are given wrong dimensions; 2) dimensions are missing from the oxidation rate constants A through G; and 3) on restart runs the radionuclide mass inventory, alpha flux, and gamma flux are given wrong dimensions.

2.3.3 Conclusions

The operation of WAPPA involves the preparation of extensive input and support data files. These should be prepared by qualified personnel who are thoroughly acquainted with the assumptions which went into the formulation of each process model.

The task of preparing input and support data files can be overwhelming for two main reasons. First, some of the input data require a pre-knowledge of how the waste package would perform. Second, the amount and quality of the needed data contrasts with the recognized paucity of pertinent data in the literature and their associated uncertainty. To that effect, it should be mentioned that WAPPA users will probably be limited to data which factor in only a few of the system variables on which they depend. Thus, it will be necessary for any WAPPA user to show that these data are conservative.

WAPPA's implemented numerical strategy lacks internal control of time step and of numerical errors. This may lead to unnecessary conservatism and place on the user the extra burden of redefining the time step vector and re-running the code several times in order to make sure that convergence is achieved. This feature, along with the large number of data whose uncertainty needs to be known, limits WAPPA's applicability for Monte-Carlo-type reliability analysis, which requires short computational time for each case run.

2.4 Conclusions and Recommendations

2.4.1 Conclusions

WAPPA is a modular code implementing radiation, thermal, mechanical, corrosion, and leach-and-transport modeling to determine system performance of

high level nuclear waste packages in groundwater saturated porous media. The code logic is conservative and the modeling level is kept simple, as expected in a system code.

WAPPA was not designed to be a self-standing code. It implements a mostly empirical approach requiring model justification, and extensive data gathering, interpretation and validation. These tasks constitute the major limitations of the code and will require a significant effort to resolve by personnel who are thoroughly familiar with the modeling.

In practice, WAPPA operates as a data base manager that simply selects which correlation and which data are applicable for each particular situation. Construction of the data base will be troublesome as the implemented correlations may be defined in terms of only a few variables, whereas the actual processes may depend on more system variables; the required data are likely to be unavailable in many cases or they may be difficult to adapt from the literature; or they may imply a pre-knowledge of future package performance, as is the case for temperatures, pressure, and groundwater flow rate at the waste package/host rock interface. Furthermore, as reported in Table 2.1, a few limitations have been identified in the process models.

The number of parameters which will have to be supplied and the number of different situations for which they may have to be specified will result in very large data files. After formation of these files, the user must make sure that the adopted data base is realistic or conservative for the problem under study. The code user will also have to prove that all assumptions that went into modeling are warranted. This will involve a detailed comparison of predictions from each process model with experimental results or with the predictions of state-of-the-art individual codes for each of the processes considered. In particular, since individual validation of each process model neglects the synergistic effects that may couple various processes, simultaneous validation of several models should be done whenever possible.

After validation of the data and models, the code user still must insure that the numerical solution procedure provides reliable calculations. At present, time step selection is determined from a user supplied input table which does not necessarily reflect the physical processes that occur, such as the breach of a barrier. Therefore, to insure the calculation is converged, the user must first run the code and determine the approximate times of major system changes. Then, the code must be rerun with a finer time step near the times of major system changes. This procedure must be repeated until the desired level of convergence has been achieved.

While adherence to the above procedures for code usage will be necessary for a license application, their rigor may be relaxed for work in site screening, preliminary design analysis, and in estimating acceptable ranges of parameters through sensitivity analysis. In this case, it may turn out to be profitable to use WAPPA once a few improvements have been made, e.g., mass conservation should be fixed in the leach-and-transport model, the temperature boundary condition could be given through a simplified far-field model, etc. All together these improvements may require a significant effort.

· WAPPA cannot be used in its present form for straightforward reliability analysis, e.g., Monte Carlo simulation through Latin Hypercube sampling. There would be too many parameters to be sampled and probability distributions for all of them would not be available. Sensitivity analysis may alleviate the task by reducing the number of parameters to be sampled. However, the need to rerun to code a number of times to insure convergence may still prove a stumbling block for the reliability analysis both in terms of computer time and trouble to the user.

2.4.2 Recommendations

1. The WAPPA code is receiving considerable attention from the DOE's Salt and Tuff programs (DOE/RW-0005, 1984). For this reason, the NRC should keep the code readily operable in its most recent form.

2. If the DOE decides to use WAPPA to obtain relevant licensing information, the NRC should request the code custodian to prepare an extensive data preparation manual which includes: a list of all the data required; a description of how the data is used; a description of model limitations; a list of appropriate references for obtaining the data; and a detailed example of how to construct the data base.

3. Any application of WAPPA should be complemented with an extensive justification of the data. Data should be prepared in accordance with the "Draft Technical Position on Waste Package Reliability" (NUREG/CR-0997n, 1983). That is, an estimate of the experimental errors in the data should be presented along with a description of experimental procedures and a citation to the original reference.

4. Further work by the NRC using WAPPA does not seem to be justified unless the DOE indicates it will use the code to obtain relevant licensing information. In that case, an effort should be made to improve upon the present modeling approach of specifying the waste package/repository boundary conditions as a user-supplied function of time. For example, WAPPA could be coupled with a temperature field analysis which calculates the required boundary temperature as the calculation proceeds. Also, the various process models should be improved to remove their internal limitations. In general, model validation will be of primary importance.

5. If the NRC desires to have the capability to independently check-waste package performance calculations, it will need, in addition to a general systems code like WAPPA, a suite of state-of-the-art analysis codes that model the various individual processes that are relevant. Examples of these processes include: groundwater flow, groundwater chemistry, heat transport, structural analysis, leaching, nuclide migration, and corrosion.

6. In the future, code manuals which provide a description of the mathematical and computational models should be prepared in accordance with the "Draft Technical Position on Documentation of Models" (NUREG-0856, 1981). In particular, the WAPPA manual, in many cases, did not provide adequate justification of the models, did not discuss the range of validity of the models, and did not address the problem of numerical stability and accuracy.

7. In the future, it would greatly assist the NRC if, in the code manual, the DOE provided a list or diagram of failure modes addressed by the code. Indeed, the preparation of a system code like WAPPA should be preceded by a failure mode and effects analysis (FMEA), in order to insure that all relevant failures are incorporated in the code. If available, this FMEA should at least be referred to in the code manual.

8. Although the modular structure of WAPPA would allow retrieval and re-adaptation of each process model to another code with a modular structure, this does not appear to be advantageous at present in view of the several shortcomings identified within each of WAPPA's process models.

2.5 References

AESD-TME-3131, 1982, Westinghouse Electric Corporation, Engineered Waste Package Conceptual Design in Salt, Sept. 1982.

Brookhaven National Laboratory, MF-125, Preliminary Review of the Leach-and-Transport Model in WAPPA, Pescatore, C., (December 1983).

Brookhaven National Laboratory, MF-126, Preliminary Review of the Metal Barriers Corrosion Models in WAPPA, Sullivan, T., (December 1983).

Brookhaven National Laboratory, MF-127, Review of WAPPA's Complex Corrosion Verification Test Case, Pescatore, C. and Sullivan, T., (February 1984).

Brookhaven National Laboratory, MF-132, Review of WAPPA's Thermal Model, Pescatore, C., (February 1984).

Brookhaven National Laboratory, MF-135, Mass Conservation in WAPPA's Leach-and-Transport Model, Sullivan, T., (February 1984).

Brookhaven National Laboratory, MF-141, Preliminary Review of the Radiation Model in WAPPA, Sullivan, T., (April 1984).

Brookhaven National Laboratory, MF-142, Derivation of the Attenuation Model Used in WAPPA, Sullivan, T., (April 1984).

Brookhaven National Laboratory, MF-149, Review of WAPPA's Mechanical Model, Pescatore, C., (June 1984).

Brookhaven National Laboratory, MF-150, Potential Problems with Using the Constant Kd Approach in Radionuclide Transport Calculations in the Near Field of a Nuclear Waste Repository, Sullivan, T., (June 1984).

Brookhaven National Laboratory, MF-151, Review of the Solution Strategy Used in WAPPA, Sullivan, T., (June 1984).

BNL-NUREG-33658, "An Evaluation of Chemical Conditions Caused by Gamma Irradiation of Natural Rock Salt, Panno, S. V. and Soo, P., 1983.

DOE/RW-0005, Mission Plan for the Civilian Radioactive Waste Management Program, Vol. II, Draft, 1984.

NUREG-0856, Draft Technical Position on Documentation of Models, Silling, S. A., 1981.

NUREG-0997R, Brookhaven National Laboratory, Draft Technical Position on Waste Package Reliability, Sastre, C., and Pescatore, C., 1983.

ONWI-302, Battelle Memorial Institute, Columbus, OH., Waste Package Performance Evaluation, Lester, D. H. et al., 1983. (Content of this report was effective as of December 1981).

ONWI-452, Battelle Memorial Institute, Columbus, OH., WAPPA: A Waste Package Performance Assessment Code, INTERA Environmental Consultants, Inc., 1983. (Content of this report was effective as of October 1982).

ORNL-5621, ORIGEN2- A Revised and Updated Version of the Oak Ridge Isotope Generation and Depletion Code, Croff, N.G., 1980.

Perry, R. H. and C. H. Chilton, 1973, Chemical Engineers Handbook, Fifth Edition, McGraw Hill Book Company, New York, N.Y., p. 10-6.

Pescatore, C., 1983. "Mechanistic Modeling of Nuclear Waste Form Leaching by Aqueous Solutions," PhD. Thesis, University of Illinois.

Pickering, H. W., et al., "Wedging Action of Solid Corrosion Product During Stress Corrosion of Austenitic Stainless Steels." Corrosion, Vol. 18, p. 230 (June 1962).

PNL-4452, Nuclear Waste Package Materials Testing Report: Basaltic and Tuffaceous Environments, p. 82., Bradley, D. J., Coles, D. G., Hodges, F. N., McVay, G. L., and Westermen, R. E.,, 1983.

RHO-BWI-LD-48, Rockwell Hanford Operations, Richland, WA., The Sorption Behavior of Selected Radionuclides on Columbia River Basalts, Salter, P. F., Ames, L. L., and McGarrah, J. E., 1981.

Rockwell, T., ed., 1956. Reactor Shielding Design Manual, Van Nostrand, Princeton, N. J.

Weber, W. J., Turcotte, R. P., Bunnell, L. R., Roberts, F. P., and Westsik, J. M., 1979. CONF-790420, "Radiation Effects in Vitreous and Devitrified Simulated Waste Glass," Ceramics in Nuclear Waste Management, p. 294.

Weber, W. J., Wald, J. W., and Gray, W. J., 1980. "Radiation Effects in Crystalline High-Level Nuclear Waste Solids." Proc. 3rd Symp. Scientific Basis for Nuclear Waste Management, p. 441.

3. DETERMINATION OF LOCAL CORROSION CONDITIONS FOR LOW-CARBON STEEL HIGH LEVEL WASTE CONTAINERS IN A BASALT REPOSITORY

3.1 Introduction

The objective of this program is to determine the chemical environment that will be present in high level nuclear waste packages emplaced in a basalt repository. For this purpose, low carbon steel (a current Basalt Waste Isolation Project, BWIP, reference container material), a basalt/bentonite packing material, and synthetic Grande Ronde basaltic water were reacted in an autoclave. The hydrothermal (i.e. high-temperature, liquid water) conditions used were 150°C and ≈10.4 MPa (1500 psi) pressure. The tests lasted for two-month periods and the gamma irradiation flux, when used, was $(3.8 \pm 0.5) \times 10^4$ rad/h.

The Phase I irradiation test incorporated an inert argon environment within the autoclave to check for radiolytic gas pressurization and leak tightness. Phase II testing involved a similar set of test conditions but a methane cover gas was used since this gas has been found in basaltic water samples taken from Borehole RRL-2 in the Grande Ronde formation. Methane was not used in Phase I since without verification of leak tightness for the autoclave, this gas could have escaped during testing and led to detonation in the gamma irradiation facility if electrical arcing was present in the heater system. The Phase III control test was also conducted in a methane environment, but in the absence of irradiation.

Measurements on the packing material slurry at the conclusion of the tests included pH and dissolved oxygen (DO) determinations. The Eh could have also been measured but, according to available information (NUREG/CR-3389, 1984), its observed value may not be very meaningful[1]. The concentrations of Cl^-, total Fe (measured as Fe^{2+}), and SO_4^{2-} ions in the filtrate were also measured, since these ions are associated with the corrosion of carbon steel[2]. Gases generated during the irradiation period may include H_2, O_2, N_2 and CO_2. Since several of these gases could have a deleterious effect on the waste container, gas analyses were made at the conclusion of the test period. The carbon steel sleeves were metallurgically evaluated for uniform and pitting corrosion. Hydrothermal alteration of the rock and clay constituents of the packing material was also investigated.

---

[1]There is no reason to believe that the potential of a platinum (or other noble metal) electrode immersed in a solution is a thermodynamic potential or even a reasonably reproducible potential. Most likely, such a measured potential is a mixed potential dependent on the kinetics of the various redox processes occurring in the system. In the absence of significant concentrations of oxygen and other possible redox active species, the potential may depend on the corrosion rate, however small, of the indicator electrode (NUREG/CR-3389, 1984).

[2]Basaltic groundwater contains F^- ion but this has not been associated with the corrosion of carbon steel (Hall, E., 1982). Qualitative tests for H_2S and S^{-2} were to be performed in the current study to determine if quantitative tests were needed.

3.2 Materials

Basalt from the Cohassett Flow of the Sentinel Bluffs Sequence of the Grande Ronde Formation (see Figure 3.1) and bentonite clay from Wyoming[3], saturated with simulated Grande Ronde groundwater, were used to prepare the packing material slurry. The major-element oxide compositions for the Middle Sentinel Bluffs Flow (assumed to be representative of other flows in the Sentinel Bluffs Sequence, including the reference Cohassett Flow) and the reference Wyoming bentonite (coded SWy-1 by the Clay Minerals Society) are given in Table 3.1. Analyses for S and F contents were not reported for the basalt but were reported as 0.05% S and 0.11% F for the bentonite. Some information is also available on the carbonate content of the bentonite. Upon ignition to 1000°C, the bentonite lost 6.43% of its weight [assumed to be due to the loss of adsorbed and structural water (5.1%) and CO_2] (Van Olphen, H., 1979). An infrared spectrum of the bentonite confirmed the trace carbonate content and a moderate content of iron in the lattice in the ferric state (Van Olphen, H., 1979). The availability of information, e.g., the infrared spectrum, and the characterization of the standard clay, SWy-1, was a primary reason for its use in the experiment. As a reference clay, it is reported to have a surface area of 31.82 ± 0.22 m^2/g (Van Olphen, H., 1979), as determined at 77K using the BET gas (N_2) adsorption method designed by S. Brunauer, P. H. Emmett and E. Teller (1938). However, it should be noted that surface areas determined by gas adsorption techniques on SWy-1 clay do not necessarily correspond to the the reactive surface areas in solution (Lerman, A., 1979). The surface that reacts with the solution may be smaller than the total measured. It is not expected that the use of an argon or methane overpressure will block reactive sites of the clay in solution, based on results of Stoessel and Byrne (1982). They showed that methane solubilities in water at 25°C and at pressures of methane up to ≈5 MPa were not significantly affected by the presence of clay and that there was no detectable sorption of methane onto SWy-1 clay, under these conditions. It is assumed that argon will behave similarly to methane because of its inertness. It is also assumed, without evidence to the contrary, that at higher pressures and temperatures, there is no blocking of reactive sites by argon or methane.

[3]Reference basalt and clay as specified by BWIP Rockwell-Hanford personnel. The density of the basalt rock that was crushed to pellet size was measured to be 2.8 g/cc. These basalt pieces are not uniform in size but are chips ranging in size from 0.187 to 0.250 inches in diameter.

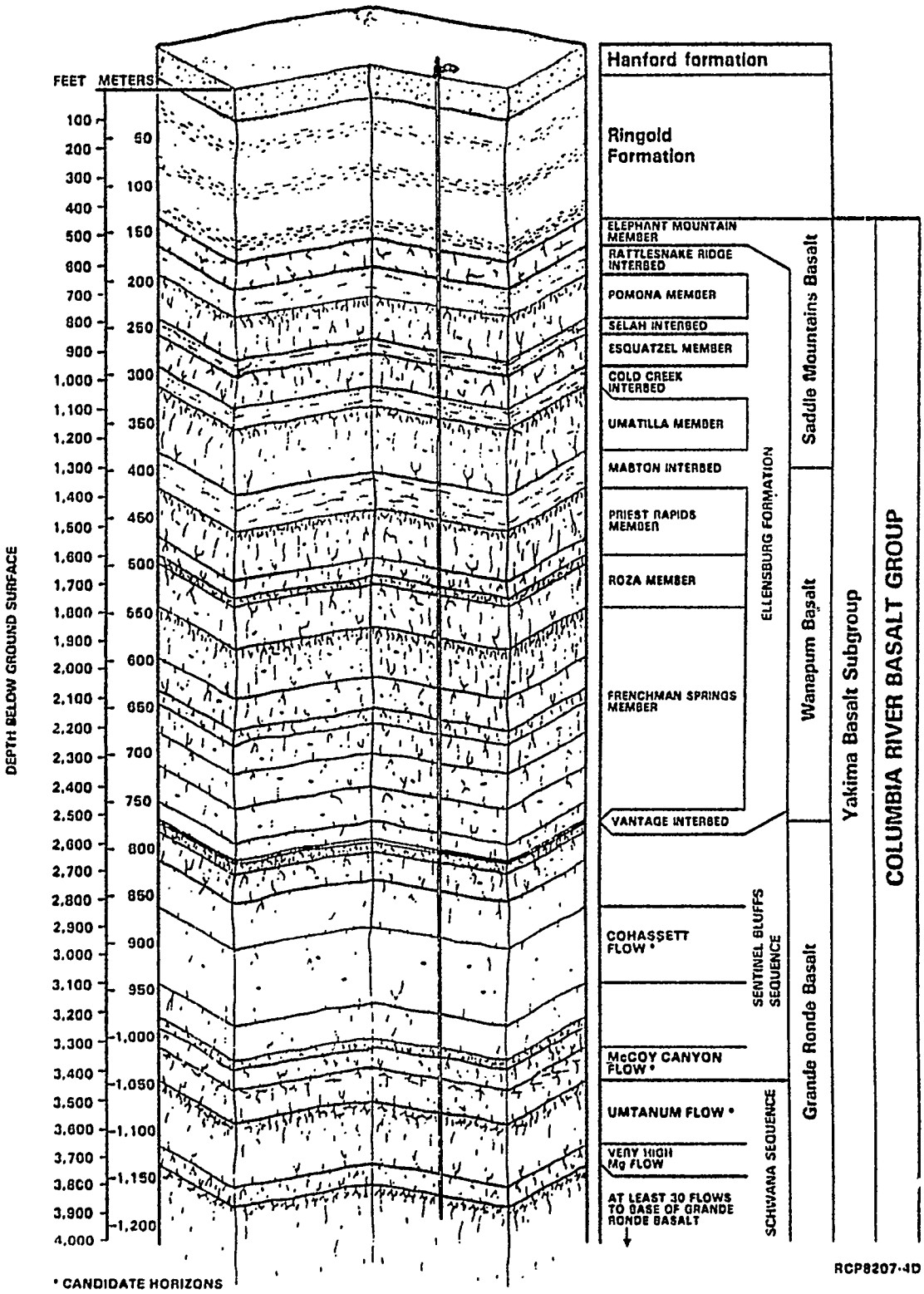

Figure 3.1. Generalized stratigraphy of the Columbia River Basalt Group, Yakima Basalt Subgroup, and intercalated and suprabasalt sediments within the Pasco Basin (RHO-BW-SA-303P, 1983). (Details of the stratigraphy are not discussed in this report.)

Table 3.1. Compositions of Middle Sentinel Bluffs Flow basalt and reference Wyoming bentonite.

Oxide Component	Basalt (Weight Percent) (DOE/RL 82-3, Vol. II, 1982)	Bentonite (Weight Percent) (Van Olphen, H, 1979)
SiO_2	53.4	62.9
TiO_2	1.79	0.09
Al_2O_3	15.0	19.6
FeO	11.7	0.32
Fe_2O_3	---	3.35
MnO	0.21	0.006
MgO	4.99	3.05
CaO	8.86	1.68
Na_2O	2.48	1.53
K_2O	1.03	0.53
P_2O_5	0.29	0.049

Mineralogically, bentonite is montmorillonite clay with some quartz present (Van Olphen, H., 1979)[4]. Steindler and others (ANL 83-19, 1983) reported the mineralogical composition of SWy-1 clay to consist of montmorillonite, quartz, calcite, and K-feldspars. No gypsum was detected.

The Grande Ronde basalt flows of the Columbia Plateau are continental flood basalts. Mineralogically, these basalts contain the principal minerals pyroxene, plagioclase, titaniferous magnetite, olivine and interstitial glass

[4]Montmorillonite is a mineral which is essentially a hydrated aluminosilicate with some substitution within the lattice. A "typical" packet of montmorillonite is formed by the bonding of a layer of alumina octahedra with two layers of silica tetrahedra. In general, Wyoming bentonite contains a mineral of the montmorillonite type as the principal component with the structural formula:

$$(Al_{1.53}\ Fe^{3+}_{0.18}\ MgO_{0.33})(Al_{0.13}\ Si_{3.87})\ O_{10}\ (OH)_2$$

(Grimshaw, R. W., 1971). (This notation indicates that Al, Fe, and Mg are present in dioctahedral coordination and that Al and Si are present in tetrahedral coordination. There are also ten divalent oxygen and two hydroxyl anions per packet, as shown by the formula.) The presence of adsorbed cations (i.e. the exchangeable cations such as Ca^{2+}, Na^{+}, Mg^{2+}, K^{+} and H^{+}) and other minerals (e.g. quartz) present in the Wyoming bentonite are not indicated by this formula.

of variable composition (DOE/RL 82-3, Vol. II, 1982). The secondary minerals are predominantly smectite clays and zeolite (clinoptilolite), with lesser amounts of SiO_2. Textures vary considerably, with typical textures dominated by a lath-shaped plagioclase and pyroxene grains locked together by an interstitial glassy matrix. Primary and secondary phases in Grande Ronde basalt are listed in Table 3.2.

Table 3.2. Petrographic characteristics of primary and secondary phases reported as present in Grande Ronde basalt (DOE/RL 82-3, Vol. II, 1982).

Characteristic Primary Phase	Abundance Volume %	Chemical Formula
Plagioclase (anorthite)	25-50	$CaAl_2Si_2O_8$
Pyroxene		
Augite	20-45	$(Ca)(Mg,Fe^{2+},Fe^{3+},Al,Ti)(Si,Al)_2O_6$
Pigeonite	0-10	$(Mg,Fe^{2+},Ca,Mn)(Mg,Fe^{2+},Mn)[Si,Al]_2O_6$
Orthopyroxene	0-trace	$(Ca,Mg,Fe^{2+})(SiO_3)$
Glassy Mesostasis	15-70	SiO_2 = 60 to 74% (by weight)
Titaniferous Magnetite	0-7	$FeO\cdot(Fe_2O_3,TiO_2)$
Apatite	0-2	$Ca_5(PO_4)_3F$, occurs as acicular crystals in the mesostasis.
Olivine	0-3	$(Mg,Fe^{2+})_2\ SiO_4$
Alteration Products (secondary phases)	1-9	Includes smectites, zeolites, SiO_2

The nominal composition of the synthetic Grande Ronde water identified as GR-3 is given in Table 3.3. Its pH at 25°C is 9.74 (RHO-RE-SR-5, 1982). In addition to the components listed, GR water has been found to contain the following gases: 25 ppm N_2, 10 ppm Ar, and up to 700 ppm CH_4 at 25°C (RHO-BW-SA-315P, 1983). The results of an analysis of the synthetic groundwater used in this experiment are also given in Table 3.3. The recipe for the synthetic groundwater is based on analyses of water samples collected from the DC-6 well in the test horizon just below the Umtanum basalt flow (990-1075 m). (The composition of GR-4 synthetic groundwater is given in Table 3 for comparison and is based on analysis of a Cohassett flow bottom sample from Borehole RRL-2 in the reference repository location. It should be noted that GR-4 water has much less sulfate content than the GR-3 water which was used in the present experiment.)

Table 3.3. Composition of synthetic Grande Ronde groundwaters.

Chemical Species	GR-3 Nominal Composition (ppm) (RHO-RE-SR-5, 1982)	GR-3 Experimental Composition (ppm)	GR-4 Nominal Composition (ppm) (SD-BWI-TP-022, 1984)
Na^+	358	363	334
Cl^-	312	312	405
SO_4^{2}	173	165	40
Si as SiO_2*	76.2	79.3	96.4
Inorganic C as HCO_3^-	54.6	---	92.0
F^-	33.4	29.9	19.9
K^+	3.43	3.63	13.8
Ca^{2+}	2.78	2.10	2.20
Mg^{2+}	0.032	0.030	---

*Total dissolved silica content is not partitioned in its speciated forms, $H_3SiO_4^-$ and H_4SiO_4.

3.3 Autoclave System Design

The hydrothermal conditions in the current tests were achieved by use of a stainless steel autoclave, which was pressurized with Ar and/or CH_4 to approximately 6.9 MPa (1000 psi) at room temperature to obtain the expected hydrostatic pressure at temperature. (The contribution to the pressure due to water vapor at 150°C is 0.52 MPa, 75 psi.) Figure 3.2 shows the exterior of the autoclave. The placement of internal components is shown in Figures 3.3 and 3.4. The autoclave weighs approximately 20.4 kg and is approximately 15.9 cm in depth and has an internal diameter of 6.3 cm. A rod-shaped resistance heater was placed vertically near the wall of the autoclave to ensure the development of a thermal gradient across the packing material. A low carbon 1020 steel sleeve was placed over the heater to simulate actual waste container/packing material conditions. It has a welded-on cap and is 25.5 mm in diameter, 143 mm in length and 2 mm in thickness. The sleeve was heated to 150°C and a temperature differential was established across the 38-mm thickness of the packing material. The temperatures at the heater (T_2) and at the wall (T_1) were monitored by thermocouples sheathed with Type 316 stainless steel. These were 3 mm in diameter and were inserted to a depth of approximately 75 mm and bent to contact the heater sleeve and inner autoclave wall. It is assumed that the thermocouples maintain contact during test. During the tests, packing material was extruded into the space between the heater and the inner surface of the steel sleeve. This would act as an insulating medium which, together with the excellent thermal conductivity of the sleeve, would greatly minimize

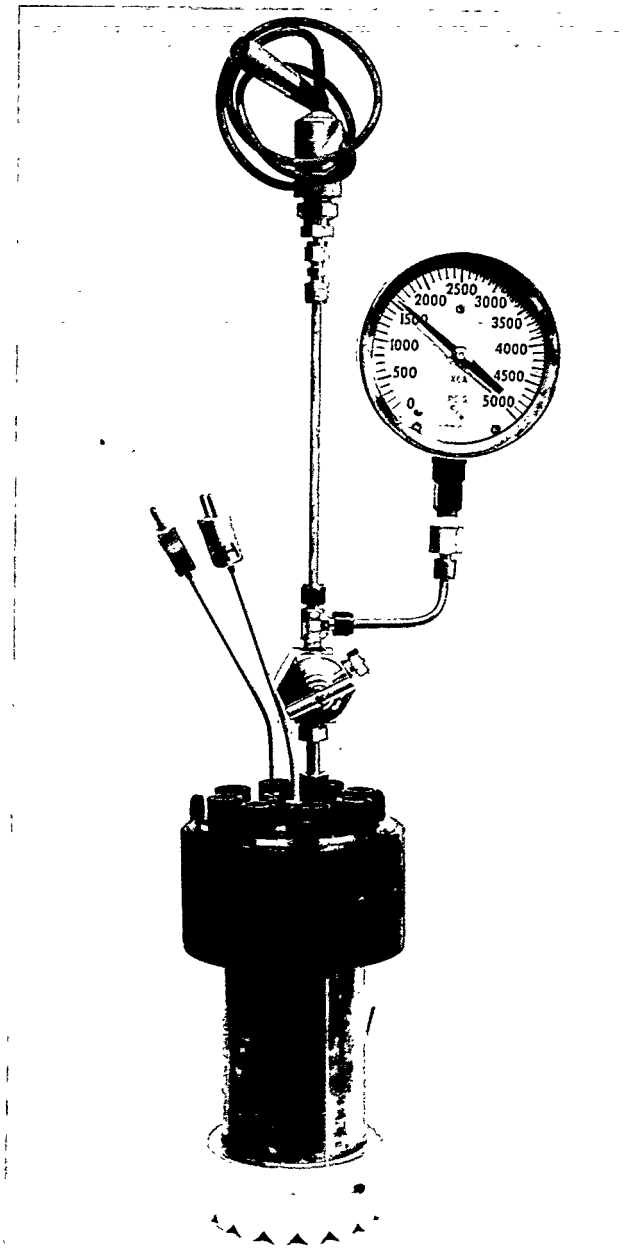

Figure 3.2. Autoclave system being leak checked. (Pressure gauge was removed prior to placement in gamma pool.) Magnification is 0.2X.

local hot spots on the latter. In the Phase I test an attempt was made to obtain water samples for analysis by incorporating two Type 304 stainless steel sampling tubes in the packing material. These were 7 mm in diameter and 150 mm in length, and each contained 23 small drilled holes to allow water ingress while retarding passage of the slurry. Since the tubes displace a volume of only 20 mL compared to a slurry volume of 440 mL, no significant changes in thermal conductivity or temperatures in the packing were expected. Sampling tubes were not used in the Phase II and III tests since the volumes of water collected by their use were minimal.

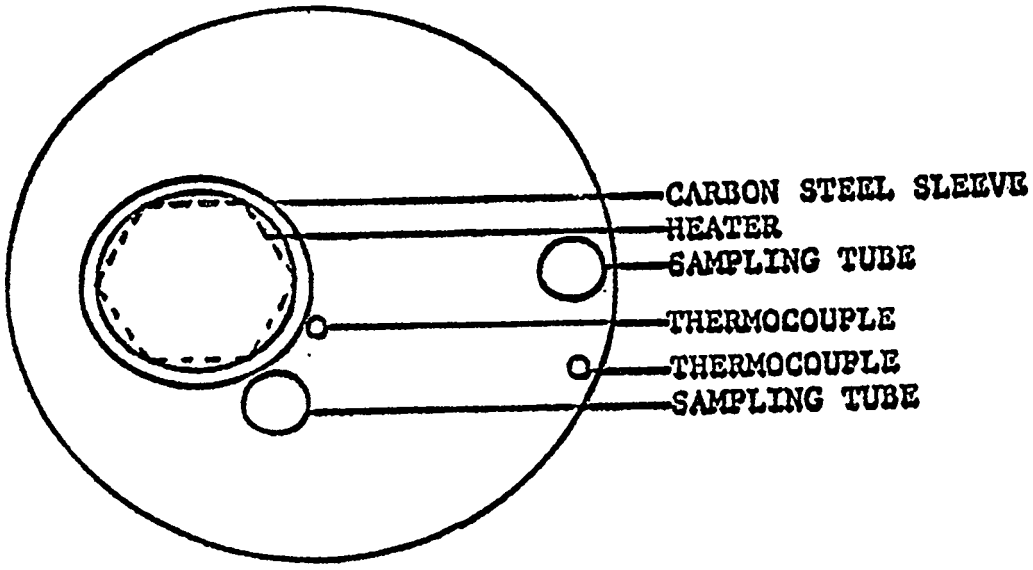

Figure 3.3. Cross section through autoclave (drawn to scale).

3.4 Experimental Procedures

3.4.1 Slurry Preparation

The bentonite was used in the as-received condition (-400 mesh, with a density of 0.78 g/cc). The basalt was crushed to pellets ranging in size from 0.187 to 0.250 inch in diameter. An excess amount of slurry was first prepared by mixing 33.5 g of bentonite with 478 mL of freshly-made synthetic groundwater which was prepared using details given in the literature (RHO-RE-SR-5, 1982). The ratio of 7:100 (by weight) of bentonite to water was selected on the basis of BWIP work which showed this composition to be optimal for restricting water flow in basalt repositories (RHO-BWI-C-66, 1980). To minimize the presence of air and voids, the slurry was prepared so that water replaced the air present in the packing material. This mixture was allowed to gel overnight in the presence of air. Pellets of basalt including fines (209 g occupying a volume of ≈129 mL) were then added to the bentonite slurry. This packing material was also allowed to equilibrate overnight in the presence of air. This procedure yielded a 3:1 (by volume) mixture of basalt:bentonite and a solution:solid

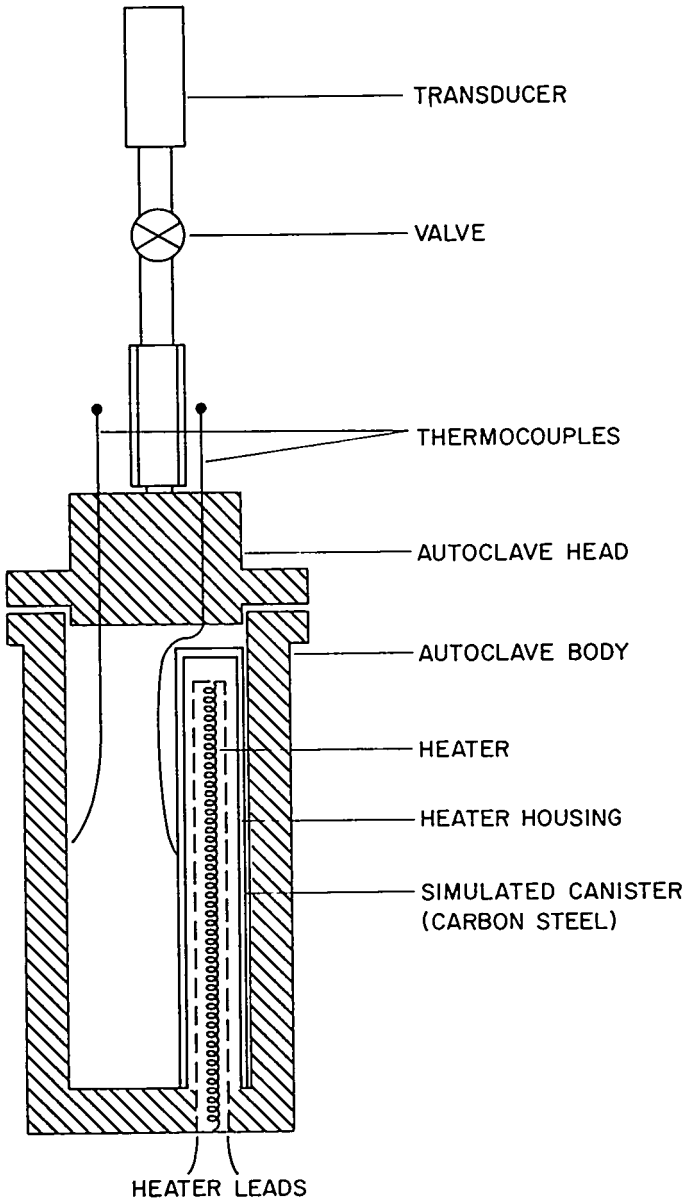

Figure 3.4. Lengthwise section through autoclave. Magnification is 0.35X.

ratio (by weight) of about 2. Most of the packing material slurry was placed in the autoclave, giving a void space below the autoclave head of approximately 20 mL. (The use of the sampling tubes gave a total void of ≈30 mL.)

3.4.2 Autoclave Pressurization

In the Phase I test, the slurry was placed in the autoclave leaving a void space of ≈30 mL. The autoclave was flushed with argon and pressurized to 6.9 MPa (1000 psi) with argon at 24°C. After lowering the autoclave and monitoring/control attachments into the gamma pool, the temperature was slowly raised to 150 ± 2°C over a period of 24 hours. A mean temperature differential of ≈37°C across the packing material test section was achieved and maintained. The temperature at the autoclave wall and pressure transducer readings were recorded hourly by use of an automatic data logger. The transducer readings in volts had previously been calibrated to pressure.

In the Phase II test, slurry was placed in the autoclave, with a void space of ≈20 mL remaining. (The sampling tubes were not used in the Phase II and Phase III tests.) Because of the ≈50 mL drop in slurry level discovered at the conclusion of the Phase I test, (due to extrusion of the packing into the heater-sleeve cavity - see Section 3.3, above) a different pressurization technique was followed in Phase II. The autoclave was pressurized to 10.4 MPa (1500 psi) at room temperature with argon and maintained overnight. The autoclave was opened and there was again found to be a noticeable drop in the slurry level. Additional slurry was added to keep an estimated void space of ≈20 mL. The autoclave was again pressurized to 10.4 MPa with argon at room temperature to check for leakage. The argon was then bled off and methane (99.93% pure, ethane 0.07%) was added to attain a pressure of 6.2 MPa (900 psi) at 18°C. After lowering the autoclave and monitoring/control attachments into the gamma pool,[5] the temperature at the sleeve was slowly raised to 150 ± 4°C over a period of 52 hours. The pressure attained at 150°C, 13.1 MPa (1900 psi), was 3.4 MPa higher than anticipated based on the pressure at 18°C. The fact that the pressure at 150°C in the Phase II experiment exceeded the predicted value may be due to the generation of a radiolytically-produced gas. In general, the pressure that developed in each of the three experiments (Phases I, II, and III) was inversely proportional to the thermal gradient that was established in the experiment. In the Phase II test, a temperature differential across the packing of approximately 22°C ± 4°C was achieved at the end of that time and was maintained throughout the experiment. After 157 hours of irradiation, a malfunction developed in the heater regulator, causing the temperature to drop to 108°C at the heater (T_2) by morning. After the regulator was replaced, the temperature was increased to normal over a period of 11 hours. The pressure reading of 11.9 MPa at 176 hours was ≈1.0 MPa lower than the pressure reading at 157 hours. It is not known whether this reduction in pressure would have occurred if the regulator had not failed; nor is the cause of the reduction clear.

[5] A methane monitor was emplaced over the tube containing the autoclave in the gamma pool. Continuous purging over the entry of the tube with argon was carried out.

In the Phase III test, a procedure similar to that described for the Phase II test was used to check for leakage. The argon was again bled off and methane added to attain a pressure of 7.4 Mpa (1074 psi) at 18.4°C. It was predicted that the system would approach a pressure of ≈10.4 MPa, with the addition of the water vapor pressure contribution. The actual pressure attained was ≈10.6 MPa. An air blower and/or cooling coils were used in this non-irradiation test in an attempt to obtain a thermal gradient in the packing similar to those obtained for the Phase I and Phase II tests which were placed in the gamma pool. Their use across the body of the autoclave increased the thermal gradient. However, an air stream across the top of the autoclave was used because its use decreased the thermal gradient. Because of the blower tests, there was some fluctuation in autoclave pressure during the first 195 hours of testing.

The initial pressurization value was kept the same for all three phases of the experiment. The fact that the pressure in the Phase II experiment exceeded that predicted may be due to the generation of a radiolytically-produced gas. Differences in pressure developing in the autoclave seem to also be inversely proportional to the size of the thermal differential across the packing material. The effect of this pressure difference between the Phase II and Phase III tests on the results is not known.

3.4.3 Irradiation Procedure

The ambient air temperature in the gamma pool test hole was 22°C. A dosimetry measurement, which was performed on the empty autoclave, indicated that a dose rate of $(3.8 \pm 0.5) \times 10^4$ rad/h was delivered to the interior of the vessel by the ^{60}Co source. This is close to a value of 2.9×10^4 mR/h estimated for a pressurized-water-reactor spent fuel container surface (AESD-TME-3142, 1982). The dose rate was measured by use of radiochromic film which is calibrated to a National Bureau of Standards (NBS) standard by comparing optical densities. No measurement of distribution of the gamma energies from the ^{60}Co source is available. In the Phase I test, the autoclave was irradiated for 1486 h, to a dose of $(5.6 \pm 0.7) \times 10^7$ rad. In the Phase II test, the autoclave was irradiated for 1727 h, to a dose of $(6.6 \pm 0.9) \times 10^7$ rad. The Phase III test did not incorporate any irradiation.

3.4.4 Post-Test Procedures

Procedures for analyses on the gas, the packing material, water and carbon steel sleeve were initiated after the autoclave had been cooled to room temperature (at a rate of approximately 5°C/min). As many as six gas samples were taken, and analyses carried out by a mass spectrometric technique. Gas remaining in the autoclave was vented to the air and the autoclave was opened in a glove bag filled with argon. Measurements of pH and DO were made at several depths in the slurry both near the heater and near the autoclave wall. The pH electrode had previously been calibrated with buffers having standardized pH values of 2, 7, and 10. Readings are accurate to ±0.05 units. The DO electrode had been calibrated against the DO content of water at 25°C, which is 8.4 ppm. Dissolved oxygen (DO) readings have an estimated accuracy of ±0.5 ppm.

The appearance of the material in the autoclave was changed after reaction in all three tests. There were portions of the slurry which were white and/or

orange in comparison to the unreacted slurry color (beige). No caking or odor were detected. Some orange coloration was also evident on the slurry adhering to the steel sleeve.

Two-core samples (each ≈5 mL) were taken from both the heater and autoclave wall regions (these are designated by the letters H and W, respectively, in subsequent discussions). Test tubes containing the slurry were centrifuged for one hour and the liquid portion was removed. Approximately 3 mL of solution were collected from the sample taken from the region near the autoclave wall and approximately 2 mL from the sample taken from the heater region. The liquid was cloudy and was passed through a membrane filter having a pore size of 0.025 μm. The filtrates were analyzed for Fe, Si, Cl^-, and SO_4^{2-} content[6]. After the cores were removed, an additional sample (i.e. samples designated R) was obtained by combining portions of the slurry that were randomly selected. The test tube containing this "combination" sample was also centrifuged, but the supernate was analyzed in the unfiltered form.

Basalt pellets were removed from the corings near the heater and the autoclave wall and prepared as thin-section specimens for microscopic analysis. Unreacted basalt thin sections were also made for comparison. Pulverized basalt and glass slides coated with reacted centrifuged slurry were also prepared for mineralogical studies using a Philips XRG 3100 X-ray diffractometer. Colloidal matter obtained from R samples, by filtration through a 0.025-micron membrane filter, was analyzed by SEM-EDX procedures.

The slurry was removed from the carbon steel sleeve by washing in water. The slurry adhering to the sleeve was isolated for SEM-EDX studies. The carbon steel sleeve was placed in a desiccator and kept for metallographic analysis.

3.5 Results and Discussion

3.5.1 Pressure Measurements

After the test temperature was attained, the pressure within the autoclave was recorded. The following ranges of pressure were found for the three tests over the two-month test periods:

9.3-9.7 MPa (1357-1404 psi) -- Phase I
11.1-13.2 MPa (1612-1919 psi) -- Phase II, and
9.8-11.7 MPa (1416-1702 psi) -- Phase III.

[6]The Fe content was determined by atomic absorption (AA). The Si content was determined by an automated standard colorimetric method using ammonium molybdate reagent. The Cl^- and SO_4^{2-} contents were measured by ion chromatography (IC). This analytical technique gives quantification of ionic species in the sub ppb to ppm range and allows for the analysis of small volumes (≈1 mL) of sample. Precision is normally ±5%, but due to the large amount present in our samples, it was approximately ±2%.

Note that the initial large pressure fluctuations in the Phase III test caused by attempts to achieve a specific thermal gradient in the packing are not included.

A plot of P/T_1 values versus time should be an indicator of change in the number of moles of gas present in the system and/or the volume that the gas occupies, since $P/T_1 = nR/V$, where R is the gas constant. It is assumed that T_1, the temperature at the autoclave wall, is representative of the average temperature experienced by the gases contained in the autoclave. Figure 3.5 gives P/T_1 values for the three tests conducted. Fluctuations in the P/T_1 values from the mean are less than ±1 percent and may be due to instrumentation characteristics or small fluctuations in volume. There is a basic trend in the pressure changes during each test involving an initial decrease in pressure over the first 500 h followed by an increase for the remainder of each test. For the Phase I test, this trend is more clearly detected by a magnified P/T_1 scale. Although the pressure at the end of each test never exceeded the initial pressure, it is possible that very long term reaction could lead to monotonic pressure increases.

Reasons for the initial decrease in pressure include consumption of gases such as oxygen and an increase in the void space in the autoclave during a test. Pressure decreases in the Phase I, II and III tests are 0.14, 0.83, and 0.48 MPa (20, 120 and 70 psi), respectively. This would represent a decrease in gaseous oxygen (sorbed or dissolved oxygen will not cause a pressure decrease after reaction) of 100-200 mg. This explanation is not likely since this relatively large amount of free oxygen (i.e. not sorbed or dissolved) would not be present in the test system. A more plausible explanation of the initial pressure decrease is a change in the volume above the packing material. Volumetric increases of only 1%, 7%, and 4% would be needed to account for the observed pressure decrease in the Phase I, II and III tests, respectively. This could be caused by shrinkage of the bentonite during hydrothermal interaction. The increases in pressure observed in the later stages of a test are likely to be partly associated with radiolytic gas generation and/or hydrogen generation by basalt/water interaction (see below).

3.5.2 Pressure Changes Due to Radiolysis

Any radiolytic effects which result in the production or consumption of gas and associated pressure changes are assumed to occur on (1) the slurry water in the Phase I and II tests, (2) methane as dissolved gas in the water in the Phase II test and (3) methane in the void space in the Phase II test. No radiation-induced structural damage to the bentonite silicate lattice is expected (Krumhansl, J. L., 1982).

3.5.2.1 Radiolysis of Water in a Closed System

Since we are concerned with the radiolytic products of water in a closed system (constant volume) in the Phase I and II tests, pressure buildup studies at Savannah River Laboratory (SRL) on the irradiation of concrete waste forms in sealed containers have yielded specific conclusions (DP-1464, 1978), which may enable an interpretation of our data to be made on the basis of radiolytic

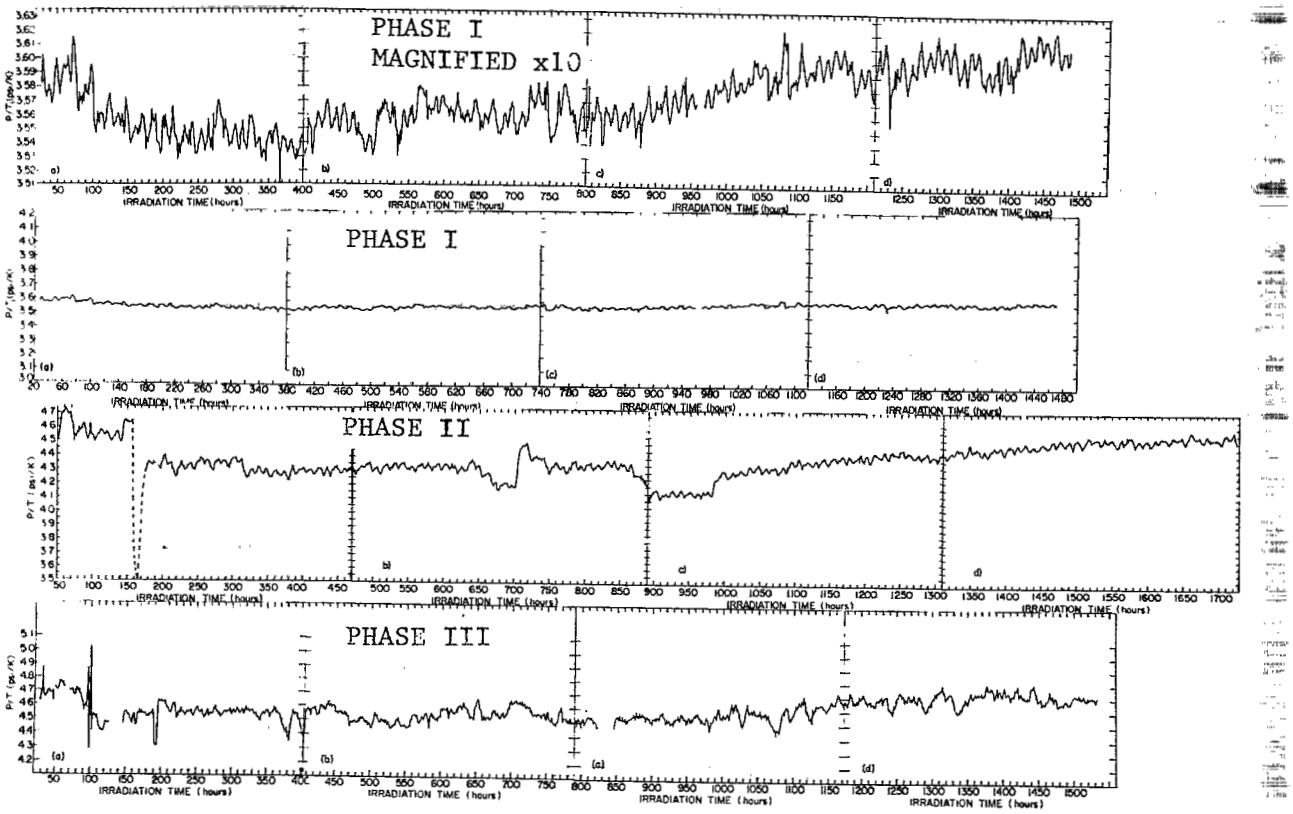

Figure 3.5. Pressure changes with time and temperature in the autoclave system for the three phases of the experiment: Phase I (absence of methane and presence of radiation), Phase II (presence of methane and radiation), Phase III (presence of methane and absence of radiation.)

effects on the amount of gas present in the system. In the SRL tests, 500-mL glass bottles containing set cement (with voids in different samples ranging from 125 to 223 mL depending on the amount of cement and water that was added to the bottle) were irradiated at 40-50°C. Both high and low dose rate tests established that the initial production rate of H_2 from the radiolysis of water was dependent upon the dose rate; but as the H_2 pressure increased, a reaction removing H_2 was initiated and the pressure reached a steady state. This equilibrium pressure was also directly dependent upon the dose rate. The gas volume and the water-to-cement ratio did not affect the pressure attained. Gas composition at the end of the test showed that O_2 content from the air sealed within the concrete was 95% consumed and N_2 content was unchanged. In water containing oxygen, the oxidizing power of the dissolved oxygen is made available by reactions of $e^-(aq)$ and $H\cdot$ to give O_2^-, which is a powerful oxidizing species. Presumably the consumed oxygen was incorporated in oxidation products. This depletion of oxygen resulted in a 0.014 MPa (≈2 psi) decrease in pressure over a period of 100 days at a constant dose rate (DP-MS-16-51, 1976). See Figure 3.6 for data on dose rate versus the steady state H_2 pressure.

It is also known that if the radiolysis occurs at a higher temperature, the increase in temperature will lead to an increase in the primary species [i.e. the hydrated electron $e^-(aq)$, the hydrogen atom and the hydroxyl radical OH] and a decrease in the number of molecules (H_2 or H_2O_2) (Draganic, I. G., 1971). It has also been determined that there is no effect of pressure on the yields of primary reducing species, hydrogen atoms, and H_2 (Draganic, I. G., 1971). Thus, we assume that the dose rate is the determinant of the final H_2 pressure from the radiolysis of water. If we chose the largest pressure at the radiation dose of $(3.8 \pm 0.5) \times 10^4$ rad/h, which is what the packing slurry receives in this experiment, this value is less than 0.17 MPa (25 psi) (assuming linear extrapolation) under ambient conditions. For a temperature of 150°C, this would correspond to a pressure of less than 0.24 MPa (35 psi). From the use of the baseline data indicated in Figure 3.5, it is clear that any increase in pressure due to H_2 production on the order of 0.24 MPa, and any decrease in pressure due to O_2 consumption, will fall within the baseline scatter and will not be observable.

3.5.2.2 Radiolysis of Methane in Aqueous Solution and in the Gaseous Phase

Gas production and consumption are also affected by the presence of methane in the Phase II test. Methane is the predominant gaseous constituent in the Saddle Mountains and Wanapum basaltic groundwaters, comprising 60 to 98 percent of the total dissolved gas. Methane comprises from <0.01 to 1.6 percent of the total dissolved gas in the groundwater of the Grande Ronde in Boreholes DB-6 and DC-14, but comprises 98 percent of the total dissolved gas in the Grande Ronde groundwater in Borehole RRL-2 (on the order of 10^2 to 10^3 ppm) (NUREG-0960, Vol. 2, 1983).

Methane (99.93%) was used to attain a pressure of 7.4 MPa (1074 psi) at 18.4°C in the Phase II test. The solubility of methane in water at 25°C at 1 atm of methane over-pressure is approximately 21 ppm (Dean, J. A., 1979). The Henry's Law coefficient for methane at this temperature is $\approx 4 \times 10^4$ atm/mole fraction (Himmelblau, D. M., 1960). A calculation using this coefficient gives

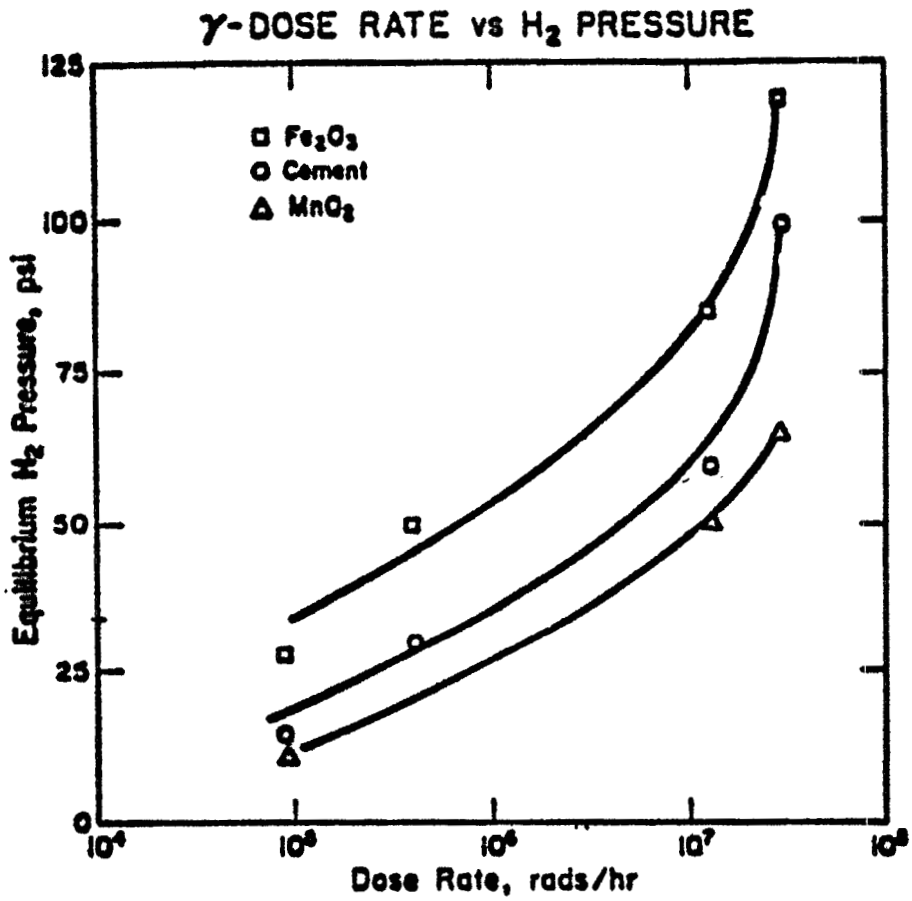

Figure 3.6. Effect of dose rate on H_2 equilibrium pressures for concrete (neat), concrete containing Fe_2O_3, and concrete containing MnO_2 (DP-MS-76-51, 1976).

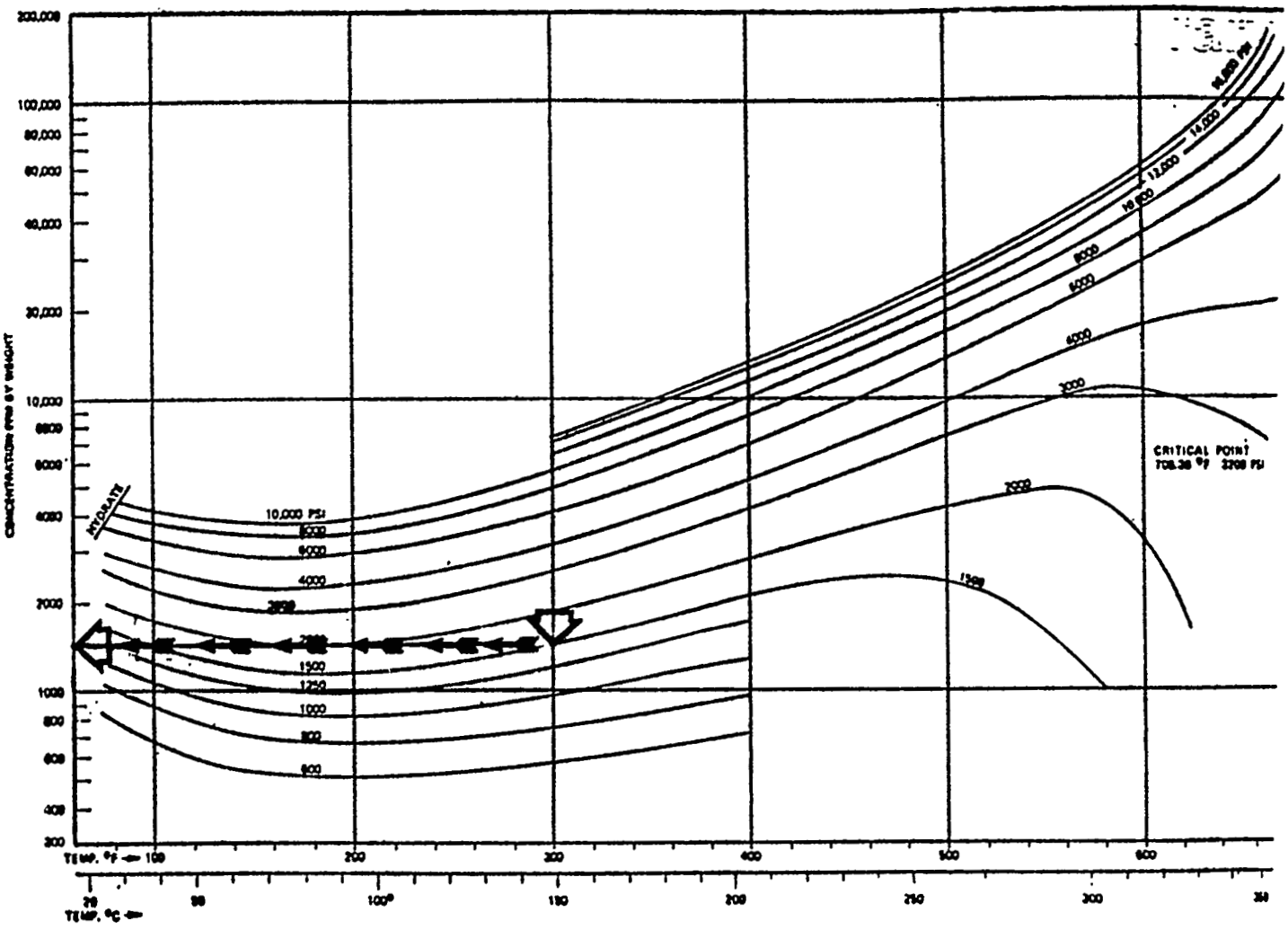

Figure 3.7. Solubility of methane in water at high temperatures and pressures (Bonham, L. C., 1978).

a concentration of ≈1600 ppm of methane in water at 7.4 MPa pressure. Solubilities at high temperature and high pressure conditions are graphically represented in Figure 3.7. At 150°C and 10.4 MPa (1500 psi) (see arrows in Figure 3.7), the solubility is approximately 1500 ppm.

Results of a study on the gamma radiolysis of aqueous methane solutions (Stevens, G. C., 1972) have indicated that only the OH free radical (from the water radiolysis) reacts with methane to any appreciable extent. Methyl radical is the product of this reaction. Methyl radical then reacts with the radiolysis products of water to yield methane, hydroxyl ion and methanol. It also reacts with another methyl radical to produce ethane. Ethane reacts with the various radicals present in the system to produce ethyl radical, methane and hydrogen. This process could continue as higher alkanes are formed which themselves interact with radicals present in the system to produce hydrogen, ethylene, propane, n-butane, i-butane, n-pentane, i-pentane, neopentane, acetylene, propylene, 1-butene and polymeric type molecules (Arai, H., 1981).

In the BNL tests, gas samples were taken from the autoclave after cooling to room temperature. Up to five separate samples were taken from each of the tests for analysis. However, some samples were discarded because of insufficient gas or because of contamination from the packing material. Detailed data are given in Table 3.4.

The largest $G(H_2)$ value from the radiolysis of methane in the gas phase and subsequent reactions is 13.26 where G is defined as the number of molecules of gas produced per 100 eV of absorbed radiation (Arai, H., 1981). No $G(H_2)$ value for the aqueous methane solution was reported in the Stevens (1972) study. Although this $G(H_2)$ value is much larger than that obtained for water (0.45), it should be noted that the methane content (≈0.1 mol) in our system is approximately 250 times less than the content of water. Thus, we could estimate that more hydrogen would be produced from the radiolysis of water than the radiolysis of methane. However, as shown in Table 3.4, more hydrogen was produced in the Phase II test than in the Phase I test.

A valid estimation of the amount of hydrogen produced by the radiolysis of methane is not possible due to the combination of major experimental factors that will affect gas production rates, viz. temperature, pressure, and increased surface area of adsorbent. The presence of other gases initially present in the system and those possibly generated by chemical reactions will also affect the dominant mechanisms in the radiolysis of methane. However, some specific effects from other studies which varied single parameters are summarized as follows:

- The G values for all products are affected by an increase in temperature (Arai, H., 1981). The G values for the formation of n-butane and acetylene decrease with increasing temperature. The G values for the formation of other significant products increase with temperature.

- An increase in pressure causes a decrease in $G(H_2)$ and $G(C_2H_6)$ (Maurin, J., 1962).

Table 3.4. Comparison of composition of gases sampled after reaction as determined by mass spectrometry. (Gas composition is given as mole percent.)

Gas	Molecular Weight	Phase I[a]	Phase II[b]	Phase III[c]
H_2	2	3.71	17.6	4.21
CH_4	16	0.019	78.3[d]	91.5[d]
NH_3	17	ND[e]	ND	ND
H_2O	18	0.020	0.028	0.063
CO	28	ND	f	ND
C_2H_4	28	ND	ND	0.03
N_2	28	1.00	0.18[f]	0.28
C_2H_6	30	ND	0.43[d]	ND[d]
NO	30	ND	ND	ND
O_2	32	0.027	ND[g]	0.020[h]
H_2S	34	ND	ND	ND
Ar	39.9[i]	95.1	3.04	3.84
CO_2	44	0.12[j]	0.17[j]	0.04[j]
NO_2	46	ND	ND	ND

[a]These values represent compositions averaged from the last two of the three gas samples taken. The two argon concentration measurements were identical within experimental error; the hydrogen concentrations differed by 2.5%.

[b]These values represent compositions averaged from the fourth and fifth samples of the six gas samples taken. The methane, argon and hydrogen concentrations varied by a maximum of 0.5, 0.8 and 3.7%, respectively, from the average values.

[c]These values represent compositions averaged from a total of five gas samples taken. The methane, argon and hydrogen concentrations varied by a maximum of 0.7, 8.1 and 31.7%, respectively, from the average values.

[d]The methane was analyzed and was found to contain 0.07% ethane. On this basis, we would predict that the Phase II test and Phase III test gas analyses would show a maximum ethane content of 0.07%.

[e]ND is an abbreviation for not detected.

[f]Carbon monoxide and nitrogen concentrations are not distinguishable at these low levels.

[g]Minimum detection limit was stated to be 0.017%.

[h]Oxygen was detected in the first two samples out of a total of five samples.

[i]The argon used contains <0.001% oxygen.

[j]Dry air contains by mole percent: 78% N_2, 20.9% O_2, 0.9% Ar, 0.03% CO_2, and 0.2% other gases.

- The influence of the basalt/bentonite mixture, due to chemical composition and increased surface area available for reaction, on the production of gases, in combination with the other variables that are present, is not known. Synergistic and/or catalytic effects may be operative. Results from Norfolk (1977) on the gamma radiolysis of methane gas adsorbed on gamma-alumina suggest that methane at the temperature under consideration will react only with radiolytic intermediates derived from surface hydration and that direct energy transfer to the adsorbed methane from the alumina did not occur.

- The presence of other gases initially present in the system and those generated by chemical reactions will also affect the radiolysis of methane. A G value for the depletion of hydrocarbon, G(-hydrocarbon), in a system containing carbon dioxide, carbon monoxide, methane, water and hydrogen has been estimated to be ≈16 (Norfolk, D. J., 1983).

3.5.3 Gas Analyses Results

3.5.3.1 Phase I Test Gas Analysis Results

In the Phase I argon-overpressure test, hydrogen, carbon dioxide, and methane were produced and radiolytic and/or adsorbed oxygen was consumed. The source of the nitrogen is assumed to be air remaining after slurry preparation. Some carbon dioxide is also present in the starting slurry, but a source of carbon must be available to account for the presence of methane and additional carbon dioxide. It is known that calcite is present in the bentonite and that the groundwater contains carbonate species. There may also be some organic surface contamination of the basalt that could act as a source of carbon.

3.5.3.2 Phase II Test Gas Analysis Results

The Phase II test system was pressurized with methane. During the course of irradiation and reaction, hydrogen, ethane, and carbon dioxide are produced and oxygen was consumed overall. A small amount of carbon monoxide may have been produced. There is some residual argon in the system from leak testing and the nitrogen is assumed to be from residual air present in the system.

Work related to the Phase II test has been conducted by PNL (RHO-BW-SA-315P, 1983) on the irradiation of synthetic Grande Ronde (GR-3) basaltic groundwater saturated with methane in the absence of basalt and bentonite at 150°C for 72-hour periods at dose rates ranging from 1.1-5.3 x 10^6 rad/h. The initial methane content of the pressurizing gas used was at least 95%, and the final methane content of the vented gas ranged from 70-85%. This decrease is due to the radiolysis of methane. Hydrogen was produced and its content in the vented gas ranged from 9.9 to 24%. In the Phase II test, the methane content was decreased to ≈78% and ≈18% H_2 was formed. However, different gases and filterable material were produced in the Phase II test than were produced in the PNL work. Carbon dioxide and ethane, and perhaps carbon monoxide, were the only carbon-containing gases found in the Phase II test. In the PNL study, carbon dioxide and higher alkanes, e.g. derivatives of propane and butane, were formed.

The filterable colloidal material in the Phase II test was mainly inorganic and contained 1.8% C, 0.3% H, and <0.03% N. The polymeric solids formed in the PNL work were mainly organic and contained ≈86% C, ≈12% H, and ≈1% O. The extent of polymerization as evidenced by weight-average molecular weights is directly dependent on the dose rate. In the PNL work, the dose rate was about two orders of magnitude greater and there was no packing material present.

3.5.3.3 Phase III Test Gas Analysis

During the course of this non-irradiation control test, hydrogen was produced and oxygen was consumed. Small amounts of carbon dioxide may also have been produced. In work performed by Siskind (NUREG/CR-3091, Vol. 3, 1983), gas analyses performed after hydrothermal reaction of packing material at 250°C (in argon and in the absence of irradiation) showed that carbon dioxide, hydrogen, and methane were produced. However, it is not possible to state whether any methane was produced during the Phase III test since this would be masked by the large volume of this gas used for pressurization.

3.5.3.4 Comparison of Gas Analyses Results

A comparison of the gas compositions from the Phase I, II, and III tests, given in Table 3.4, results in the following conclusions:

- Hydrogen is produced in all three tests, i.e. in the presence and in the absence of radiation. More hydrogen appears to be produced in the Phase II test, probably as a result of methane radiolysis. Hydrogen in the Phase I and II tests probably forms by basalt/water reactions in which magnetite reacts to form hematite:

  $$2Fe_3O_4 + H_2O = 3\ Fe_2O_3 + H_2$$

  In the irradiation tests, some additional hydrogen will be formed by radiolytic reactions.

- Since no methane is known to be present in the initial gas composition of the Phase I test, its detection indicates formation during this test. Because methane was used to pressurize the Phase II and Phase III test systems, it is difficult to determine whether any methane was produced. However, there is less methane remaining at the end of the Phase II test when compared to Phase III. This difference may be attributable to the radiolysis of methane which would explain the relatively large volume of hydrogen in Phase II.

- There is more nitrogen present in the gas at the end of the Phase I test than for the other two tests. This difference is indicative of the change in pressurization techniques after the Phase I test (see above).

- Oxygen was detected in the Phase I and III gas samples. The concentrations of 0.027 and 0.020 percent, respectively, correspond to partial

pressures (at 6.9 MPa, 1000 psi) of 0.018 atm (0.27 psi) and 0.014 atm (0.20 psi). Using a Henry's Law coefficient of 5×10^4 atm/mole fraction from Figure 8, these oxygen partial pressures give the following DO levels: 0.6 ppm (Phase I) and 0.5 ppm (Phase III). See Section 3.5.4 for measured values.

- Carbon dioxide in amounts exceeding that in dry air (i.e. 0.03%) was found in all three tests.

3.5.4 Measurement of pH and DO and Calculation of Eh

3.5.4.1 Measurement of pH and Dissolved Oxygen of Unreacted Packing Material Slurry

The pH electrode was calibrated with buffer solutions having pH values of 2, 7, and 10. The accuracy of the pH measurement is ±0.05 units. Prior to testing, the pH in the bentonite/basalt packing material was determined to be 8.14 at mid-depth and 7.84 at the bottom of the beaker containing the mixture.

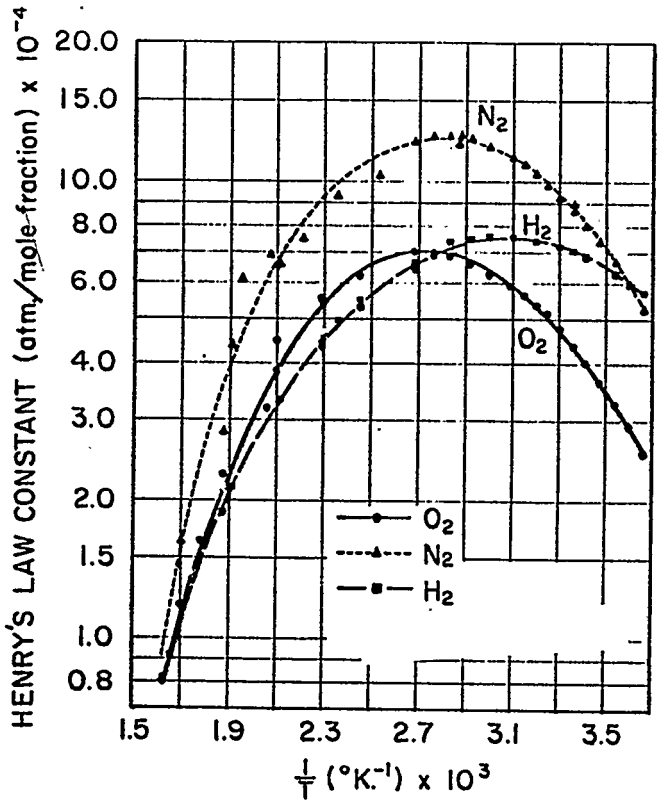

Figure 3.8. Solubilities of O_2, N_2, and H_2 in water as a function of temperature (Himmelblau, D. M., 1960). Note that the solubility of O_2 goes through a minimum near 100°C.

The DO electrode was calibrated against the DO content of water at 25°C, which is 8.4 ppm. The DO of the starting bentonite slurry without basalt was

found to be 8.3 ± 0.5 ppm. It was concluded on the basis of obtaining this 8.3 ppm value that readings are not affected by the presence of a solid phase. After the addition of basalt to the slurry, DO was measured near the surface and at mid-depth, at three locations. Results for the near-surface measurements ranged from 4.1 ppm to 6.5 ppm, with an average value of 5.4 ppm. Results for the mid-depth measurement ranged from 2.8 ppm to 3.7 ppm, with an average value of 3.2. It is clear that the DO content of the bentonite/basalt slurry is reduced by basalt/water interaction. The wide range of results obtained in the DO values led to uncertainty in the accuracy of the measurements. Accuracy is taken to be ±0.5 ppm based on DO measurements on a solution prepared to contain zero dissolved oxygen (Method 421F, A. Greenberg, 1980).

3.5.4.2 Measurement of pH and Dissolved Oxygen of Reacted Packing Material Slurry

The following general procedure was used for each of the three tests: The autoclave was opened and kept in a glove bag filled with argon. The pH and DO measurements were made, almost immediately, at several depths in the slurry near the heater and near the autoclave wall. It was felt that these in situ measurements would be most representative of the conditions achieved during a test. It should be noted, however, that autoclave depressurization forces gases such as carbon dioxide and oxygen out of solution and causes the pH reading to be higher and DO to be lower than those under the pressurized condition. The use of these measurements after decompression in the calculation of the Eh would, therefore, result in a more reducing value.

3.5.4.2.1 Measurement of Phase I Test pH and Dissolved Oxygen and Calculation of Eh

In the irradiated Phase I test, pH values near the heater increased from 6.84 to 6.92 as the depth of measurement increased. The three pH values obtained averaged 6.88. Near the autoclave wall, the pH was found to be 7.16 near the surface of the slurry, 6.73 in the middle and 6.88 near the bottom. These pH values averaged 6.92. If the average pH value at the heater is compared to the average pH value at the wall, there does not appear to be a significant difference across the thermal gradient. The average pH of the Phase I test irradiated system was, therefore, taken to be 6.90 in the Eh calculations described below.

Dissolved oxygen measurements taken near the heater gave values of 0.64 ppm near the surface, and 0.56 ppm at a depth of approximately 5 cm. For measurements near the autoclave wall, the DO was found to be 0.70 ppm near the surface and 0.52 ppm at a depth of approximately 5 cm. These values may be compared to the average of 3.2 ppm for a system containing only bentonite, basalt, and synthetic groundwater and open to the air. There is significantly less DO in the reacted system which is probably due to reaction with various system components, i.e. packing and carbon steel, during irradiation to form corrosion products and colloids. However, there does not seem to be a significant difference between the DO content across the thermal gradient. The average DO content of the Phase I irradiated system was taken to be 0.6 ppm for the Eh calculation given below.

It has been speculated by BWIP that the environment in a basalt repository will be sufficiently reducing to inhibit corrosion of the carbon steel. Reducing conditions, however, were not achieved in the Phase I test based on the following calculation of Eh. The Eh was calculated using the experimental DO and pH results from the following equation (DOE/RL 82-3, Vol. II, 1982)[7] for a temperature of 24°C (297.2°K) to compare with BWIP estimates:

$$Eh\ (V) = 1.23 + 0.0147 \log fO_2 - 0.0590\ pH + 0.000136.$$

If we assume that the pressure exerted by the dissolved oxygen on the system is equivalent to the fugacity of oxygen needed as input to the equation and that the use of this oxygen pressure rather than the oxygen overpressure (1670 Pa)[8] leads to a smaller value for fO_2, then the fugacity is calculated to be 46.3 Pa by use of the Ideal Gas Law, based on a DO content of 0.6 ppm (1.875×10^{-8} mol/mL)[9]. Accordingly, the Eh is +0.85 V, indicating that an oxidizing environment existed in the Phase I test after quenching the autoclave.

3.5.4.2.2 Measurement of Phase II Test pH and Dissolved Oxygen and Calculation of Eh

Measurements for the Phase II test were similar to those for Phase I. Adjacent to the heater, the pH was 6.62 near the surface of the slurry, 6.52 in

---

[7]The total range of Eh values for the Middle Sentinel Bluffs and Umtanum flows from 51°C to 300°C was estimated to be -0.54 to -0.37 V (DOE/RL 82-3, Vol. II, 1982). The equation used to calculate Eh should be applicable at a temperature of 24°C, because the equations for pH and fO_2 used in the derivation are valid at this temperature (Equations 11-6 and 11-16, DOE/RL 82-3, Vol. II, 1982).

[8]By use of the Henry's Law coefficient for oxygen at 25°C ($\approx 5 \times 10^4$ atm/mole fraction), it was calculated that an overpressure of 0.0165 atm of oxygen is needed to sustain an oxygen solubility in water of 0.6 ppm (The mole fraction of oxygen was calculated to be 3.3×10^{-7}.) The amount of oxygen overpressure expressed as a volume per cent of the mixture of gases at 1000 psi (68 atm) is 0.024%, which is very close to the measured oxygen content of the gas vented after quenching. It should be noted that an oxygen content of 0.2 ppm in water at 25°C would require an overpressure of 0.0055 atm of oxygen, which would constitute 0.008% of a gas mixture at 68 atm, and which would be below the mass spectrometric detection limit for oxygen of 0.017%.

[9]The compressibility factor of oxygen at 1 atm of oxygen and 300 K is 0.9994, indicating that oxygen behaves as an ideal gas under the conditions for which fugacity is calculated (Braker, W., 1980). It is interesting to also note that the compressibility factors (Z) for 100 atm of methane and 100 atm of argon at 300 K are 0.8493 and 0.9553, respectively. At higher temperatures, the values for Z increase and approach 1.0000, indicating more ideal behavior of methane and argon.

the middle, and 6.68 near the bottom, with an average value of 6.61. Adjacent to the wall, the pH was 6.53 near the surface of the slurry, 6.49 in the middle, and 6.70 near the bottom, with an average value of 6.57. Although there does not seem to be a significant change in pH across the thermal gradient, there does appear to be a significant change in pH with depth. The pH of the Phase II test for the purpose of Eh calculations will be taken as 6.60.

Near the heater, the DO was 0.21 ppm near the surface of the slurry and 0.22 ppm at a depth of approximately 5 cm. The DO near the autoclave wall was 0.16 ppm at similar depths. There does not appear to be a significant change in DO across the thermal gradient. The value of DO for Eh calculations will be taken as 0.2 ppm.

The Eh was calculated to be 0.86 V using the values for pH and fugacity of oxygen of 15.4 Pa (based on a DO of 0.2 ppm).

3.5.4.2.3 Measurement of Phase III Test pH and Dissolved Oxygen and Calculation of Eh

Adjacent to the heater, the pH was 7.10 near the surface of the slurry, 7.05 in the middle, and 7.28 near the bottom, with an average value of 7.14. Adjacent to the wall, the corresponding pH values were 7.03, 7.02 and 7.06, respectively, with an average value of 7.03. There does not appear to be a significant difference in pH as measured across the thermal gradient. The pH measured at 24°C is taken to be 7.10.

Near the heater, the DO was 0.6 ppm near the surface of the slurry and 0.5 ppm at a depth of approximately 5 cm. The DO near the autoclave wall was 0.4 ppm at similar depths. The DO content does not vary significantly across the thermal gradient. The average DO content in the test is taken to be 0.5 ppm.

Using the equation cited above, the Eh (after quenching) was calculated to be 0.83 V.

3.5.4.3 Comparison of pH and DO Measurements and Eh Calculations for All Tests

The pH and DO data for the three tests along with the calculated Eh values after quenching are summarized in Table 3.5.

The unreacted slurry components are basic in contrast to the reacted slurries. The latter are either slightly basic (the non-irradiated Phase III test) or slightly acidic (the irradiated Phase I and Phase II tests). Comparison of the DO data for the reacted (closed system) and unreacted (open system) shows that there is approximately an order of magnitude difference in the DO levels. The addition of basalt in an open system reduced the DO content and it was further reduced in the irradiated and non-irradiated tests. Within the accuracy of the measurements, there is no obvious difference in DO content among the three tests. The calculated Eh values show a more oxidizing environment in the closed reacted systems than in the open unreacted systems, due to lower pH values in the closed reacted system. It would appear that radiation does not significantly affect the Eh of the system under consideration.

Table 3.5. pH and DO as measured for packing material slurry and Eh as calculated for all tests.

	pH[a]	DO (ppm)[b]	Eh (V)[c]
Phase I test slurry	6.9 ± 0.05	0.6 ± 0.5	0.85 ± 0.01
Phase II test slurry	6.6 ± 0.05	0.2 ± 0.5	0.86 ± 0.01
Phase III test slurry	7.1 ± 0.05	0.5 ± 0.5	0.83 ± 0.01
Unreacted bentonite slurry	8.7 ± 0.05	8.3(mean) ± 0.6(2σ)	0.76
Unreacted bentonite + basalt slurry	8.0(mean)	4.3(mean) ± 3(2σ)	0.79
Unreacted groundwater	9.7 ± 0.05	8.4	0.70

[a]These reported pH values represent the average of six readings made with a pH electrode which was calibrated with buffer solutions having pH values of 2, 7, and 10. The accuracy of the pH measurement is 0.05 units.
[b]The reported DO values represent the average of four or more readings. Accuracy is taken to be 0.5 ppm. The DO electrode was calibrated with the oxygen content of water at 25°C, which is 8.4 ppm.
[c]These Eh values are calculated based on the pH and DO measurements of the slurry at 24°C.

3.5.5 Measurement of Ionic Concentrations in Slurry Water

It was considered important to measure the concentrations of ions particularly associated with the corrosion of carbon steel and to determine whether significant differences occurred across a thermal gradient. Therefore, the concentrations of Cl^-, Fe(total), and SO_4^{2-} in W samples (filtered) and H samples (filtered) were measured as detailed in the experimental section. These concentrations in R samples (unfiltered) were also measured to determine differences in content between filtered and unfiltered samples. The concentration of Si, reported as SiO_2, was also determined but only for the Phase I test samples. Results of these analyses are summarized in Table 3.6 and uncertainties are given wherever they are known. However, it must be emphasized that these are the results of one analysis on single samples after quenching has

occurred[10]. Any conclusions derived from these data would have to be supported by valid experiments that have eliminated any effects due to quenching. Therefore, these results should be regarded only as indications of possible differences in ionic concentration across a thermal gradient.

Table 3.6. Comparison of ionic concentrations of reacted Grande Ronde GR-3 groundwater (in ppm).

Sample	Cl^-	SO_4^{2-}	Fe(Total)	SiO_2
GR-3 (initial composition)	312	165	0	79
Sample H-I (filtered)[a]	305±6	260±5	ND(<2)	29
Sample W-I (filtered)[b]	321±6	300±6	ND(<2)	39
Sample R-I (unfiltered)[c]	357±7	330±7	500±100	116
Sample H-II (filtered)[d]	263±5	220±4	1.4	---
Sample W-II (filtered)[b]	328±7	272±5	0.9	---
Sample R-II (unfiltered)[c]	---d	330±7	700±140	---
Sample R-II (filtered)[c]	177±3	145±3	2.4	---
Sample H-III (filtered)[a]	388±8	204±4	0	---
Sample W-III (filtered)[b]	429±9	258±5	1.0	---
Sample R-III (unfiltered)[c]	---d	345±7	500±100	---
Sample R-III (filtered)[c]	368±7	200±4	2.5	---

[a]Sample H is the designation for the supernate of the centrifuged slurry removed from the heater region in the autoclave. Experimental phases are designated by Roman numeral I, II or III.
[b]Sample W is the designation for the supernate of the centrifuged slurry, removed from the wall region in the autoclave.
[c]Sample R is the designation for the supernate of the centrifuged slurry removed from random locations in the autoclave.
[d]Insufficient sample remained for this analysis to be performed.

[10]Evidence exists (RHO-BWI-C-105, 1981) that the state of leachates under hydrothermal conditions is not completely preserved in quench rates of ≈25°C/min. Experiments conducted on the interaction of seawater and basalt (Seyfried, W. E., 1979) at 150°C showed that significant retrograde changes occurred in ionic concentrations and pH measurements after a quenching period of 45 minutes. Approximate cooling time for all tests in the current study was 25 minutes.

3.5.5.1 Measurement of Ionic Concentrations in Phase I Test

The concentrations of Cl^-, SO_4^{2-} and Si were greater near the cooler end (the wall) of the thermal gradient which was at approximately 113°C. The change in concentration of Cl^- across a thermal gradient may be significant. However, the difference in concentration of SO_4^{2-} across the gradient does seem significant, based on these single measurements. It is not known whether the Si concentrations are significant, since the precision is not known and they are an order of magnitude smaller than the Cl^- and SO_4^{2-} concentrations. Comparison of these ionic concentrations with those measured in the synthetic groundwater (see Table 3.6) reveals a decrease of Si and an increase of SO_4^{2-} in the filtrates. If any Fe was present in the filtrates, it was in amounts <2 ppm, the detection limit of the analysis. Total iron in Sample R-I was determined quantitatively after acidification of the unfiltered liquid with HF. It was also determined that a significant portion of the total Fe was in the ferrous state (Fe^{2+})[11].

It appears that the bulk of the Fe and Si content of the unfiltered water is present in the colloidal state. This is also reflected by relatively low concentrations of Si and below detection for Fe in filtered samples. The filterable material appears to be acting as a sink for iron, the source of which can be the basalt, bentonite, or carbon steel.

3.5.5.2 Measurement of Ionic Concentrations in Phase II Test

The only measurements that appeared to change significantly across the temperature differential of ≈22°C were the concentrations of SO_4^{2-} and Cl^-. Concentrations were lower at the hotter end of the gradient, i.e. near the heated carbon steel sleeve.

From the results of these single determinations, it appears that less Cl^- and more SO_4^{2-} than are present in the starting groundwater would be found near the carbon steel sleeve. It is clear that, for the Phase I test results, the bulk of the Fe content of the unfiltered supernate is present in the colloidal form. However, very small amounts of iron remain in the filtered supernates.

3.5.5.3 Measurement of Ionic Concentrations in Phase III Test

As was the case in the previous tests, concentrations of Cl^- and SO_4^{2-} were significantly lower at the hotter end of the gradient. Again, the bulk of the iron is present in colloidal material.

---

[11]The Fe^{+2} content was estimated using the phenanthroline standard method. Three molecules of 1,10-phenanthroline chelate each atom of ferrous ion to form an orange-red complex. The intensity of the color is dependent on the amount of ferrous ion present. A visual comparison with color standards was made to determine content of ferrous ion. Another portion of Sample R was treated to convert any ferric ion to ferrous and another phenanthroline complexation determination was made. The color of the reduced solution was very similar to that of the first determination, indicating that most of the iron was in the ferrous state in the original sample.

3.5.5.4 Comparison of Measured Ionic Concentrations For All Tests

The results of the water analyses for Fe(total), Cl^-, and SO_4^{2-} from the three tests were summarized in Table 3.6. There were different thermal differentials established across the packing materials in each test. For Phases I, II and III, these were, respectively, 1.0, 0.6 and 2°C/mm. Results from the three tests, therefore, cannot be quantitatively compared. However, qualitative differences among ionic concentrations are noted for the three tests. It must be emphasized that these results are from the analyses of single specimens from individual tests. Therefore, in the absence of statistical information, a difference is deemed significant if one measured value differs from another by a quantity that exceeds the experimental error. Experimental precision is indicated in the table where it is known. The results for the chloride and sulfate concentrations are based on IC measurements and are estimated to vary by ±2%. On this basis the following conclusions can be drawn by comparing and contrasting the ionic concentrations measured in the three tests after quenching:

- Compared to unreacted groundwater, the chloride content of filtered reacted water is usually decreased in hotter regions of the packing material and increased in cooler regions. The exception occurred in the Phase III control test where increases in chloride level were evident for both the hotter and cooler regions. Nevertheless, there was still the same general behavior in terms of higher chloride in the cooler regions.

- Compared to unreacted groundwater, the sulfate content of filtered reacted water is always increased. The increase is larger in the cooler regions of the packing material.

- For unfiltered reacted groundwater the concentrations of chloride, sulfate, and especially SiO_2 and total iron, are significantly increased. This shows that the colloidal particles present in the groundwater contain relatively high concentrations of these three constituents.

- In terms of the effect of thermal gradients on the concentration differences across the packing it was found that chloride and sulfate differences were largest for the Phase II test, which had the smallest thermal gradient. These concentration trends were very similar for Phase I and Phase III even though the temperature differentials across the packing were quite different (viz. 37 and 73°C, respectively). It is, therefore, unclear what factors controlled the changes in concentration along the thermal gradient.

Similar increases in chloride concentrations were reported by Wood (RHO-BW-SA-219P, 1983), who studied changes in ionic concentrations with time for closed non-irradiated systems containing Umtanum basalt (free of fines) or Baroid National Western[12] bentonite and GR-3 synthetic groundwater at 300°C

[12]The Baroid bentonite contained 85% montmorillonite, 5% quartz, 5% feldspar, 2% illite, and 1% calcite and gypsum.

and 29.9 MPa for one month. However, in Wood's work, the sulfate concentration was lower in the reacted bentonite/groundwater system and was unchanged in the reacted basalt/groundwater system. This would seem to indicate that for these particular systems basalt and bentonite are sources of chloride and that the bentonite can act as a sink for sulfate. An additional experiment containing bentonite/basalt/groundwater reacted under the same hydrothermal conditions for three months showed that sulfate concentration was slightly increased at 28 days and was significantly decreased at the 56-day sampling. In the same test, chloride concentration increased and reached a maximum between 28 and 56 days.

Also, in Wood's study it was found that the iron concentrations in reacted groundwater were highest in the bentonite/water system (up to 0.14 ppm) and similar for basalt/water and basalt/bentonite/water systems (up to 0.08 ppm). This indicates that bentonite is a prime source of iron in the water. In another study, carried out at a 200°C test temperature, a basalt/water system gave a reacted water containing 35.4 ppm of iron after 718 hours (RHO-BW-ST-21P, 1982). The trend to higher total iron concentrations, as the test temperature is decreased from 300 to 200°C, is evident from Wood's work. In the BNL study, however, much of the iron originated from the carbon steel present in the system and iron was present in colloidal form which was not reported as present in Wood's work.

3.5.6 SEM-EDX Analysis of Colloidal Material

A part of R sample from each of the tests was passed through a 0.025-μm membrane filter to collect colloidal material for analysis. The latter was removed as a film from the filter when it dried. They were mounted with epoxy on a graphite holder and examined using a scanning electron microscope with an X-ray energy-dispersive analysis system attached (SEM-EDX). It should be noted that comparatively less colloidal material was extracted from the Phase III (non-irradiated) test.

3.5.6.1 SEM-EDX Analysis of Colloidal Material Removed From Phase I Test Solution

A micrograph of the dried colloidal material film from the Phase I test is given in Figure 3.9. A rod-shaped phase and a small rectuangular particle are seen to be embedded in the colloidal material. SEM-EDX analyses given in Figures 3.10 through 3.12 show that the colloidal material is rich in Si, Fe, Ca and Al with smaller quantities of Mg and K. The rod-shaped phase also contains Si with significant amounts of Mg, Ca, Ba, Zn K and Al present. In the case of the small particle, the dominant element detected is Ca with a minor proportion of Si. The colloidal material substrate in Figure 3.9 has an elemental composition consistent with that for clay particles, as expected (Table 3.1). The small calcium-rich phase is possibly calcite which has been found in bentonite by other workers (ANL-83-19, 1983). At the present time, the identification of the rod-shaped phase is unknown. Zinc has been observed in small crystals found in bentonite (ANL-83-19, 1983) but this phase could have also originated from the basalt component of the packing material. More work is needed to characterize the colloidal material obtained from the current studies.

An interesting effect was observed as the colloidal material was bombarded with 17-kV electons in the SEM as shown in Figure 3.13. Small protuberances developed in the sample film which could have been caused by vaporization of residual moisture.

3.5.6.2 SEM-EDX Analysis of Colloidal Material Removed From Phase II Test Solution

Micrographs of the dried colloidal material recovered from the Phase II test heater and wall regions are shown in Figures 3.14 and 3.15. Both of these samples were analyzed by EDX and were found to be high in Si and Al along with some Fe and Ca. This is similar to the composition determined by EDX for the Phase I test material, except that no K or Mg was detected (see Figure 3.10).

However, several differences are evident upon comparison of the two micrographs taken at the same magnification. The material from the heater region is much coarser in texture. This may be due to different thicknesses of material deposited on the filter. Additionally, there is a dendritic structure lying on the substrate in the material taken from the wall region (see Figure 3.15). The structure was analyzed by EDX and found to contain large amounts of Ca and S. See Figure 3.16 for a micrograph taken at alower magnification (300X) of the material recovered from the heater region in the Phase II test. Analysis by EDX of the nodule present shows a high content of Ca, S and Si along with some Al.

3.5.6.3 SEM-EDX Analysis of Colloidal Material Recovered from the Phase III Test Solution

Micrographs of the colloidal material recovered from the heater and wall regions of the Phase III control test are shown in Figures 3.17 and 3.18. Corresponding EDX analyses for these materials are given in Figures 3.19 and 3.20. Both have essentially the same composition: high Si and Al content with moderate Fe and Ca amounts along with some trace elements. No differences in composition were noted for localized variations in substrate texture. Additionally, the presence of oxygen was confirmed in the sample taken from the wall region by use of transmission electron microscopy (TEM)-EDX (see Figure 3.21). The dried sample taken from the heater region was too thick to permit an analysis by TEM-EDX.

3.5.6.4 Comparison of SEM-EDX Analyses of Colloidal Materials

A comparison of the information gained by use of SEM-EDX techniques in the three test systems yields the following conclusions:

- The bulk composition of all colloidal materials, from both the wall and heater regions, is essentially the same. There is a high Si and Al content, some Ca and Al, along with trace elements. Oxygen is believed to be present in all samples but was only confirmed by TEM-EDX in the colloidal material taken from the wall region of the Phase III test.

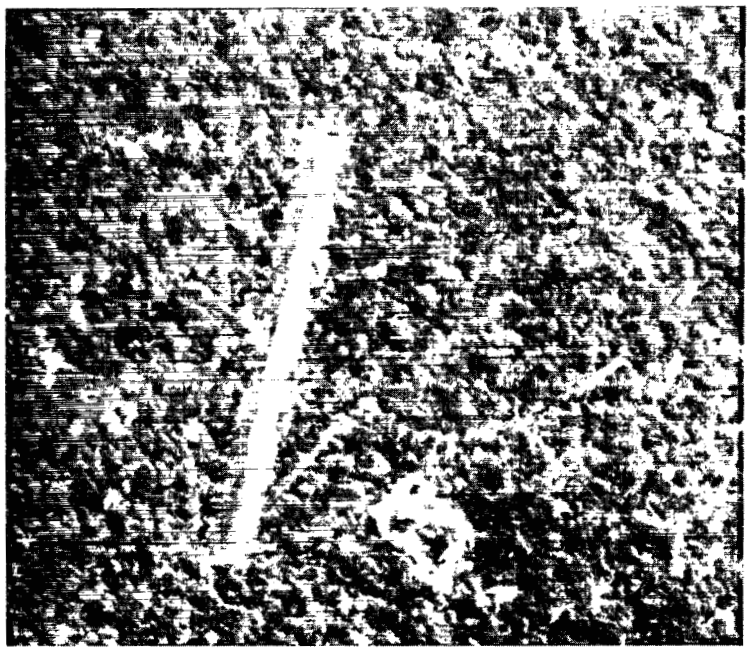

Figure 3.9. Micrograph of colloidal material recovered from the Phase I test (800X).

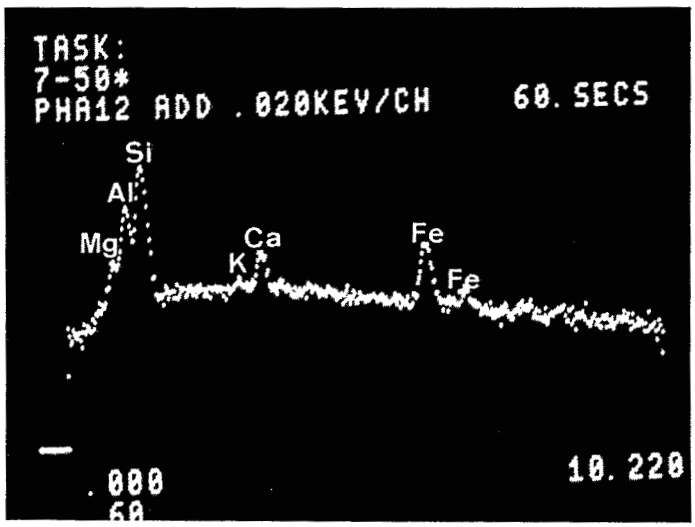

Figure 3.10. EDX analysis of colloidal material recovered from the Phase I test.

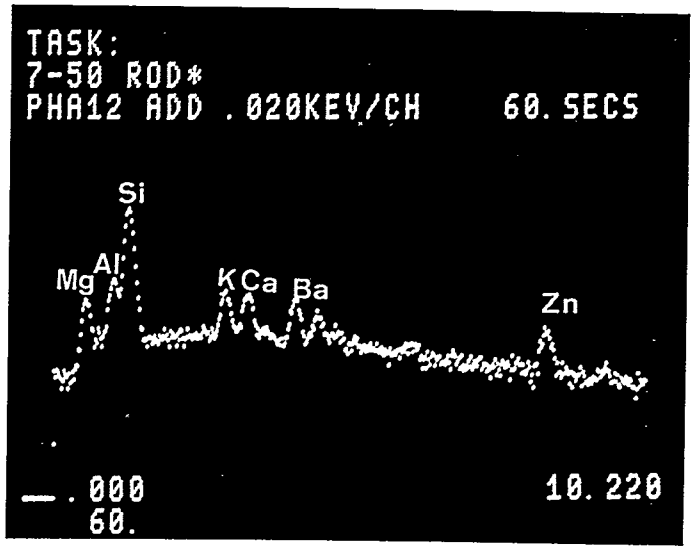

Figure 3.11. EDX analysis of rod in colloidal material recovered from the Phase I test.

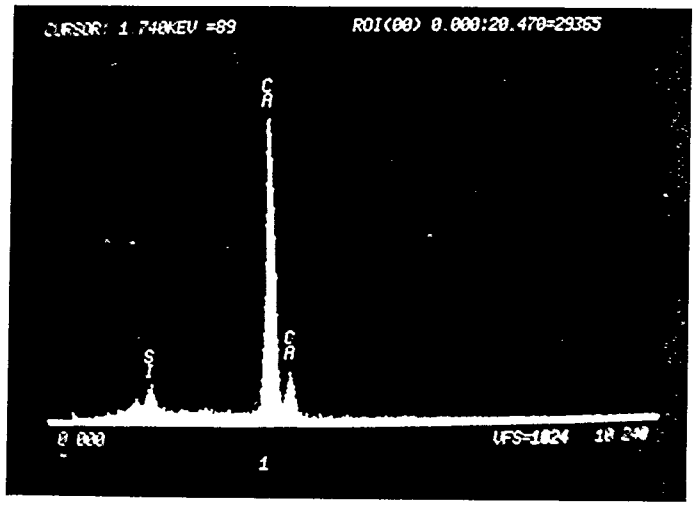

Figure 3.12. EDX analysis of crystal in colloidal material recovered from the Phase I test.

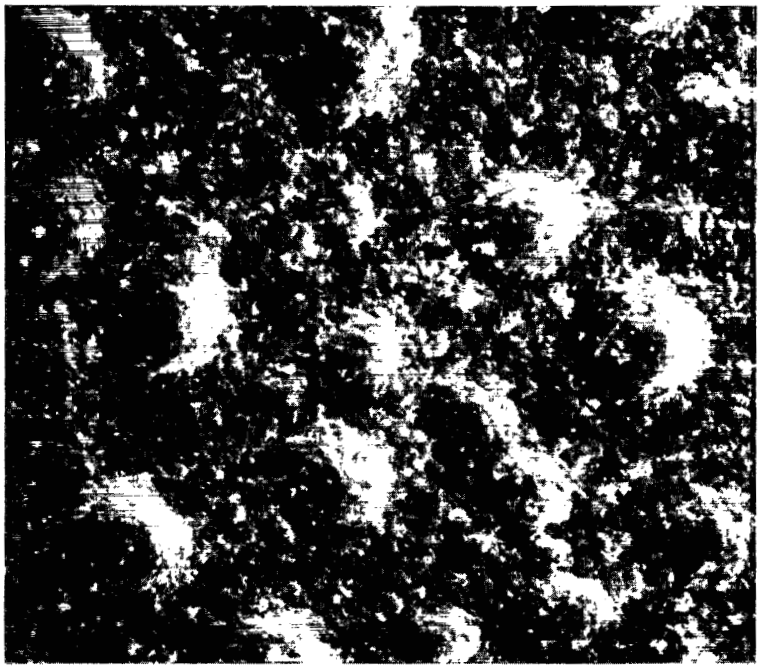

Figure 3.13. Micrograph of protuberances appearing in colloidal material recovered from the Phase I test after bombardment with 17-kV electrons (1000X).

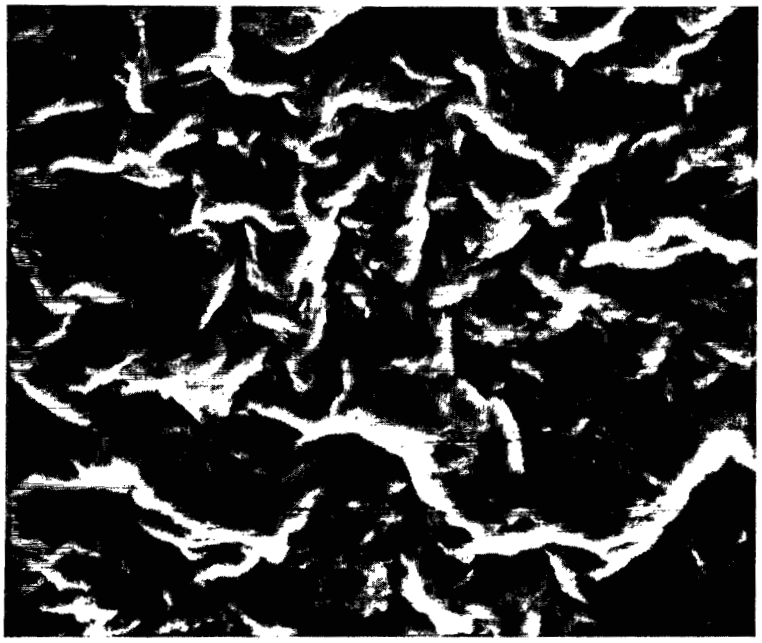

Figure 3.14. Micrograph of colloidal material recovered from the Phase II test heater region (1000X).

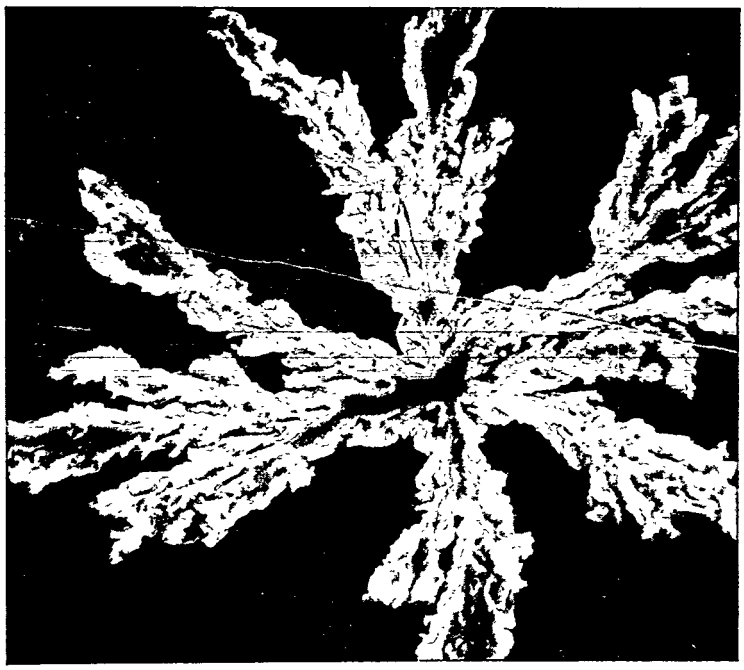

Figure 3.15. Micrograph of colloidal material recovered from the Phase II test wall region (1000X).

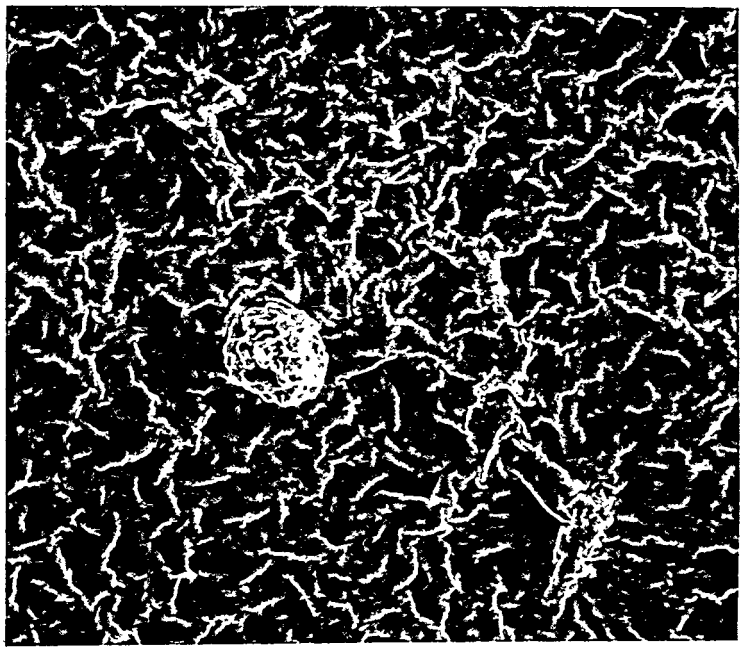

Figure 3.16. Micrograph of colloidal material recovered from the Phase II test heater region (300X).

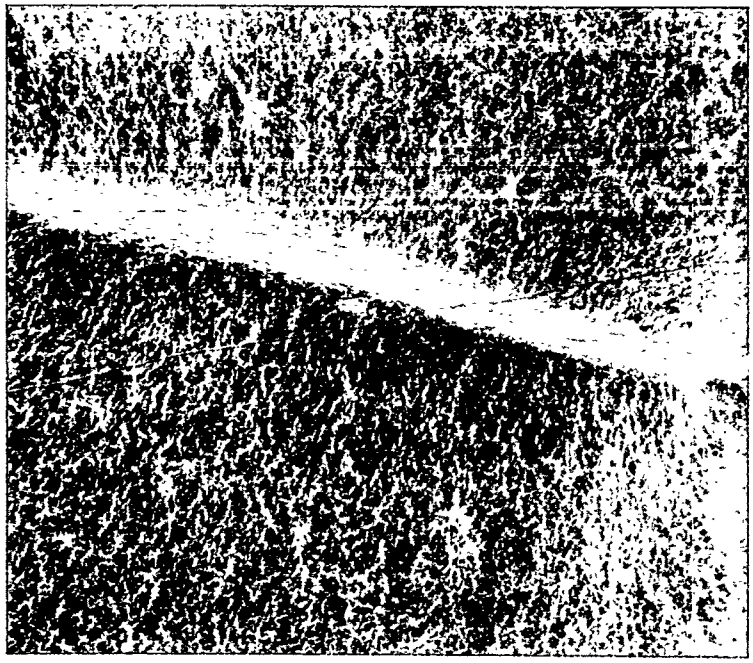

Figure 3.17. Micrograph of the colloidal material recovered from the Phase III test heater region (100X).

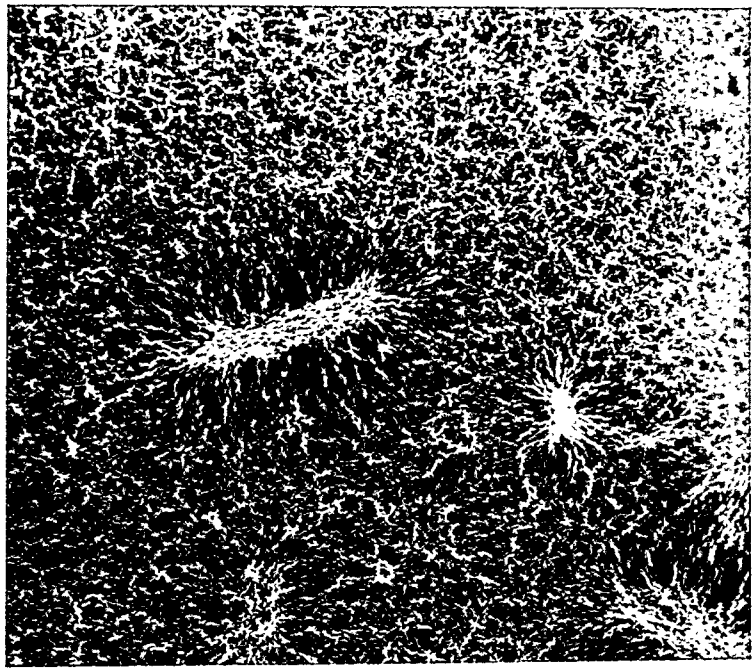

Figure 3.18. Micrograph of the colloidal material recovered from the Phase III test wall region (100X).

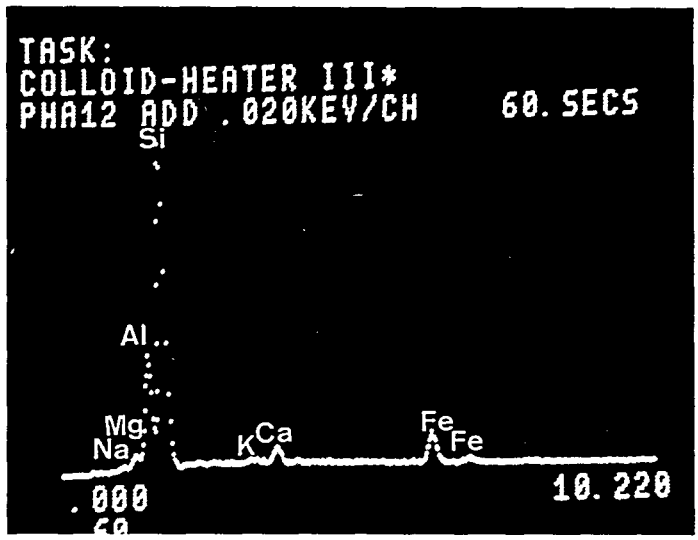

Figure 3.19. EDX analysis of colloidal material recovered from the Phase III test heater region.

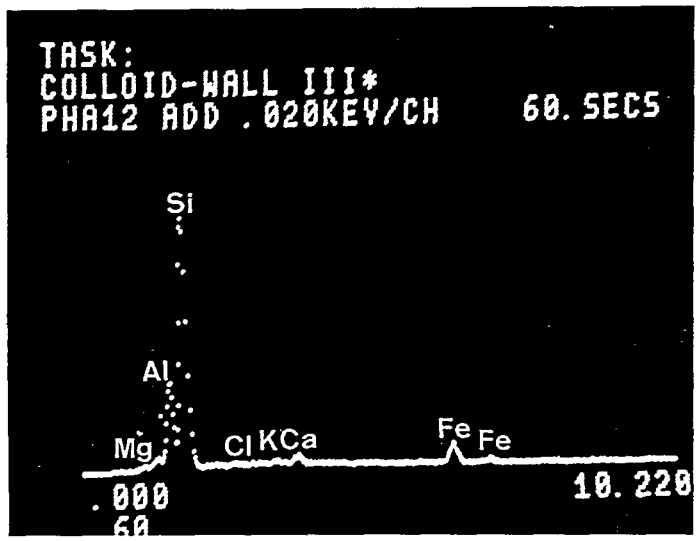

Figure 3.20. EDX analysis of colloidal material recovered from the Phase III test wall region. The presence of oxygen was confirmed by EDX, see Figure 21.

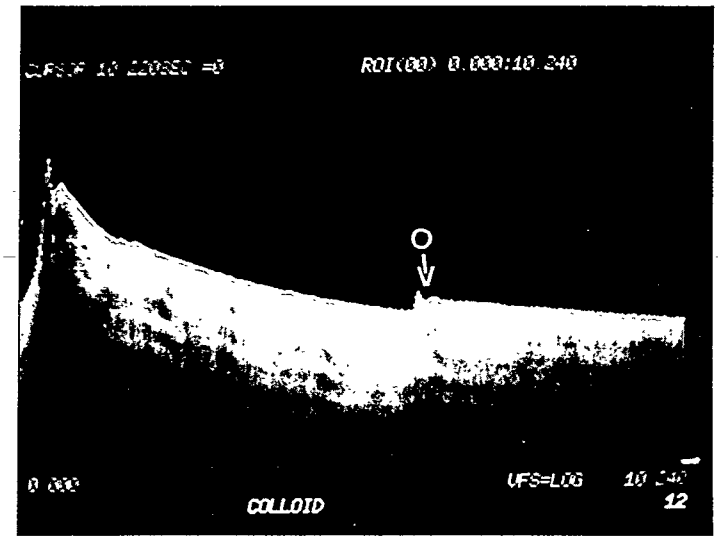

Figure 3.21. EDX(TEM) analysis of colloidal material recovered from the Phase III test wall region.

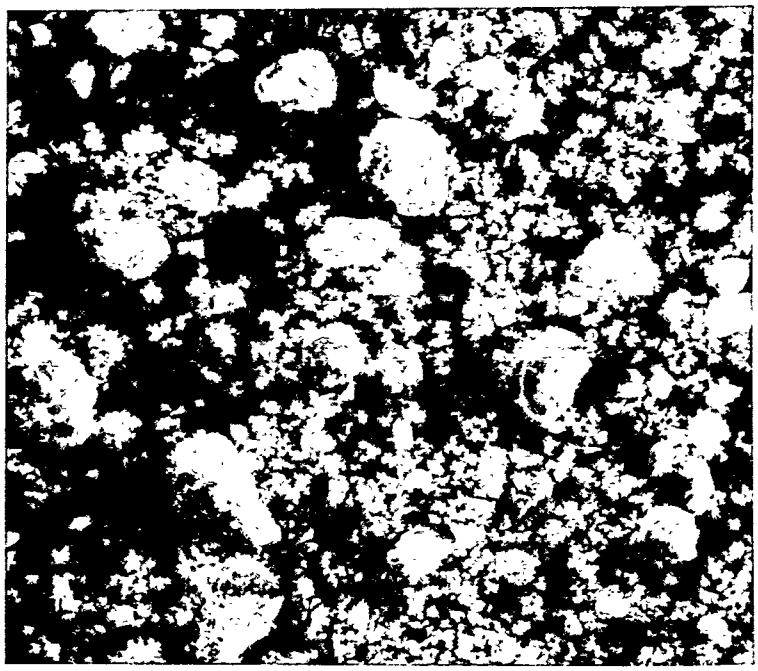

Figure 3.22. Micrograph of unreacted bentonite clay (100X).

- A variety of embedded and deposited phases that differ in shape and composition can be seen in the micrographs of the colloidal material recovered from the Phase I and Phase II tests. None of these was seen in the colloidal material recovered from the Phase III test. This indicates that radiation plays some role in the formation of these phases.

3.5.7 Analysis of Unreacted Bentonite and Reacted Bentonite Portion of Slurry

3.5.7.1 Analysis of Bentonite

A micrograph of unreacted SWy-1 bentonite is given in Figure 3.22. The semi-quantitative EDX analysis shows that the following elements were present at two locations in the sample: Si (≈75%), Al (≈15%), Fe (≈6%), 4% (Mg, K, Ca, V, Na, Cu, Zn, Ti).

Reacted bentonite portions of the packing material were centrifuged, and the solid placed on a glass slide and allowed to dry. There were no basalt pellets in any of these specimens. They were examined with an X-ray diffractometer in the range $2\theta = 3\text{-}37°$ using Cu K_α radiation and the resulting patterns are shown in Figures 3.23, 3.24, 3.25. The 2θ values were converted into d-spacings using standard tables (Rose, A. J., 1957). A comparison is given in Table 3.7. It is clear that differences exist in the d-spacings of the Phase I, Phase II and Phase III test samples. For illustrative purposes, the materials remaining after centrifugation and removal of the supernatant liquid in the Phase I test are shown in Figure 3.26. This appearance is similar to those for materials from the Phase II and Phase III tests. Samples from near the heater (Tubes A and D in Figure 3.26) were a combination of orange, white and tan in color. Material samples near the wall (Tubes B and E in Figure 3.26) was mostly tan and white in color. A tube of unreacted slurry (Tube C in Figure 3.26) was centrifuged for comparison purposes and was tan in color. See Section 3.5.8.1 for the results of solids analysis performed in the study by Wood (RHO-BW-SA-219P, 1983).

3.5.7.2 Analysis of Montmorillonite Portion of Bentonite

The major peaks attributable to the montmorillonite in the control samples appear in the range $2\theta = 7.1$ (d = 12.4 Å) to $2\theta = 7.8$ (d = 11.3 Å). These single peaks are shown for Phase I, Phase II and Phase III test samples in Figures 3.27b to 3.29b, respectively. These peaks shift in the reacted, glycolated, and heat-treated slurry samples.

3.5.7.2.1 Montmorillonite XRD Phase I Test

The two reacted samples in the Phase I test gave very similar results but the strongest peak obtained was significantly shifted compared to the equivalent peak for the control, which may indicate that the incorporation of a large cation in the interlayer sites occurred and that the distance between successive layers of the smectite (i.e. basal spacing) increased due to swelling. There is some illite present in the samples before and after reaction, as evidenced by the peak at $\approx 2\theta = 9°$ (d ≈ 9.9 Å). See the last three columns of Table 3.8 for a tabulation of these data.

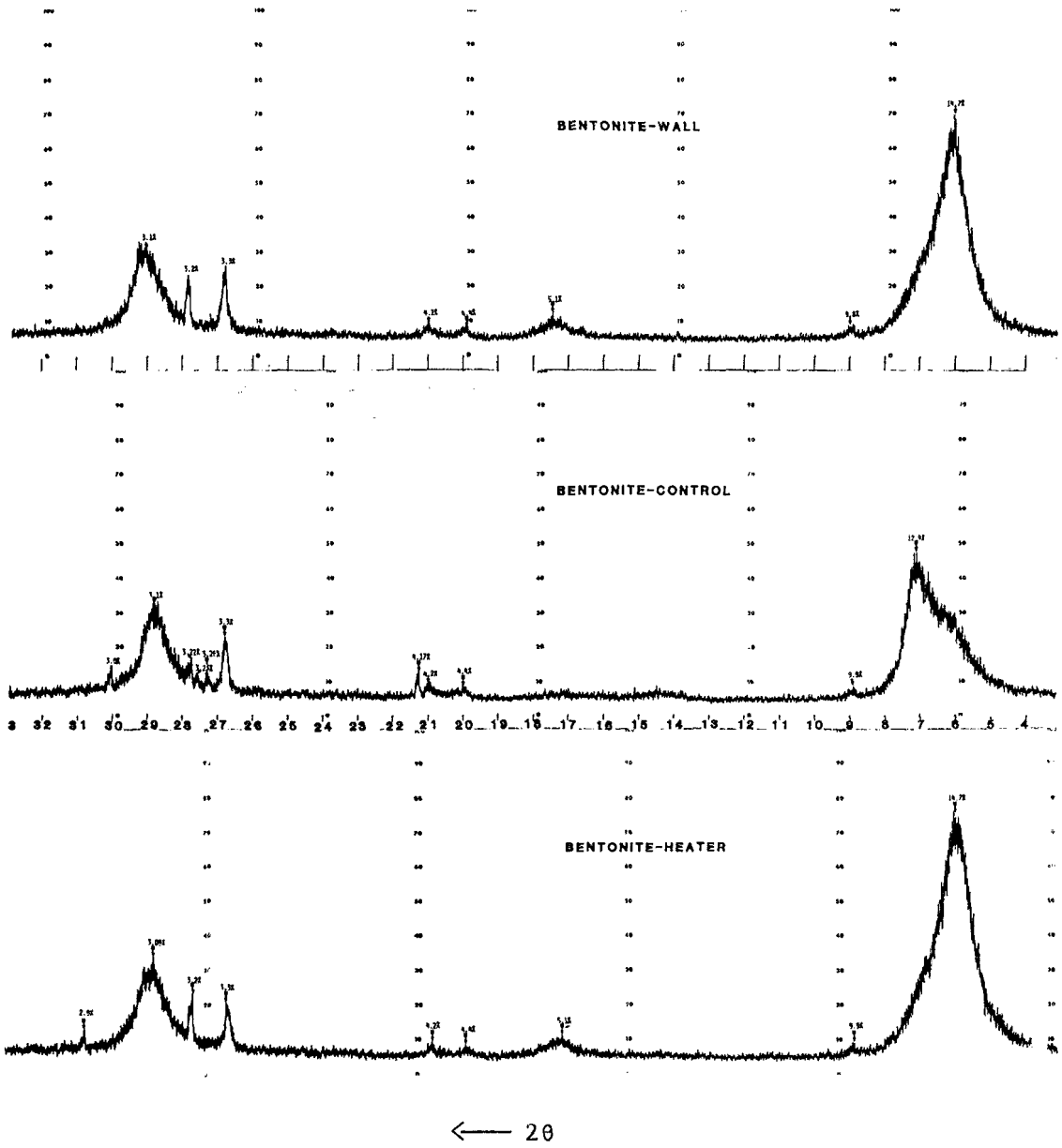

Figure 3.23. Comparison of X-ray diffraction patterns of reacted and unreacted bentonite present in the Phase I centrifuged packing material slurry samples prepared as oriented clay mounts by evaporation of slurry on glass slides. [Range of scan: 2θ = 3-37° (d = 2.43-29.4 Å).](Control sample consisted of a slurry of bentonite and basalt withsynthetic groundwater.)

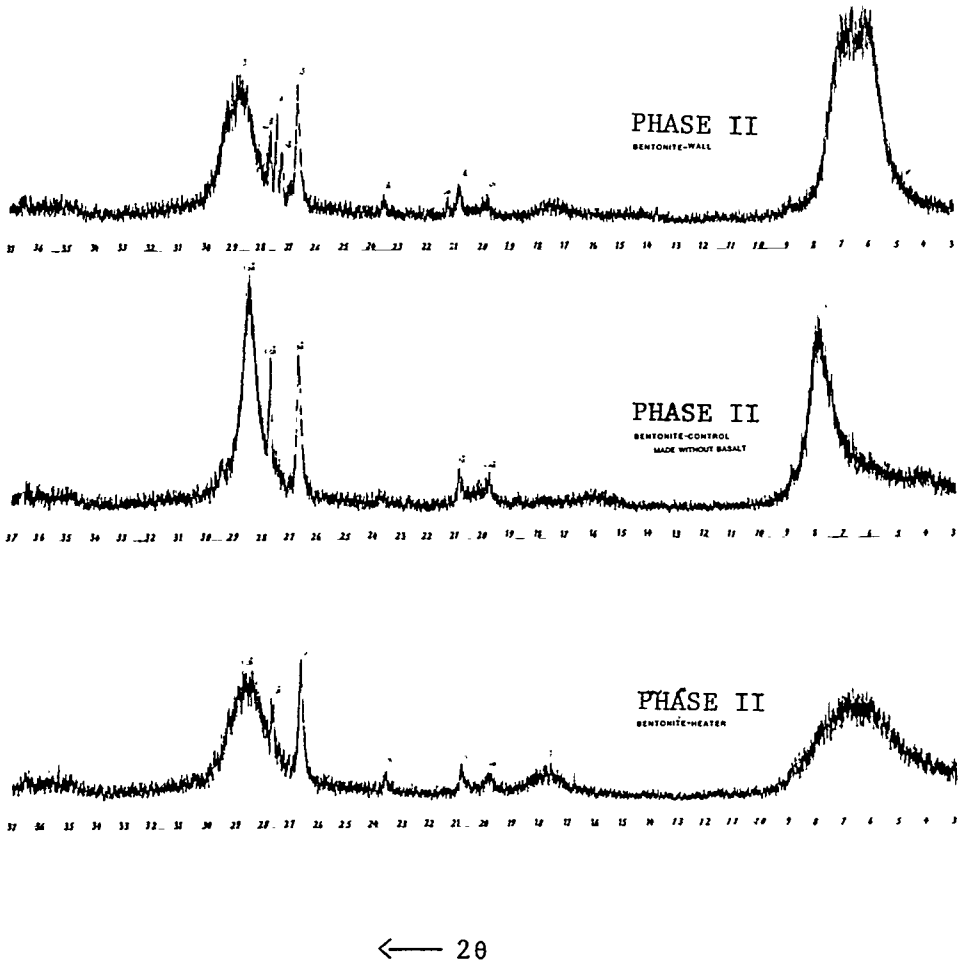

Figure 3.24. Comparison of X-ray diffraction patterns of reacted and unreacted bentonite present in the Phase II test centrifuged packing material slurry samples prepared as oriented clay mounts by evaporation of slurry on glass slides. [Range of scan: $2\theta = 3\text{-}37°$ ($d = 2.43\text{-}2.94$ Å)]. (Control sample consisted of a slurry of bentonite with synthetic groundwater.)

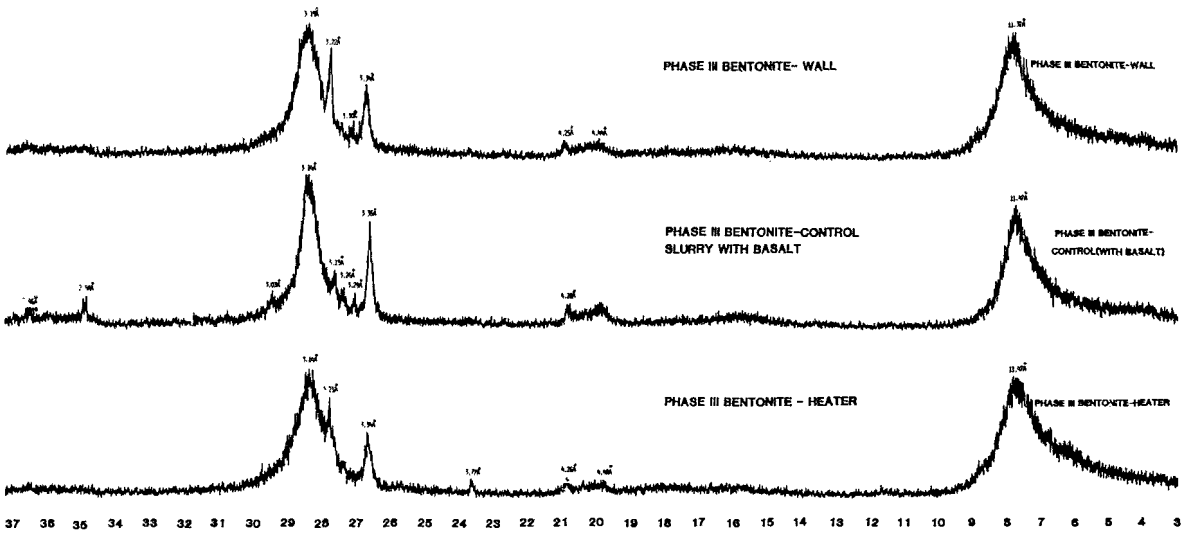

← 2θ

Figure 3.25. Comparison of X-ray diffraction patterns of reacted and unreacted bentonite present in the Phase III test centrifuged packing material slurry samples prepared as oriented clay mounts by evaporation of slurry on glass slides. [Range of scan: 2θ = 3-37° (d = 2.43-29.4 Å)]. (Control sample consisted of a slurry of bentonite and basalt with synthetic groundwater.)

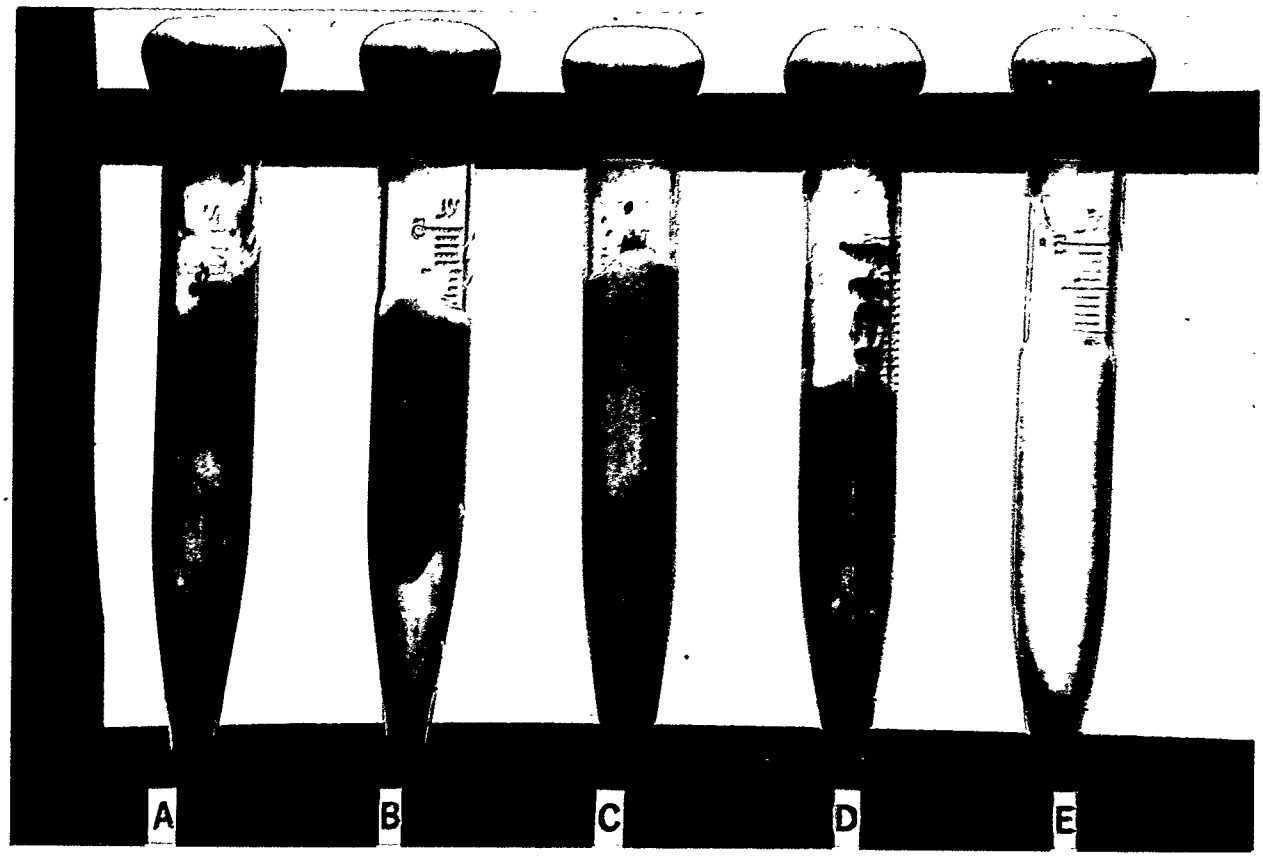

Figure 3.26. Appearance of Phase I centrifuged packing material slurries before and after reaction. (Tubes are shown full-scale. Black material in bottom of tubes is basalt fines.)
(A) Sampled near heater
(B) Sampled near autoclave wall
(C) Control unreacted
(D) Sampled near heater
(E) Sampled near autoclave wall.

Table 3.7. Comparison of (00ℓ) d-spacings based on X-ray diffractometer studies of reacted and unreacted bentonite portions of centrifuged packing material slurries prepared as oriented clay mounts by evaporation of centrifuged slurry on glass slides. [Intensities not specified. Range of scan: $2\theta = 3\text{-}37°$ (d = 2.43-29.4 Å).]

d (Å) Wall Sample	d (Å) Heater Sample	d (Å) Control Sample[a]
Phase I Test		
14.7	14.7	12.4
----	9.9	9.9
5.1	5.1	----
4.4	4.4	4.4
4.2	4.2	4.2
----	----	4.17
3.3	3.3	3.3
----	----	3.26
----	----	3.23
3.2	3.2	3.22
3.1	3.09	3.1
----	----	3.0
Phase II Test		
13.6	13.4	11.3
6.50	----	----
----	----	5.53
5.09	5.01	----
4.47	4.48	4.49
4.27	4.27	4.25
3.77	3.77	3.77
3.34	3.35	3.34
3.28	----	----
3.25	----	----
3.23	3.22	3.22
3.11	3.13	3.14
Phase III Test		
11.3	11.5	11.5
4.44	4.48	4.49
4.25	4.26	4.28
----	3.77	----
3.34	3.34	3.35
3.30	----	3.29
----	----	3.26
3.22	3.21	3.23
3.15	3.14	3.14
----	----	3.03
----	----	2.58
----	----	2.46

[a]Control samples for each test were prepared separately and contained bentonite/basalt in Phase I and III tests but contained only bentonite/groundwater for the Phase II test.

Table 3.8. Comparison of (00ℓ) d-spacings based on X-ray diffractometer studies of Phase I test reacted and unreacted montmorillonite, prepared as oriented clay mounts by evaporation of centrifuged packing material slurry on glass slides; treatment by glycolation at 60°C, followed by heating to 300°C for one hour. [Intensities not specified. Range of scan: 2θ = 3-9.5° (d = 9.30-29.4 Å).]

d (Å)								
Heater	Wall	Control	Heater	Wall	Control	Heater	Wall	Control
Samples Glycolated			Samples Glycolated and Heat Treated			Samples Untreated		
17.0	16.0	16.6	15.2*	15.2*	15.5*	14.7	14.7	12.4
9.9	9.7	9.9	----	9.9	----	9.9	9.8	9.9

*Peak intensity is drastically reduced when compared to the peak intensities in the diffraction patterns of the untreated and glycolated samples. This decrease in intensity is due to the collapse of the smectite structure.

The slides, coated with centrifuged reacted and unreacted (control) packing material slurries, were subsequently given standard glycolation[13] and heat treatments to study the changes in the (001) reflections of the montmorillonite clay (Carroll, D., 1970). The first treatment consists of glycolation. See the first three columns of Table 3.8 for tabulation of the data on the glycolated samples and Figures 3.27d, e, and f for the diffraction patterns of the glycolated samples. An expandable clay such as montmorillonite will characteristically swell upon glycolation due to the increase in basal spacing between layers because of the incorportion of organic molecules in the interlayer sites and this will be evidenced by a shift in the d-spacing at ≈12-15 Å to ≈16-18 Å. Compare Figures 3.27a and d; Figures 3.27b and e; Figures 3.27c and f. The sample taken from the heater region had the largest d-spacing value, followed by that for the control sample, followed by that for the sample taken from the wall region.

[13]Samples are glycolated by placing the coated slides in a desiccator, which contains ethylene glycol in the well normally filled with desiccant, and by heating in an oven at 60°C for at least an hour.

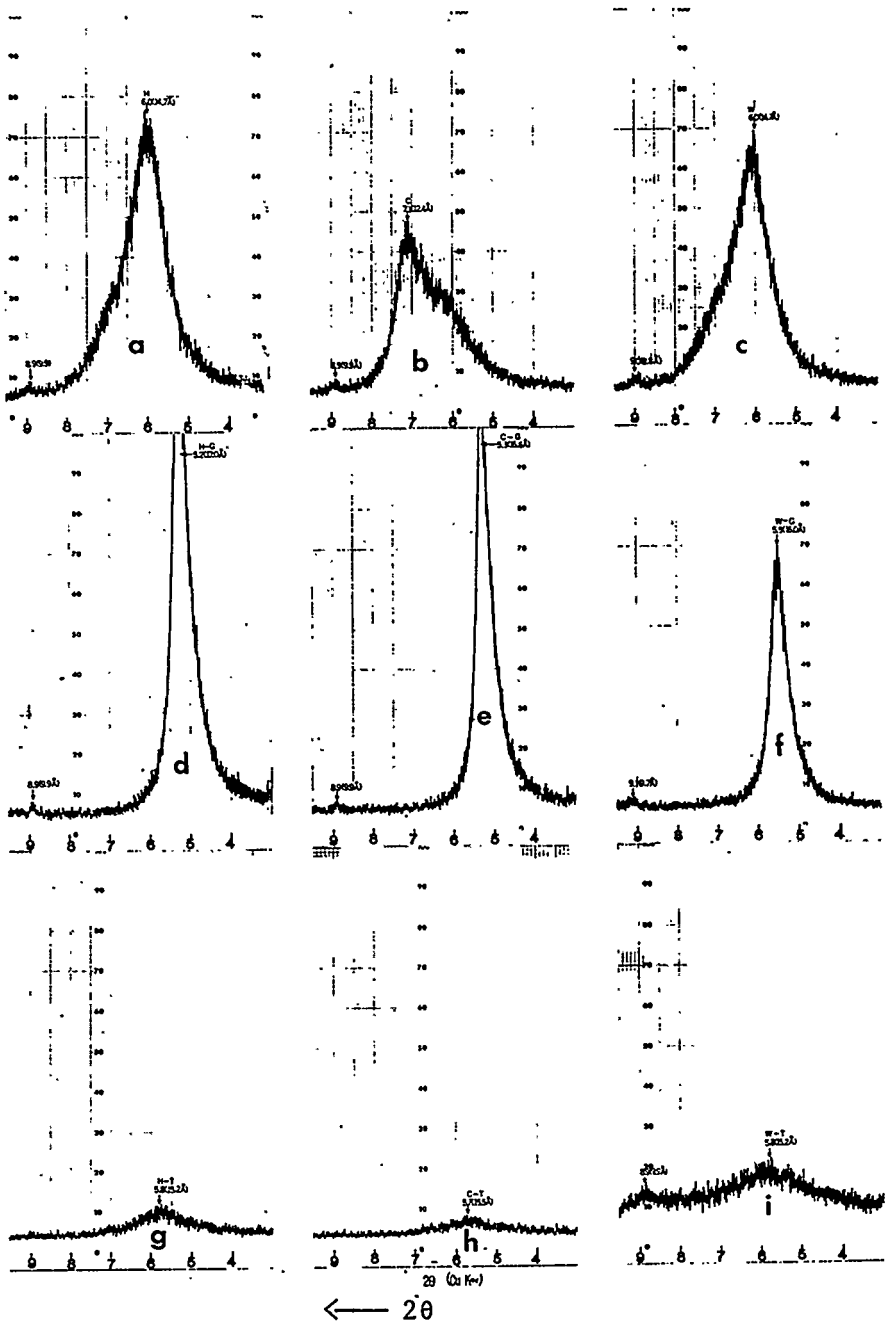

Figure 3.27. Comparison of X-ray diffraction patterns of Phase I test reacted and unreacted montmorillonite present in the centrifuged packing material slurry samples prepared as oriented clay mounts by evaporation of slurry on glass slides; treatment by glycolation, followed by heating to 300°C for one hour. [Range of scan: 2θ = 3.9-5° (d = 9.30-29.4 Å)].

(a) Untreated slurry sampled from heater region
(b) Untreated slurry (control)
(c) Untreated slurry sampled from wall region
(d) Glycolated (60°C) slurry sampled from heater region
(e) Glycolated (60°C) slurry (control)
(f) Glycolated (60°C) slurry sampled from wall region
(g) Heat-treated (300°C) slurry sampled from heater region
(h) Heat-treated (300°C) slurry (control)
(i) Heat-treated (300°C) slurry sampled from wall region.

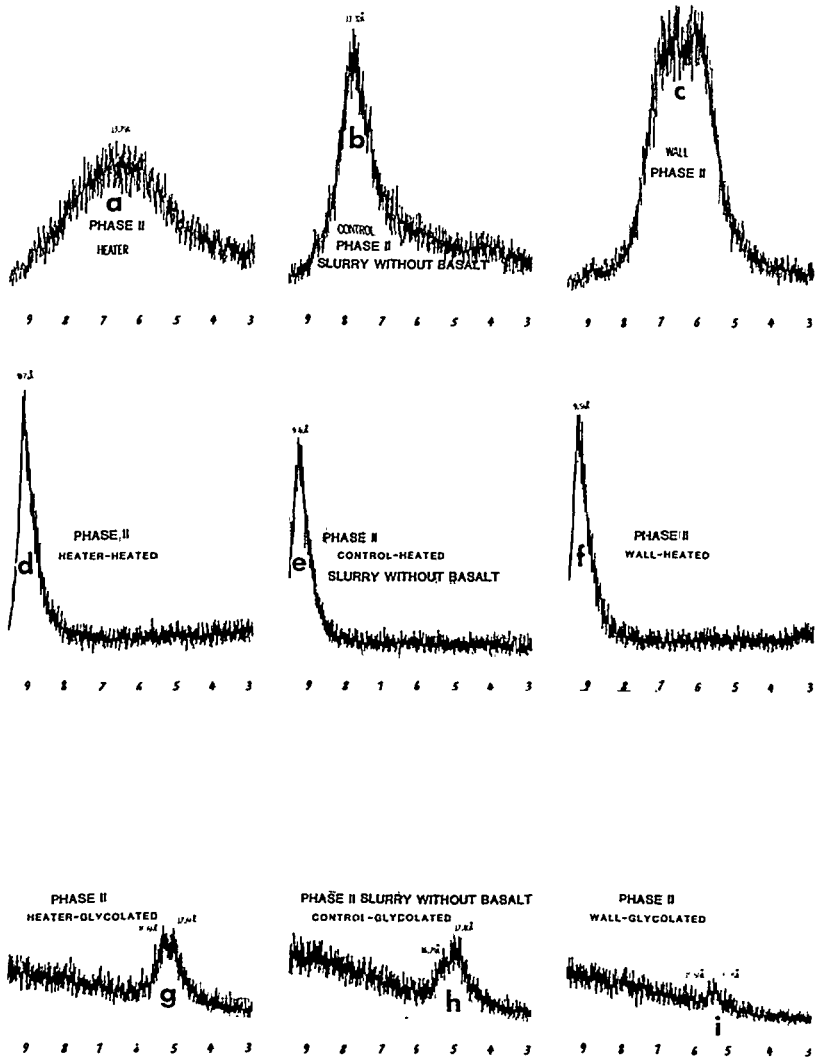

⟵ 2θ

Figure 3.28. Comparison of X-ray diffraction patterns of Phase II test reacted and unreacted montmorillonite present in the centrifuged packing material slurry samples prepared as oriented clay mounts by evaporation of slurry on glass slides; heat-treated at 300°C for 18 hours, followed by glycolation at 60°C. [Range of scan: 2θ = 3-9.5° (d = 9.30-29.4 Å)].

(a) Untreated slurry sampled from heater region
(b) Untreated slurry (control)
(c) Untreated slurry sampled from wall region
(d) Heat-treated (300°C at 18 h) slurry sampled from heater region
(e) Heat-treated (300°C at 18 h) slurry (control)
(f) Heat-treated (300°C at 18 h) slurry sampled from wall region
(g) Glycolated (60°C) slurry sampled from heater region
(h) Glycolated (60°C) slurry (control)
(i) Glycolated (60°C) slurry sampled from wall region.

The second standard treatment for a smectite consists of heating the glycolated samples to 300°C for at least one hour. The interlayer water is removed by this procedure and, characteristically the original (001) reflection collapses and is replaced by one in the ≈9-10 Å region. This is evident upon comparison of Figures 3.27a and g; Figures 3.27b and h; and Figures 3.27c and i. See Columns four through six of Table 3.8. Although these heat-treated samples were not rehydrated to see if the (001) reflection due to swelling would reappear, it is obvious that after heating to 300°C, the expandability has been drastically reduced. The reflection at ≈9-10 Å attributable to the formation of a non-expandable clay was not observed. Additional heating at 300°C may be needed to see this effect. With the loss of interlayer water, montmorillonite may be transformed into hydromica (illite) if sufficient potassium is available, or into chlorite, if sufficient magnesium is present. The main effect of pressure and temperature on a hydrous mineral will be dehydration. Reviews of the literature concerning the hydrothermal stability of the packing material can be found in NUREG/CR-2482, Vols. 3 and 5 (1983) and NUREG/CR-3091, Vols. 1 and 2 (1983).

3.5.7.2.2 Montmorillonite XRD Phase II Test

Similar treatments were given to the Phase II test samples, except that the order of glycolation and heating was reversed. This was done in order to see to what extent swelling would occur after heating. See Figures 3.28a to i. The shifts in d-spacings evident in the diffraction patterns after these treatments are summarized in Table 3.9.

Table 3.9. Comparison of (00ℓ) d-spacings based on X-ray diffractometer studies of Phase II reacted and unreacted montmorillonite, prepared as oriented clay mounts by evaporation of centrifuged packing material slurry on glass slides; treatment by heating to 300°C for 18 hours, followed by glycolation at 60°C. [Intensities not specified. Range of scan: $2\theta = 3\text{-}9.5°$ (d = 9.30-29.4 Å).]

d (Å)								
Heater	Wall Samples Heat-Treated	Control	Heater	Wall Samples Heat-Treated and Glycolated	Control	Heater	Wall Samples Untreated	Control
9.7	9.5	9.60	17.7*	16.0*	17.8*	13.8	13.6	11.3
----	----	----	16.7*	15.6*	16.8*	----	----	----

*Peak intensity is drastically reduced when compared to the peak intensities in the diffraction patterns for the untreated and heated samples.

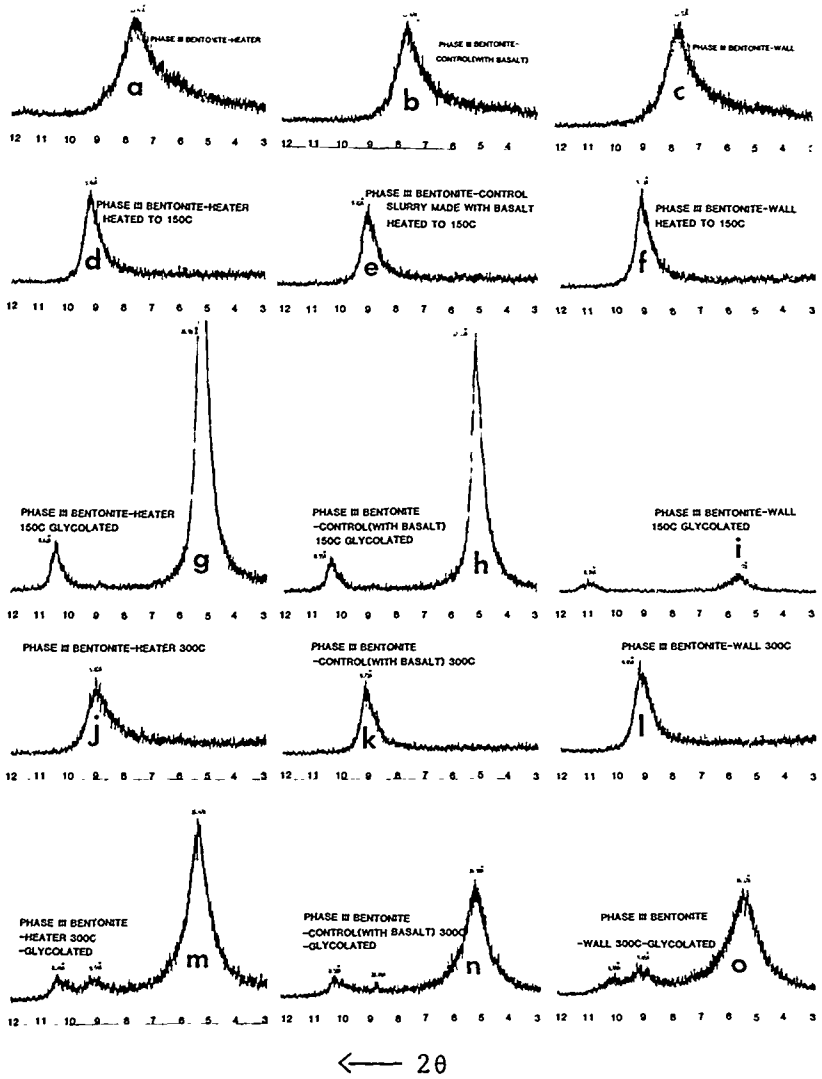

⟵ 2θ

Figure 3.29. Comparison of X-ray diffraction patterns of Phase III test reacted and unreacted montmorillonite present in the centrifuged packing material slurry samples prepared as oriented clay mounts by evaporation of slurry on glass slides; heat-treated at 150°C, followed by glycolation at 60°C, followed by heat-treatment at 300°C, followed by glycolation at 60°C. [Range of scan: 2θ = 3-9.5° (d = 9.30-29.4 Å)].

(a) Untreated slurry sampled from heater region
(b) Untreated slurry (control)
(c) Untreated slurry sampled from wall region
(d) Heat-treated (150°C) slurry sampled from heater region
(e) Heat-treated (150°C) slurry (control)
(f) Heat-treated (150°C) slurry sampled from wall region
(g) Glycolated (60°C) slurry sampled from heater region after heating to 150°C
(h) Glycolated (60°C) slurry (control) after heating to 150°C
(i) Glycolated (60°C) slurry sampled from wall region after heating to 150°C
(j) Heat-treated (300°C) slurry sampled from heater region
(k) Heat-treated (300°C) slurry (control)
(l) Heat-treated (300°C) slurry sampled from wall region
(m) Glycolated (60°C) slurry sampled from heater region after heating to 300°C
(n) Glycolated (60°C) slurry (control) after heating to 300°C
(o) Glycolated (60°C) slurry sampled from wall region after heating to 300°C)

Swelling of the montmorillonite occurred in the Phase II test as evidenced by the shift in d-spacing from 11.3 Å to 13.8 Å (in the sample taken from the heater region) and to 13.6 Å (in the sample taken from the wall region). This is shown in Figures 3.28a to c. Upon heating of the samples to 300°C, the d-spacings of the major montmorillonite peak shifted to a range of 9.5-9.7 Å, indicative of dehydration and collapse of the smectite structure. See Figures 3.28d to f for the XRD patterns of the heated samples. These samples were subsequently glycolated and some swelling did occur as can be seen in Figures 3.28g to i by the shift in the d-spacings to a range of 15.6-17.8 Å. However, the intensity of the peaks is drastically reduced when compared to the intensity of the peaks of the hydrated montmorillonite (Figures 3.28a to c). This seems to indicate that dehydration may not be reversible.

3.5.7.2.3 Montmorillonite XRD Phase III Test

The X-ray diffraction patterns of the samples from the Phase III unirradiated test are shown in Figures 3.29a to c. Various treatments were applied and X-ray diffraction studies subsequently made to determine the effects of the treatments on the expandability of the montmorillonite. The d-spacings for each of the patterns are given in Table 3.10. There was a slight increase in the basal spacing of the untreated reacted samples when compared to the untreated unreacted sample. See Figures 3.29a to c. After heating the samples to 150°C for 12 hours, dehydration with the accompanying decrease in basal spacing occurred, as shown in Figures 3.29d to f. Up to this point, all XRD patterns for the Phase III test samples were very similar to each other. The samples were subsequently glycolated at 60°C to determine differences in expandability. The XRD patterns of the glycolated Phase III test control sample and the Phase III test sample taken from the heater region shown in Figures 3.29g and h show a large increase in the montmorillonite basal spacing, along with the appearance of a new peak. Intensities of these two peaks are similar and are much greater than the corresponding intensities in the XRD patterns of the untreated samples. The XRD pattern of the glycolated heat treated sample taken from the wall region of the Phase III test system shows less expandability of the montmorillonite and decreased intensities of the montmorillonite major peak and of the newly formed one. These samples were then heated to 300°C for several hours and XRD patterns were obtained. Significant and similar decreases in basal spacings are evident in all three samples, as shown in Figures 3.29j to l. Samples were then subjected to glycolation at 60°C. Similar expansion of the basal spacing occurred in all samples, indicating that swelling of the montmorillonite was still occurring and that dehydration was apparently reversible in the case of these samples and their successive treatments.

Table 3.10. Comparison of (00ℓ) d-spacings based on X-ray diffractometer studies of Phase III reacted and unreacted montmorillonite, prepared as oriented clay mounts by evaporation of centrifuged packing material slurry on glass slides; heat-treatment at 150°C, followed by glycolation at 60°C, followed by heat-treatment at 300°C, followed by glycolation at 60°C. [Intensities not specified. Range of scan: 2θ = 3-9.5° (d = 9.30-29.4 Å).]

	d(Å)		
	Heater	Wall	Control
Untreated	11.5	11.3	11.5
Heat-treated (150°C)	9.6	9.7	9.8
Glycolated (60°C)	17.0	15.8*	17.1
	8.6	8.0	8.6
Heat-treated (300°C)	9.8	9.7	9.7
Glycolated (60°C)	16.5	16.2	17.0
	9.5	9.7	10.1
	8.5	8.7	8.6

*Peak intensity is drastically reduced when compared to the peak intensities in the diffraction pattern of the untreated sample.

3.5.7.2.4 Comparison of Montmorillonite XRD Studies For All Tests

A comparison of the d-spacings obtained for untreated and treated montmorillonite samples from the three tests yielded the following conclusions:

- The basal spacings in the samples taken from the wall and heater regions of the irradiated systems are increased in comparison to an unreacted control sample. This suggests that irradiation may enhance expandability.
- The shape and intensity of the major montmorillonite peak in the Phase II test samples differs significantly for the heater sample and the wall sample. This is not true for the corresponding samples of the Phase I and Phase II tests.

- Expandability may be affected by heat treatments. After heating the samples from the Phase II tests for 18 hours at 300°C, and subsequent glycolation, it was apparent that the major montmorillonite peak had almost disappeared. This did not occur in the case of the Phase III test samples after heating at 300°C for several hours. But it should also be noted that other peaks appeared in the Phase III test XRD patterns, indicating that other minerals had been produced. This is also supported by the XRD patterns obtained over the entire range. Qualitatively it can be seen by comparison of the overall patterns that differences exist between the reacted and unreacted clays in each test and in the three different test systems.

3.5.8 Analysis of Reacted Basalt

3.5.8.1 Comparison of XRD Patterns of Pulverized Basalt

The basalt pellets removed from regions near the heater and near the wall in each of the three phases and an unreacted control sample were pulverized and analyzed by XRD to detect any differences due to reaction. Interpretation of the complex diffraction patterns to identify specific changes in mineralogical composition would require a significant effort and is beyond the scope of this work. Polished thin section basalt samples were also prepared and examined with a polarizing microscope to help detect changes in basalt mineralogy.

The XRD patterns for all basalt samples are reproduced in Figure 3.30. The data for the observed (hkℓ) reflections are summarized in Table 3.11. If a comparison of the patterns shown in Figure 3.30 is made, it is obvious that there are differences among the patterns, showing that changes occur in the mineralogical composition of the basalt upon reaction. For example, there is a d-spacing of 4.67 Å for samples taken from the heater region in the irradiated systems which is not present in the samples taken from the wall or heater regions in the unirradiated system. More detailed and comprehensive studies are needed to characterize the changes that occur and to determine the effects of these changes in composition on the repository environment.

A preliminary solids analysis and solution analysis performed in the Wood hydrothermal bentonite/basalt/groundwater non-irradiated experiment (RHO-BW-SA-219P, 1983) at 300°C and 28.9 MPa suggests that the primary reaction in the basalt-bearing system is the dissolution of basalt glass followed by the precipitation of a pure silica phase (that is, cristobalite and/or quartz) and smectite, illite, and mordenite (zeolite). It was thought that some alteration of the bentonite to illite may have occurred but this was not seen when a bentonite/groundwater system was tested in a similar manner.

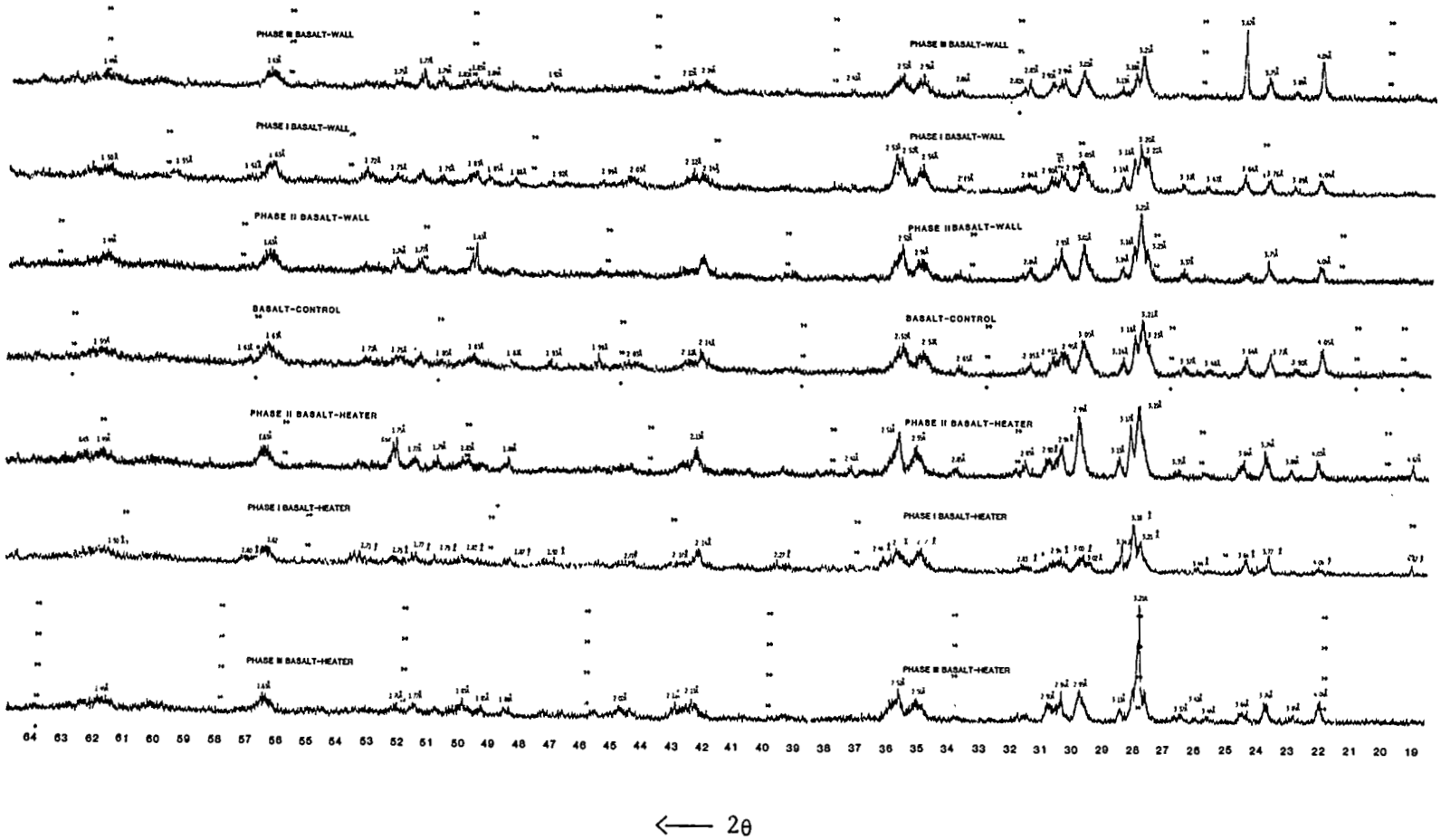

Figure 3.30. Comparison of X-ray diffraction patterns for reacted and unreacted basalt, prepared as unoriented mounts of pulverized basalt. [Range of scan: $2\theta = 3\text{-}65°$ (d = 1.43-29.4 Å)].

Table 3.11. Comparison of (hkℓ) d-spacings based on X-ray diffractometer studies of reacted and unreacted basalt, prepared as unoriented mounts of pulverized basalt. [Intensities not specified. Range of scan: 2θ = 3-65° (d = 1.43-29.4 Å).]

d (Å)						
Wall Sample Phase I Test	Wall Sample Phase II Test	Wall Sample Phase III Test	Heater Sample Phase I Test	Heater Sample Phase II Test	Heater Sample Phase III Test	Control Sample
----	----	----	4.67	4.67	----	----
4.04	4.04	4.04	4.04	4.03	4.04	4.05
3.89	3.88	3.89	----	3.88	3.89	3.90
3.76	3.75	3.75	3.77	3.74	3.74	3.77
3.64	3.64	3.67	3.64	3.64	3.64	3.64
3.47	----	3.47	----	3.46	3.48	3.48
----	3.45	----	3.44	----	3.42	----
3.37	3.37	----	----	3.35	3.37	3.37
3.22	3.23	----	----	----	3.23	3.23
3.20	3.21	3.21	3.21	3.19	3.21	3.21
3.18	3.18	3.18	3.18	3.17	3.18	3.18
3.14	3.14	3.13	3.14	3.13	3.13	3.14
----	----	----	3.02	----	----	----
3.00	3.01	3.01	3.00	2.99	2.99	3.00
2.94	----	2.94	2.94	2.94	2.94	2.95
2.93	2.93	2.93	----	----	----	----
2.90	2.92	2.90	----	2.90	2.90	2.91
2.84	2.84	2.83	2.83	2.83	2.84	2.85
----	2.82	2.82	----	2.80	2.81	----
2.65	2.65	2.66	----	2.65	2.65	2.65
2.56	2.56	2.56	2.57	2.55	2.56	2.57
2.52	2.52	2.52	2.51	2.51	2.52	2.52
2.51	----	2.51	2.48	----	----	----
2.41	----	2.41	----	2.41	----	----
----	----	----	2.27	2.27	----	----
2.14	2.14	2.14	2.14	2.13	2.13	2.14
2.12	2.11	2.12	2.10	2.11	2.11	2.12
2.03	----	2.03	2.02	2.02	2.02	2.03
1.99	1.99	----	----	----	1.99	1.99
----	----	----	----	----	1.95	----
1.92	1.92	1.92	1.92	----	1.93	1.93
1.88	1.87	1.88	1.87	1.88	1.88	1.87
1.85	1.85	1.84	----	1.85	1.85	----
1.83	1.83	1.83	1.83	1.83	1.83	1.83
1.79	1.80	1.79	1.79	1.79	1.79	1.80
1.77	1.77	1.77	1.77	1.77	1.77	1.77
1.75	1.74	1.75	1.75	1.75	1.76	1.75
1.72	1.72	1.72	1.71	1.71	----	1.72
1.63	1.63	1.63	1.62	1.63	1.63	1.63
1.61	1.61	----	1.60	----	----	1.61
1.55	----	----	----	----	----	----
1.50	1.49	1.49	1.50	1.50	1.49	1.50

3.5.8.2 Comparison of Micrographs of Polished Basalt Thin Sections

Examination of polished basalt thin sections under a polarizing microscope revealed the presence of at least three mineralogical phases: plagioclase, pyroxene, and olivine. These were identified by their respective characteristic shapes and optical properties (Kraus, E. H., 1959; Deer, W. A., 1966). The three phases are shown in Figure 3.31. Examination of reacted basalt samples taken from the heater region for each test under the polarizing microscope indicates that plagioclase and olivine appear to be relatively unchanged. However, the pyroxene appears to have been altered, as evident from the alteration features observed on pyroxene grains from a Phase I test sample shown in Figure 3.32. Additionally, there are red-brown areas in the reacted basalt that are not present in the unreacted basalt in samples from the three tests. See Figure 3.33. There do not seem to be gross differences in the irradiated and non-irradiated basalt thin sections under the polarizing microscope. It was observed that there were very few red-brown areas in the Phase III specimen. In the Phase III specimen, they were mainly yellow-brown in color. Compare Figures 3.33 and 3.34. An additional observation is that these areas not present in the unreacted basalt specimen appear to be more numerous in the samples taken from the wall region than in the samples taken from the heater region in all three tests.

Work has been done at BWIP on identifying alteration products resulting from the reaction under hydrothermal conditions at 150°C for 120 days of basalt/bentonite/groundwater (BWIP/NRC Geochemistry Workshop, 1984). It was observed that (1) partial dissolution of basalt mesostasis and clay occurred, (2) smectite structure was preserved, and (3) iron and potassium were substituted in the smectite structure. The reaction product was identified as Fe-smectite. In the present work, XRD analysis of the powdered basalt samples did not reveal any basal spacings $\geq$ 9.6 Å, which is the minimum basal spacing a smectite can display and corresponds to the fully collapsed state (Deer, W. A., 1966)[14].

Much work needs to be conducted to identify the specific mineralogical changes that are occurring in the basalt after reaction. In particular, the effects of the repository conditions on the basaltic glassy phases need to be determined. Also, correlations need to be made between the changes seen microscopically and the changes seen in the XRD patterns.

3.5.9 Metallography of Carbon Steel Sleeve and Identification of Surface Products

In the three phases of the test program, individual 1020 carbon steel sleeves were used to simulate the waste container. End caps were welded on to isolate the internal heater. The sleeves (25.4-mm diameter, 155-mm length and

[14]The observable range of d-spacings was 1.43-29.4 Å. Any d-spacings greater than 29.4 Å would not have been seen.

Figure 3.31. Minerals in unreacted basalt as determined with a polarizing microscope under crossed polars (100X). (Key: Pl = plagioclase, P_y = pyroxene and O = olivine.)

Figure 3.32. Minerals in Phase I test reacted basalt sampled from the heater region as determined with a polarizing microscope under crossed polars (100X). (Key: Pl = plagioclase, P_y = pyroxene and O = olivine.)

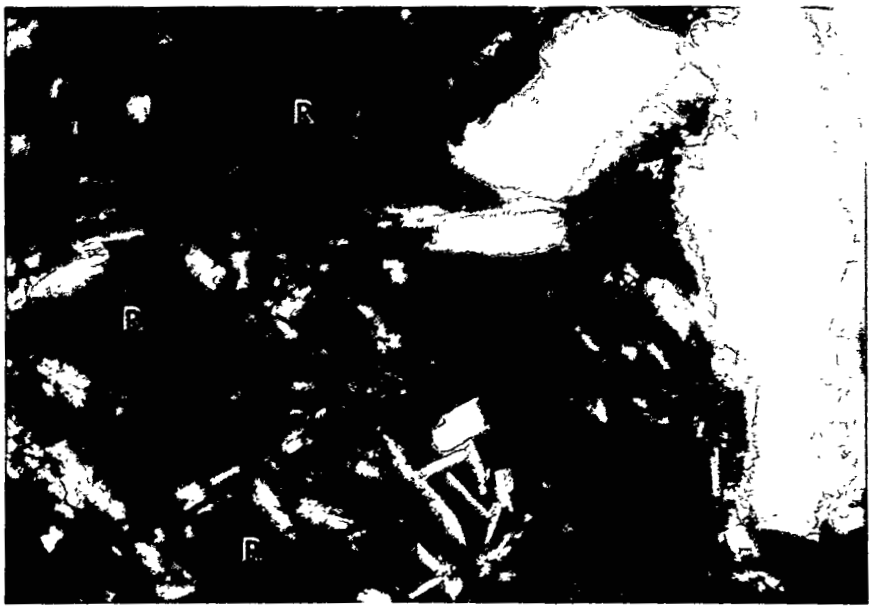

Figure 3.33. Minerals in Phase I test reacted basalt sampled from the wall region as determined with a polarizing microscope under crossed polars (100X). (Red-brown areas are indicated by R in photo.)

Figure 3.34. Minerals in the Phase III test reacted basalt sampled from the wall region as determined with a polarizing microscope under crossed polars (100X). (Yellow-brown areas are indicated by y in photo.)

2-mm thick) were removed from the stainless steel autoclave after the packing material slurries had been examined after the 60-day test periods. Figure 3.35 shows the reacted sleeve after the Phase I test and compares it to one which was not tested. It should be noted that the sleeve for the Phase I test was in the as-received condition whereas the Phase II and Phase III test sleeves were polished through 600-grit silicon carbide paper, in an attempt to remove the decarburized surface layer which was introduced by tube manufacturing processes.

3.5.9.1 Metallography of Phase I Test Sleeve

Figure 3.36 shows a metallographic section perpendicular to the axis of the Phase I steel sleeve. The steel consists primarily of white ferritic grains interspersed with dark pearlitic regions. A thin gray oxide layer is observed on the outer surface, which was in contact with the packing material. The oxide is adherent but in certain locations is found to be fractured. Within the two-month testing period at 150°C, no obvious surface pitting or intergranular corrosion was observed. Small indentations which were present originated in the starting material. Immediately above the oxide, a slightly thicker black layer (indicated by arrow) is just discernible between the oxide and plastic compound used to mount the sample for metallographic preparation. Figure 3.37 is a micrograph taken at a different location and shows a thicker dark layer (between the arrows). This represents an adherent orange-red clay layer which remained after most of the basalt/bentonite mixture contacting it was removed. Samples of this layer were mechanically removed and subjected to X-ray diffraction. It seems from a comparison of Figures 3.36 and 3.37 that the metal oxide layer is thinner in regions where the orange-red layer is thick. This indicates that this adherent layer minimized uniform corrosion.

Analysis by SEM-EDX of the sleeve surface product revealed the presence of a material similar in composition to a sample of bentonite that was examined separately. However, there were some compositional differences at various locations on the sleeve, as the semi-quantitative elemental analyses revealed. The elemental analysis of bentonite clay by SEM-EDX shows that Si is the most abundant element (≈75%), with some Al (≈15%) and Fe (≈6%), and minor amounts of other elements (≈4%). At some sites on the sleeve, the surface products that were probed showed more Fe relative to the amount indicated in bentonite. For some sites, the Fe and Si peaks were similar in intensity but in others the Fe peaks were much stronger than those for Si. One surface product sample, shown in Figure 3.38, is a layered material whose elemental composition was mainly Fe with some Si and a small amount of Mg. There was not sufficient material, however, to pursue more quantitative experiments.

As noted above, the Phase I test sleeve, which was used in the as-received condition, was decarburized to a depth of approximately 50 microns (Figures 3.36 and 3.37). Figure 3.39, showing a section through a non-reacted steel tube, proves that decarburization was a result of standard manufacturing processes rather than from hydrothermal testing.

During the Phase I test, the slurry level inside the autoclave had fallen to a level below the top of the carbon steel sleeve. Above this waterline,

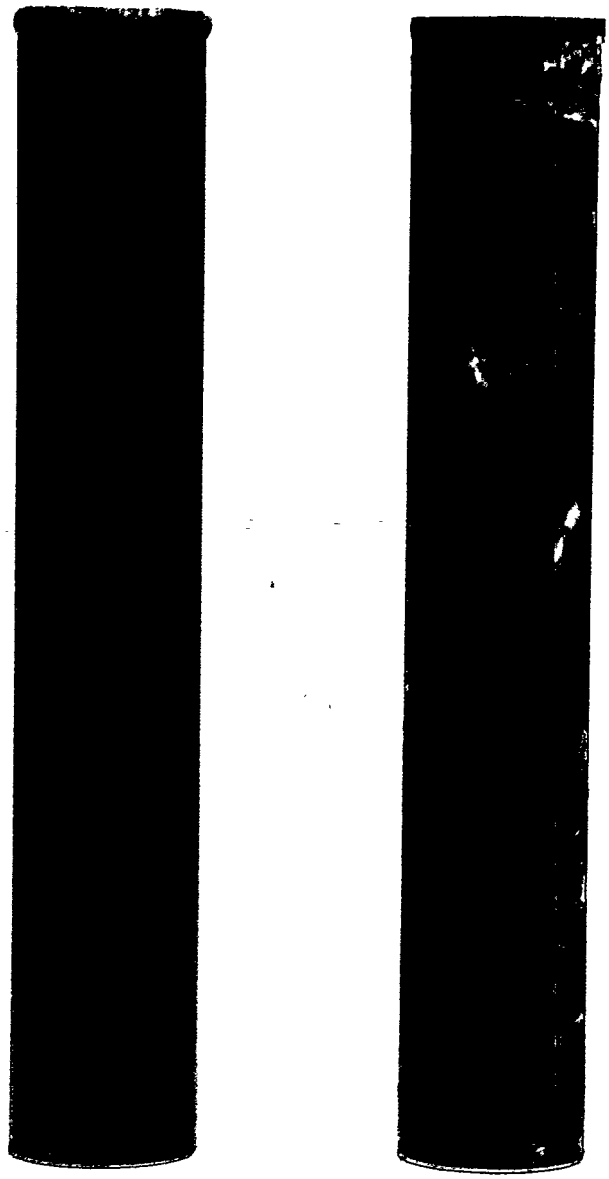

Figure 3.35. Appearance of carbon steel sleeve prior to reaction (left) and subsequent to Phase I test reaction (right). (Sleeves are shown full-scale.)

Figure 3.36. Micrograph of outside diameter of carbon steel sleeve subsequent to Phase I test rection showing metal oxide and thin clay deposition layer (marked by arrow) (250X).

Figure 3.37. Micrograph of outside diameter of carbon steel sleeve subsequent to Phase I test reaction showing metal oxide and thick clay deposition layer between arrows (250X).

Figure 3.38. SEM-EDX micrograph of iron-rich layered material in Phase I test carbon steel surface product (1000X).

Figure 3.39. Micrograph of outside diameter of carbon steel sleeve prior to Phase I test reaction (250X). (Note the presence of decarburized surface.)

accelerated corrosion at the welded end cap was evident (Figure 3.35). The occurrence of more severe corrosion on the steel exposed to vapor has been reported in another study (PNL-4452, 1983). In that work, cast ductile iron was placed in an autoclave with oxic basaltic groundwater and crushed basalt at a temperature of 250°C, a pressure of 5.2 MPa (700 psi) and a gamma dose rate of $\approx 2 \times 10^5$ rad/h for periods up to three months with no bentonite present. Between the one- and three-month test periods, the autoclave operated in the vapor phase for several days, apparently because of a slightly elevated temperature. The present observation of accelerated corrosion in the vapor phase could, therefore, be associated with higher oxygen levels or, possibly, with waterline corrosion.

Figure 3.40 shows the appearance of weld metal at the top of the Phase I test steel sleeve. A thin broken oxide layer is just visible. Fusion of the metal has removed the decarburized layer and ferrite-rich grain boundary regions are formed. Again, no pitting or intergranular attack was detected.

3.5.9.2 Metallography of Phase II Test Sleeve

In the Phase II test, prior polishing of the sleeve had removed the decarburized surface layer (Figure 3.41). A very thin, irregular surface oxide is seen above which is a thin clay layer (between arrows). Several hemispherically-shaped pits are present. These are approximately 12 microns in depth after the 60-day reaction period. If one makes the highly conservative assumption that the pit depth increases linearly with time, then the depth after the minimum 300-year radionuclide containment period would be 2.2 cm. This would be insufficient to penetrate any of the carbon steel containers specified by Westinghouse Electric Corporation for conceptual waste package designs (AESD-TME-3142, 1982). For these, the container wall thicknesses vary between 5.3 and 8.7 cm.

The adherent materials on the Phase II test sleeve were studied with SEM-EDX, electron diffraction, and electron energy loss spectroscopy (EELS) in an attempt to identify the orange-brown portion and magnetic green-yellow portion. Micrographs of these materials are shown in Figures 3.42 and 3.43, respectively. The EDX analyses of these samples showed that (1) the orange-brown material contained large amounts of Si, Fe and Al with some Ca, Mg and S in the darker areas, and some Ca, Mg and K in the lighter areas and (2) the green-yellow material contained large amounts of Fe and Si with some Al, Mg and Ca. The samples were shown to be well-defined crystalline materials that contained oxygen by use of EELS. See Figure 3.44 for the two-point plot of the EELS spectrum of the orange-brown material. A similar one was obtained for the green-yellow specimen. Subsequently Debye-Scherrer patterns were obtained (see Figures 45 and 46). The d-spacings were calculated by measuring the patterns, which had been calibrated against a gold standard and are listed in Table 3.12. They did not match any of the spacings reported for common iron-silicate materials. It is believed that these specimens contain hydroxyl groups and/or water molecules because they were degraded by an electron beam. The identify of these materials is not presently known.

Figure 3.40. Micrograph of weld metal in carbon steel sleeve subsequent to Phase I test reaction (250X).

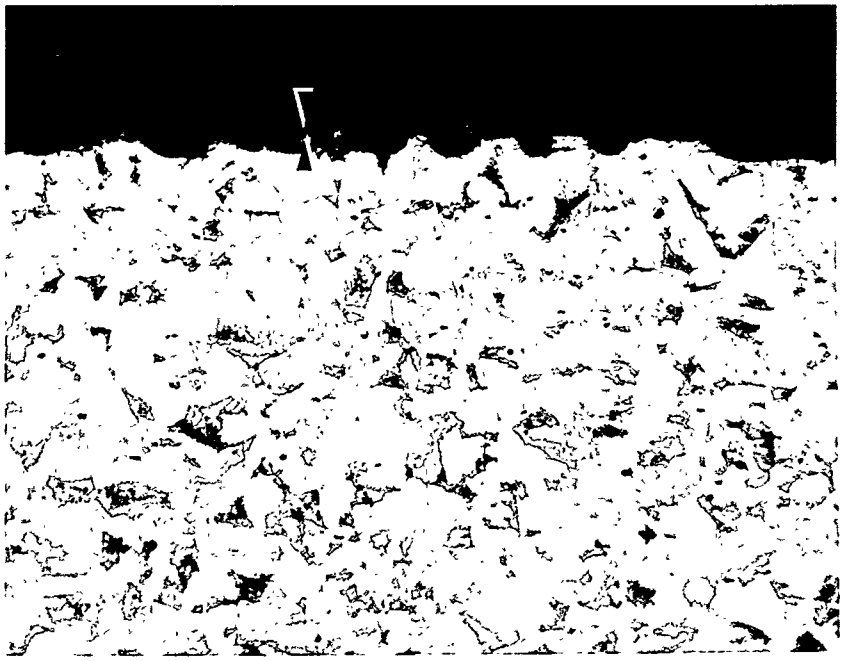

Figure 3.41. Micrograph of outside diameter of carbon steel sleeve subsequent to Phase II test reaction showing metal oxide and thin clay deposition layer (marked by arrows) (250X).

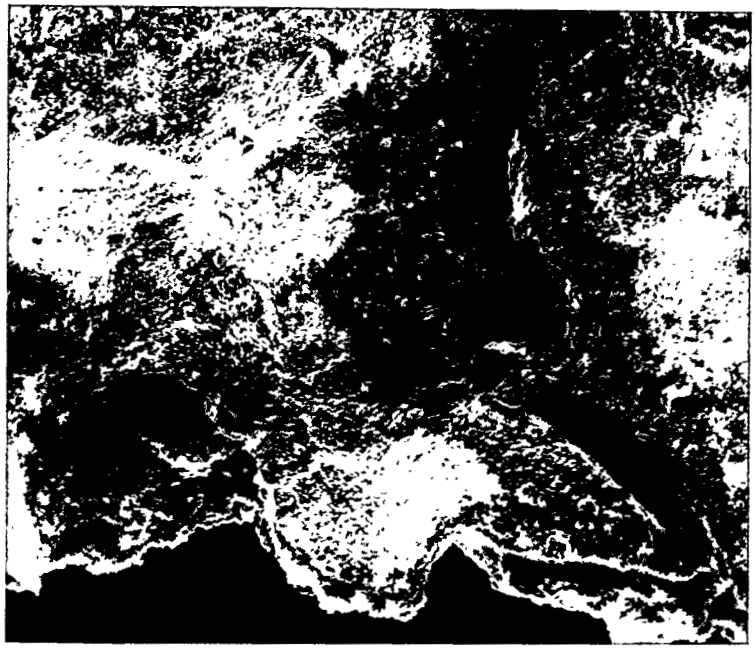

Figure 3.42. Micrograph (SEM) of orange-brown sleeve surface product from Phase II test (100X).

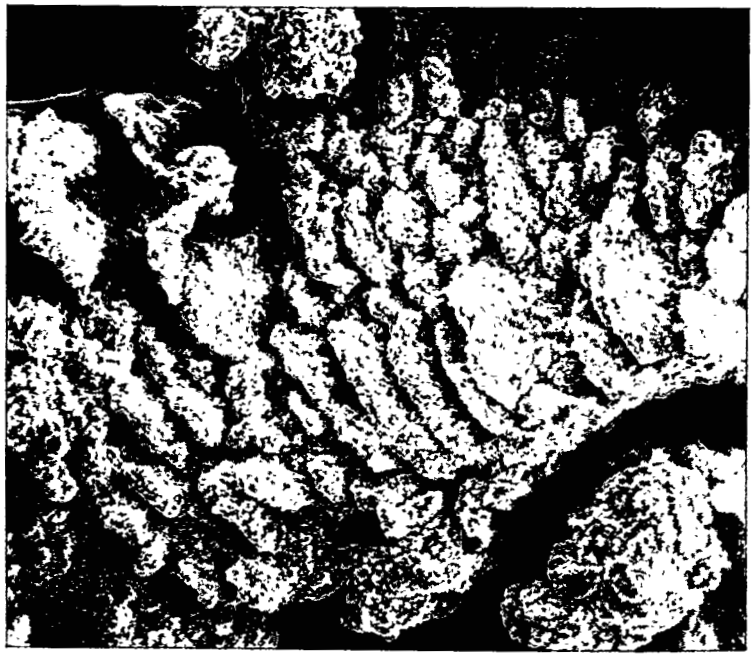

Figure 3.43. Micrograph (SEM) of magnetic green-yellow sleeve surface product from Phase II test (100X).

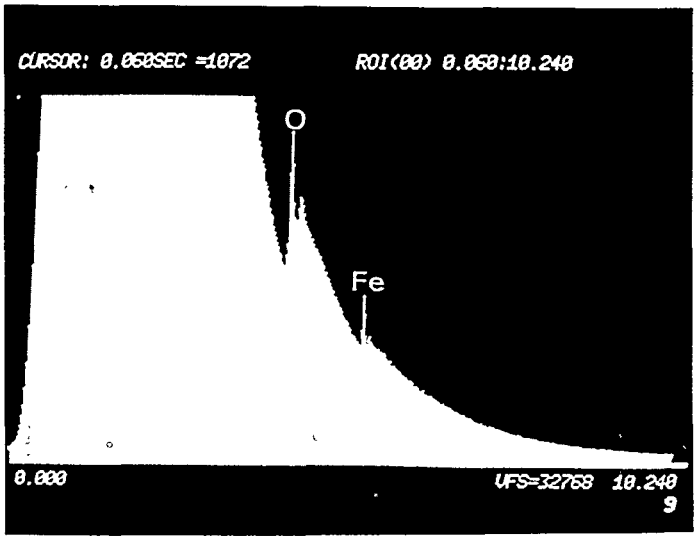

Figure 3.44. Point plot of EELS spectrum of orange-brown sleeve surface product from the Phase II test showing well-defined crystalline material containing iron and oxygen.

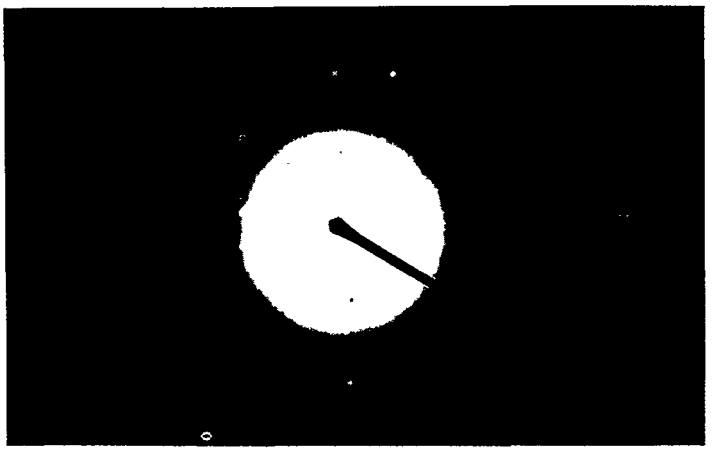

Figure 3.45. Debye-Scherrer powder pattern for orange-brown sleeve surface product from Phase III test.

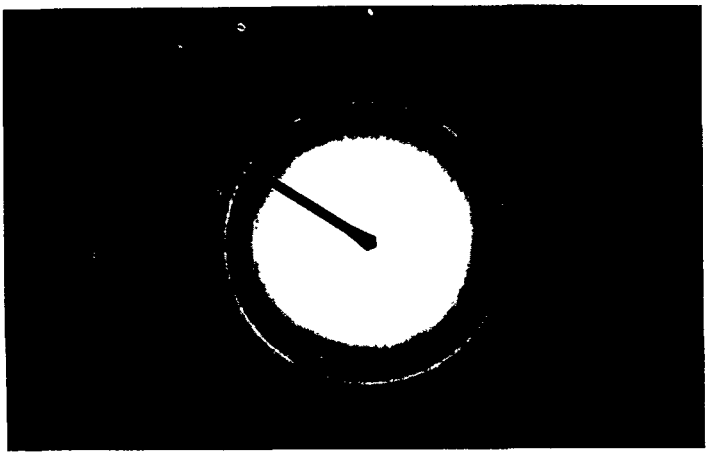

Figure 3.46. Debye-Scherrer powder pattern for green-yellow sleeve surface product from Phase II test.

Table 3.12. Calculated d-spacings of Phase II test sleeve surface product based on measured Debye-Scherrer electron diffraction powder patterns.[a]

d (Å) Green Oxide[b]	d (Å) Red (Orange) Oxide[b]
4.69	4.40
2.60	2.49
1.76	1.63
1.55	1.47
1.36	1.26
1.00	----

[a]Spacings were calculated based on the measured patterns. A gold standard was used for calibration.
[b]Oxygen was determined to be present by use of EELS (electron energy loss spectroscopy).

3.5.9.3 Metallography of Phase III Sleeve

In the Phase III control test, carried out in a non-irradiation environment, pitting is also observed (see Figure 3.47). The pits in this case are more shallow and more closely spaced than those in the Phase II experiment (Figure 3.41). Based on an assumed linear pit propagation rate, the pit depth after 300 years would be about 1.5 cm. It should be noted that polishing the carbon steel sleeve prior to testing did not completely remove the surface-decarburized layer. Therefore, pit initiation and growth do not seem to be dependent on the presence of carbide phases. Figure 3.47 also shows a thin oxide layer which was detached from the metal substrate. It is approximately seven microns in thickness, which is similar to the oxide thickness for the Phase I test sleeve shown in Figure 3.36. If the oxide is assumed to be magnetite (Fe_3O_4), it may be shown that the 7-μ oxide layer was formed from 3.2 μ of steel during the 60-day test period[15]. Again, a highly conservative assumption of a linear rate for uniform corrosion gives a metal loss of 0.6 cm in 300 years. Thus, uniform corrosion will not be a significant failure mode for a carbon steel container in a basalt repository.

The material adhering to the Phase III test carbon steel sleeve was analyzed by SEM-EDX and X-ray diffraction to determine if an identification could be made. One product was green in color. A micrograph and EDX analysis of

[15]The amount of O_2 present in this amount of magnetite is estimated to be ≈140 mg. There is a maximum of 22 mg of O_2 in the plenum and dissolved in the water. The remaining O_2 probably originates from adsorbed oxygen and/or radiolysis of water.

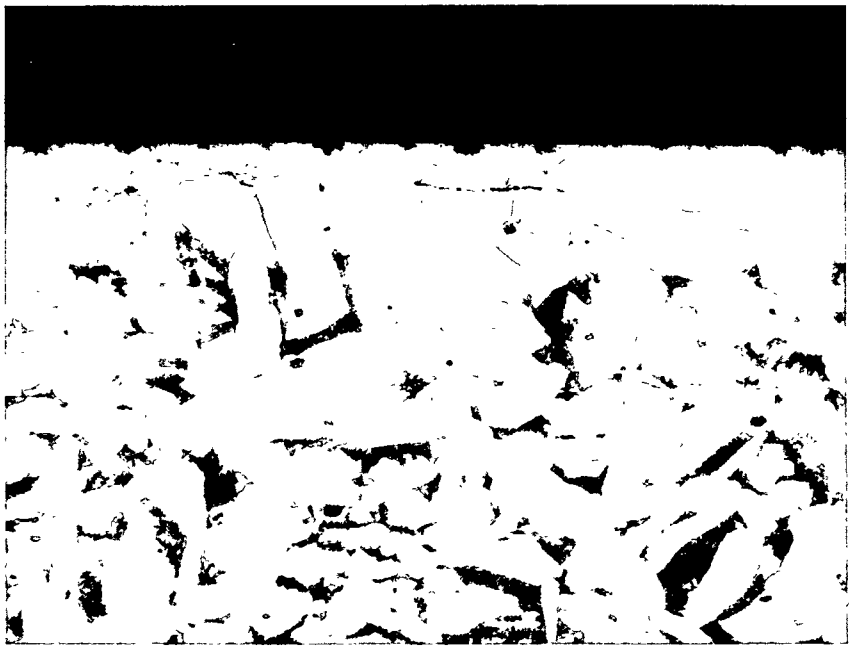

Figure 3.47. Micrograph of outside diameter of carbon steel sleeve subsequent to Phase III test showing pitting, and a thin detached oxide layer (250X).

this material are shown in Figures 3.48 and 3.49. The other product was orange-brown in color and relevant information is given in Figures 3.50 and 3.51. Both materials contain large amounts of Si and Fe. The green product also has a high Ca content. Some Mg, Al, and Cl are also present in each. The XRD diffraction pattern (scan range $2\theta = 3\text{-}68°$) of the orange-brown material yielded five sets of d-spacings: 3.03-3.08 Å, 2.51-2.56 Å, 2.10-2.11 Å, 1.91-1.93 Å and 1.88-1.89 Å. This compound or mixture of compounds was not identifiable.

3.5.9.4 Comparison of Pitting Corrosion For All Tests

The results of the carbon steel corrosion evaluations show that pitting may occur during 60-day tests at 150°C in the presence of basalt/bentonite packing material. Gamma irradiation and surface decarburization of the steel did not have a significant influence on the initiation of pitting. Pits were only found, however, on pre-polished metal surfaces exposed to methane-containing water. It is not clear whether the surface polishing or the methane was responsible for this type of corrosion. Although the pitting rates obtained in this study were found to be too low to penetrate a typical steel container for a basalt repository, it must be realized that the test temperature of 150°C is much lower than the maximum value of about 300°C relevant to actual container conditions.

3.6. Summary

The objective of this program was to determine the chemical environment that will be present within high level nuclear waste packages emplaced in a basalt repository. For this purpose, low carbon 1020 steel (current BWIP reference container material), synthetic basaltic groundwater and a mixture of bentonite and basalt were exposed in an autoclave to a specific repository condition after sealing (150°C, 1500 psi) in a gamma radiation environment with a dose rate of $(3.8 \pm 0.5) \times 10^4$ rad/h. The experiment consisted of three test phases.

The Phase I test involved a two-month irradiation test in an argon environment. The Phase II test is a similar test in a methane environment in the presence of radiation. These two tests were followed by a Phase III control test which is similar to the Phase II study but which was conducted in the absence of radiation.

A summary of findings is given below:

- Over the two-month test periods, the gas pressure in the autoclave ranged from 9.3-9.7 MPa in the Phase I test, from 11.1-13.2 MPa in the Phase II test and from 9.8-11.7 MPa in the Phase III test. There was a trend to decreasing pressures followed by a trend to pressures approaching or slightly exceeding the initial values.

- In all three tests, hydrogen was produced and oxygen was consumed, as determined by gas analyses and dissolved oxygen measurements. More hydrogen was produced in the Phase II test than in the Phase I and III

Figure 3.48. Micrograph of Phase III test green carbon steel surface product (100X).

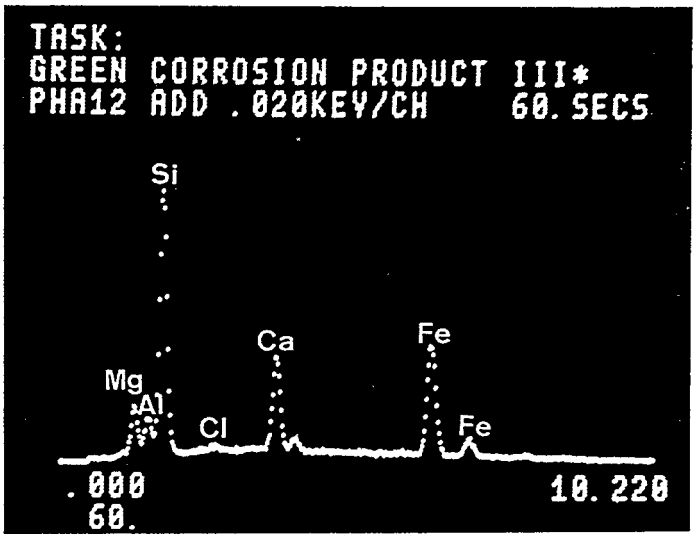

Figure 3.49. EDX of Phase III test green carbon steel surface product.

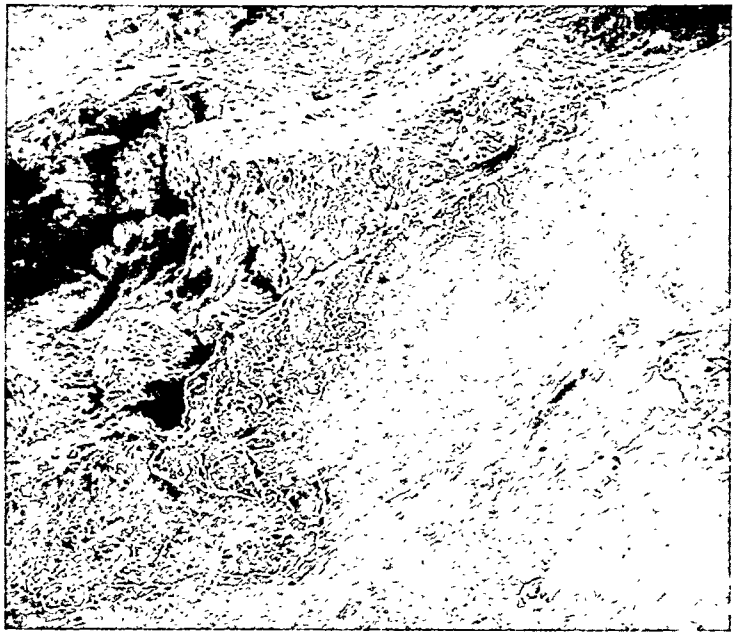

Figure 3.50. Micrograph of Phase III test orange-brown carbon steel surface product (100X).

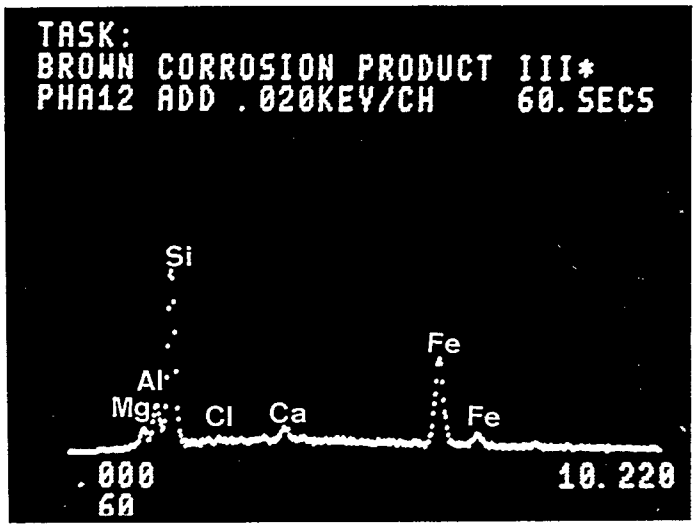

Figure 3.51. EDX of Phase III test orange-brown carbon steel surface product.

tests due to the radiolysis of methane. Similar amounts of hydrogen were produced in the irradiated Phase I test and in the non-irradiated Phase III test.

- After cooling the autoclave over a period of 25 minutes, the pH of the water in the basalt/bentonite packing material measured at room temperature was nearly neutral. There did not appear to be a significant change in pH across the thermal gradient in the packing material in any of the three tests.

- There did not appear to be a significant change in DO across the thermal gradient of the packing material in any of the three tests.

- The calculated Eh values indicated that an oxidizing environment existed after quenching the contents of the autoclave. Radiolysis of groundwater did not appear to increase the oxidizing potential overall.

- The concentration of Cl^- and SO_4^{2-} measured at room temperature were significantly greater near the cooler end of the thermal gradient in the tests.

- The bulk of the Fe and Si content of the reacted water is present as colloidal material that is filterable. Gamma radiation enhanced colloid formation.

- Hydrothermal conditions cause some change in the bentonite component of the packing material including dehydration and loss of the smectite structure. Such changes will likely influence water migration rates through the packing material.

- Optical and XRD studies indicate that some changes occur in the mineralogical content of basalt during hydrothermal testing. However, these were not quantified in this program.

- There was no pitting on the carbon steel sleeve or the steel weldment in the Phase I test. There were hemispherically-shaped pits approximately 12 μ in depth after 60 days of irradiation in the Phase II test. In the Phase III test, shallower (approximately 8 μ in depth) and more closely-spaced pits were formed on the carbon steel sleeve. At this time it is not clear whether surface polishing of the steel or the presence of methane is responsible for the pitting. Based on a highly conservative assumption of linear pitting rates the maximum pit-depth after 300 years is about 2.2 cm.

- Adherent surface products removed from the carbon steel sleeve in the Phase I test contained mainly montmorillonite clay. SEM-EDX analysis indicated the presence of other materials containing more Fe than that found in the montmorillonite. Surface products removed from the carbon steel sleeve in the Phase II test were analyzed by SEM-EDX and electron diffraction but were not readily identifiable. (An orange-brown product contained large amounts of Si, Fe, and Al, while the green-yellow product was largely composed of Fe and Si.) Identification was

also not possible for the Phase III surface products, which were analyzed by SEM-EDX and XRD. Both Phase III surface products contained large amounts of Si and Fe, with the green phase also containing a large amount of Ca.

3.7. Recommendations for Future Work

The following recommendations are made for additional and confirmatory experiments:

- A number of identical experiments need to be performed to establish statistical variations.
- Longer term experiments should be performed to determine changes in gas composition and pressure buildup.
- The effect of quenching the autoclave on the measured values of pH, DO, Cl^-, SO_4^{2-} and Fe needs to be determined.
- Changes in the clay and basalt during hydrothermal reaction need to be specified and explained to predict long term performance.
- Full characterization of the colloidal material in terms of composition and size distribution needs to be performed.
- Mineralogical changes in the basalt, especially with regard to the glassy phases, need to be fully evaluated. Correlations could be made with predictions generated by use of geochemical codes, such as WATEQ and PHREEQE.
- Long term corrosion studies are needed to determine the extent of localized corrosion in container steels. Hydrogen uptake by steel, and its effect on embrittlement also needs to be established.
- Applicability of the current laboratory data to repository environments needs to be established by in situ experiments. These experiments should simulate hydrothermal conditions and may involve pressurizing a test borehole. Similar tests will need to be developed and conducted for waste package performance experiments. Repository field tests, such as those which have been carried out by WIPP (SAND 83-1516C, 1983), may provide a basis for designing tests relevant to a basalt repository.

3.8. References

AESD-TME-3142, "Waste Package Conceptual Designs for a Nuclear Repository in Basalt," C. R. Bolmgren and others, Westinghouse Electric Corporation, 1982.

ANL-83-19, "Fuel Cycle Programs - Quarterly Progress Report, October-December 1982," J. J. Steindler and others, Argonne National Laboratory, 1983.

Arai, H., S. Nagai, K. Matsuda and M. Hatada, "Effect of Irradiation Temperature on the Radiolysis of Methane," Radiat. Phys. Chem. 17, 151-157, 1981.

Bonham, L. C., "Solubility of Methane in Water at Elevated Temperatures and Pressures," American Association of Petroleum Geologists Bulletin 62, 2478-2488, 1978.

Braker, W. and A. L. Mossman, Gas Data Book, Matheson Gas Products, Inc., Secaucus, New Jersey, 1980.

Brunauer, S., P. H. Emmett and E. Teller, "Adsorption of Gases in Multimolecular Layers," J. Amer. Chem. Soc. 60, 309-319, 1938.

BWIP/NRC Geochemistry Workshop, January 9-12, 1984, Richland, Washington.

Carroll, D., Clay Minerals: A Guide to Their X-Ray Identification, Geological Society of America, Boulder, Colorado, 1970.

Dean, J. A., Lange's Handbook of Chemistry, McGraw-Hill, 1979, p. 10-5.

Deer, W. A., R. A. Howie and J. Zussman, An Introduction to the Rock-Forming Minerals, London, Longnam Group Ltd, 1966.

DOE/RL 82-3, Vol. II, "Site Characterization Report for the Basalt Waste Isolation Project," November 1982.

DP-1464, "Radiolytic Gas Production From Concrete Containing Savannah River Plant Waste," N. E. Bibler, Savannah River Laboratory, January 1978.

DP-MS-76-51, "Radiolytic Gas Production During Long-Term Storage of Nuclear Wastes," N. E. Bibler, Savannah River Laboratory, October 1976.

Draganic, I. G. and Z. D. Draganic, The Radiation Chemistry of Water, New York, Academic Press, 1971.

Greenberg, A. E., J. T. Connors and D. Jenkins, Standard Methods for the Examination of Water and Wastewater, American Public Health Association, Washington, D. C., 1981.

Grimshaw, R. W., The Chemistry and Physics of Clays and Other Ceramic Materials, New York, John Wiley and Sons, 1971.

Hall, E. E., "Corrosion of Cast Iron and Low Carbon Steel Nuclear Waste Containers in a Basalt Repository," U. S. Nuclear Regulatory Commission, August 1982.

Himmelblau, D. M., "Solubilities of Inert Gases in Water, 0°C to Near the Critical Point of Water," J. Chem. Eng. Data, Vol. 5, 10-15, 1960.

Kraus, E. H., W. F. Hunt and L. S. Ramsdell, Mineralogy, New York, McGraw-Hill, 1959.

Krumhansl, J. L., "Mineralogic Stability of a Bentonite Backfill in a Bedded Salt Repository Environment," Abstract for 1982 Meeting Geological Society of America.

Lerman, A., Geochemical Processes Water and Sediment Environments, New York, Wiley, 1979, p. 389.

Maurin, J., "Etude de la Radiolyse due Methane en Phase Gazeuse, J. Chim. Phys. 59, 15-26, 1962.

Norfolk, D. J. and T. Swan, "Gamma Radiolysis of Methane Adsorbed on Gamma-Alumina - Part I: Development of Sites Active in Energy Transfer," J. Chem. Soc. Faraday Trans. I 73, 1454-1466, 1977.

Norfolk, D. J., R. F. Skinner and W. J. Williams, "Hydrocarbon Chemistry in Irradiated $CO_2/CO/CH_4/H_2O/H_2$ Mixtures - I," Radiat. Phys. Chem. 21, 307-319, 1983.

NUREG-0960, Vol. 2, "Draft Site Characterization Analysis of the Site Characterization Report for the Basalt Waste Isolation Project," U. S. Nuclear Regulatory Commission, March 1983.

NUREG/CR-2482, Vol. 3, BNL-NUREG-51494, "Review of DOE Waste Package Program: Subtask 1.1 - National Waste Package Program, April 1982-September 1982," P. Soo and others, Brookhaven National Laboratory, March 1983.

NUREG/CR-2482, Vol. 4, BNL-NUREG-51494, "Review of DOE Waste Package Program: Subtask 1.1 - National Waste Package Program, October 1982-March 1983," P. Soo and others, Brookhaven National Laboratory, September 1983.

NUREG/CR-3091, Vol. 1, BNL-NUREG-51630, "Review of Waste Package Verification Tests: Semiannual Report Covering the Period April-September 1982," P. Soo and others, Brookhaven National Laboratory, April 1983.

NUREG/CR-3091, Vol. 2, BNL-NUREG-51630, "Review of Waste Package Verification Tests: Semiannual Report Covering the Period October 1982-March 1983," P. Soo and others, Brookhaven National Laboratory, August 1983.

NUREG/CR-3091, Vol. 3, BNL-NUREG-51630, "Review of Waste Package Verification Tests: Biannual Report," B. Siskind and others, December 1983.

NUREG/CR-3389, "Valence Effects on the Sorption of Nuclides on Rocks and Minerals," R. E. Meyer, W. D. Arnold and F. I. Case, Oak Ridge National Laboratory, February 1984.

PNL-4452, "Nuclear Waste Package Materials Testing Report: Basalt and Tuffaceous Environments," D. J. Bradley and others, Pacific Northwest Laboratory, March 1983.

RHO-BW-SA-219P, "Experimental Investigation of Sodium Bentonite Stability in Hanford Basalt," M. I. Wood, Rockwell Hanford Operations, 1983.

RHO-BW-SA-303P, "Repository and Waste Package Designs for High Level Nuclear Waste Disposal," M. J. Smith and others, Rockwell Hanford, 1983.

RHO-BW-SA-315P, "Gamma Radiolysis Effects on Grande Ronde Basalt Groundwater," W. J. Gray, Pacific Northwest Laboratory, October 1983.

RHO-BW-ST-21P, "Evaluation of Sodium Bentonite and Crushed Basalt as Waste Package Backfill Materials," M. I. Wood, G. D. Aden and D. L. Lane, Rockwell Hanford Operations, October 1982.

RHO-BWI-C-66, "Preliminary Geochemical and Physical Testing of Materials for Plugging Man-Made Accesses to a Repository in Basalt," C. L. Taylor and others, Rockwell Hanford, April 1980.

RHO-BWI-C-105, "The Geochemical Behavior of Supercalcine Waste Form: Its Stability in a Basalt Environment," J. R. Halloway and others, Rockwell Hanford Operations, June 1981.

RHO-RE-SR-5, "Reference Material Chemistry - Synthetic Groundwater Formation," T. E. Jones, Rockwell Hanford Operations, April 1982.

Rose, A. J., Tables permettant le depouillement des diagrammes de rayons X et Abaques de reglage des monochromateurs a lame caurbe, Paris, Centre National de la Recherche Scientifique, 1957.

SAND 83-1516C, "The Waste Package Materials Field Test in S. E. New Mexico Salt," M. A. Molecke and T. M. Torres, Sandia National Laboratories, November 1983.

SD-BWI-TP-022, "Barrier Materials Test Plan," Rockwell Hanford Operations, March 1984.

Seyfried, W. E., Jr. and J. L. Bischoff, "Low Temperature Basalt Alteration by Seawater: An Experimental Study at 70°C and 150°C," Geochimica et Cosmochimica Acta 43, 1937-1947, 1979.

Stevens, G. C., R. M. Clarke and E. J. Hart, "Radiolysis of Aqueous Methane Solutions," J. Phys. Chem. 76, 3863-3867, 1972.

Stoessell, R. K. and P. A. Byrne, "Methane Solubilities in Clay Slurries," Clays and Clay Minerals 30, 67-72, 1982.

Van Olphen, H., An Introduction to Clay Colloid Chemistry, New York, Wiley, 1977.

Van Olphen, H. and J. J. Fripiat, Data Handbook for Clay Materials and Other Non-Metallic Minerals, Oxford, England, Pergamon Press, 1979, p. 19.

4. TESTING FOR STRESS CORROSION CRACKING OF HIGH LEVEL WASTE CONTAINER MATERIALS IN TUFF REPOSITORY ENVIRONMENTS

4.1 Introduction

The Nevada Nuclear Waste Storage Investigations (NNWSI) project is developing a waste package for the disposal of high level nuclear waste in a tuff repository. One of the reasons that prompted NNWSI to consider emplacing waste in the tuff unsaturated zone at the Nevada Test Site was the greatly decreased amounts of water that would be present in the vicinity of the waste package. This was considered highly desirable since container corrosion and waste leaching would be reduced.

From a literature survey, Russell and others (1984) assessed the likely performance of 17 candidate canister materials using corrosion resistance, mechanical properties, weldability, and cost as equally-weighted selection criteria. The reference material was stated to be Type 304L stainless steel (SS) with Type 316L SS, Type 321 SS, and Incoloy 825 as alternates. The applicability of the selection criteria used by these authors to a repository situation is questionable since corrosion resistance is much more important with respect to containing the waste than, for example, mechanical strength or cost. There is also evidence in the literature that some of the alloys being considered by NNWSI are susceptible to stress corrosion cracking (SCC) in steam and in water environments very similar to those expected in a tuff repository. Below is given a brief literature survey of stainless steel stress corrosion behavior in environments which are similar or extrapolatable to tuff repository conditions. It shows that there is a very strong potential for stress corrosion cracking and an experimental verification would be highly desirable. On this basis a detailed testing program was initiated at BNL to check the integrity of the NNWSI reference materials.

4.2 Survey of Stress-Corrosion Behavior of Austenitic Stainless Steels in Relatively Pure Steam/Water/Air Environments

Figure 4.1 shows that austenitic stainless steels exposed to the steam phase of alkaline-phosphate treated boiler water, and given intermittent wetting cycles, will fail by stress-corrosion craking even though the water contains very low Cl^-/O_2 levels (Williams, W. L., 1957). For example, 5 ppm O_2 and 5 ppm Cl^- in the boiler water will cause failure of stainless steels exposed to the steam phase. Tuff repository water will contain about 7.5 ppm Cl^- and this will be saturated with oxygen from the surrounding air (UCRL-89988, 1983). Initial evaporation of groundwater and subsequent dissolution of previously precipitated salt can make the concentration of Cl^- and other ions in the water coming in contact with a waste package much higher than the values currently assumed.

Data in Figure 4.2 show results from bent-beam tests on Type 321 stainless steel. Strained samples were maintained at 200° and 300°C in the steam phase above water containing 5 ppm Cl^-. For strains as low as 10^{-3} failure readily occurs in times of 40-100 hours (Birchon, D., 1964).

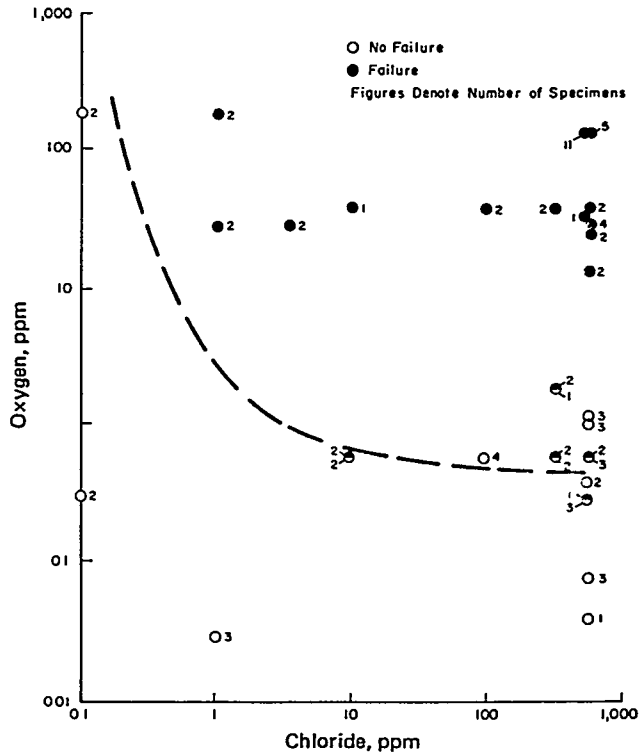

Figure 4.1. Proposed relationship between chloride and oxygen content of alkaline phosphate treated boiler water and susceptibility to stress corrosion cracking of austenitic stainless steel exposed to the steam phase with intermittent wetting (Williams, W. L., 1957).

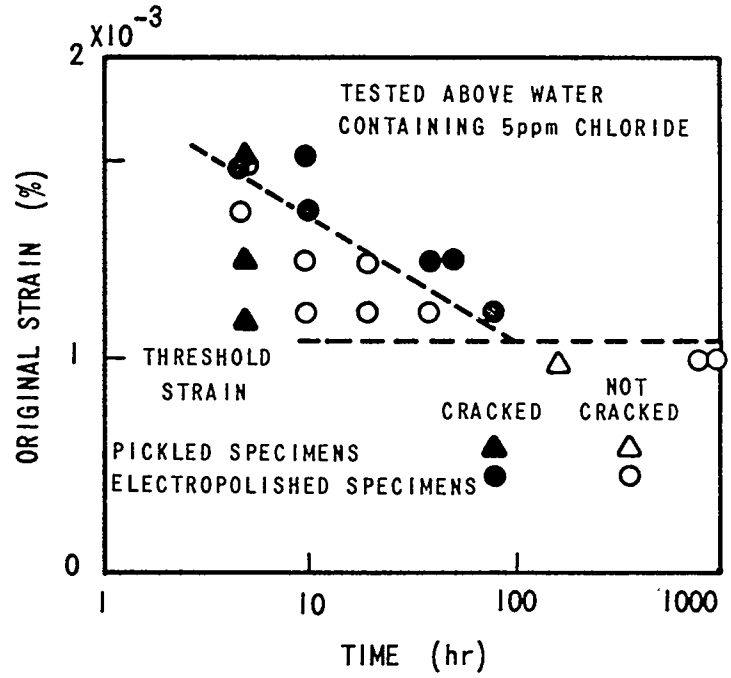

(a)

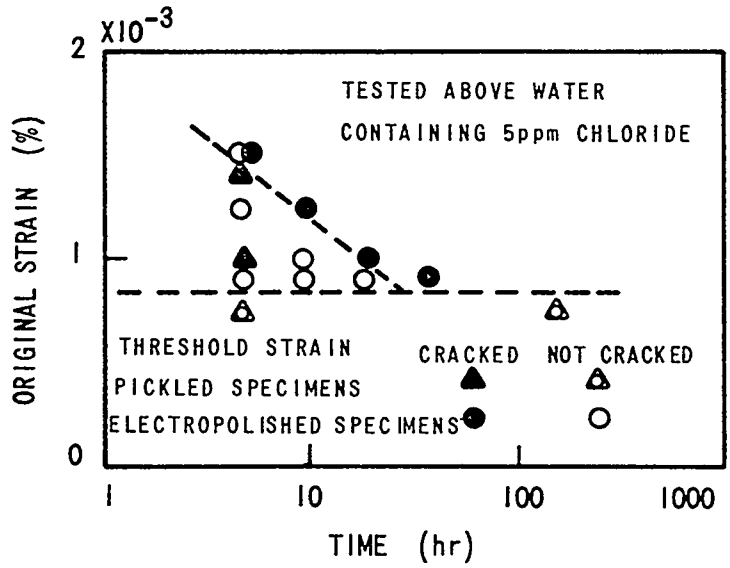

(b)

Figure 4.2. The relationship between original strain in bent-beam specimen and time-to-crack for (a) Type 321 stainless steel at 300°C and (b) Type 304 stainless steel at 200°C (Bircon, D., 1964).

There is also much information on the aqueous (as opposed to steam) corrosion of stainless steel. This type of data would be pertinent to the situation where boiling of water around the waste package has ceased and liquid water from the surface of the repository percolates past the container. Figure 4.3 shows that Type 304 SS U-bend samples will fail by stress corrosion cracking in 100°C water containing 10 ppm Cl^- (Warren, D., 1960). Failures begin after about one month and all exposed samples failed after about nine months.

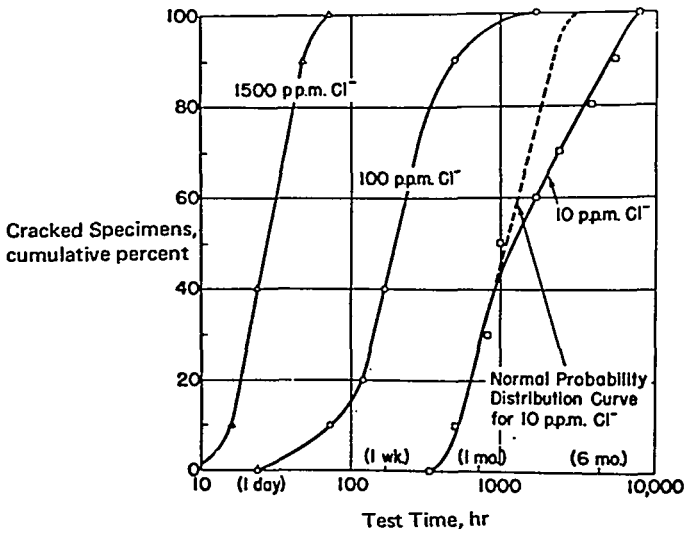

Figure 4.3. Effect of chloride added as NaCl on cracking of Type 304 stainless steel at 100°C. Solution transported by porous material to specimen (Warren, D., 1960).

Other data from Japan (JAERI-M-82-145, 1983) on a range of stainless steels and high nickel alloys in boiling deionized water also show that even these "benign" conditions can cause failure. The test apparatus is shown in Figure 4.4. Double-U-bend samples were used, some containing V notches at the specimen apexes to give stress concentration effects. Table 4.1 shows that Type 304 and Type 304L display stress corrosion cracking behavior without irradiation and also under a gamma dose rate of 1.1×10^5 R/h. Usually, cracking occurs on the inner U-bend specimens, but it also occurs on the outer specimens which have V notches. Irradiated solutions are more damaging than non-irradiated ones.

The observations that cracking is more likely on the inner U-bend samples is probably connected with crevice type conditions in which small volumes of trapped water can alter their composition and Eh/pH conditions more rapidly than those exposed to large amounts of free solution. Crushed tuff packing adjacent to the HLW container will likely give such crevice-like conditions.

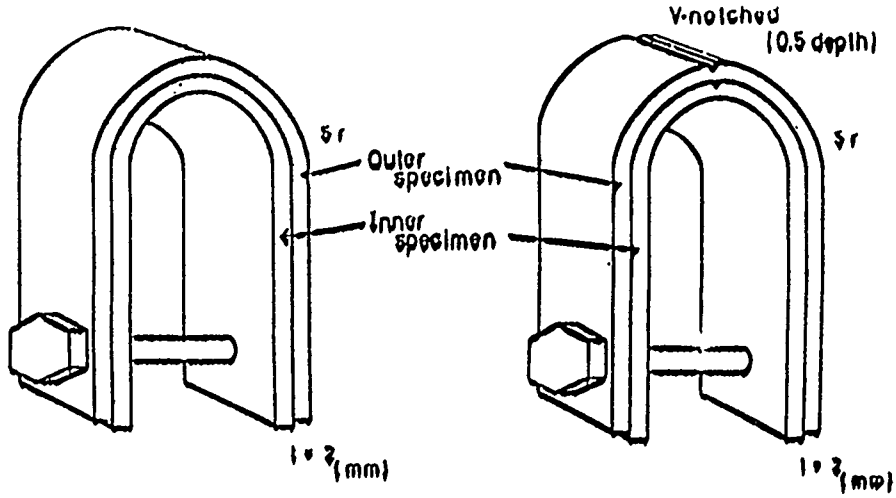

Figure 4.4(a). Schematic diagram of double U-bend type specimen.

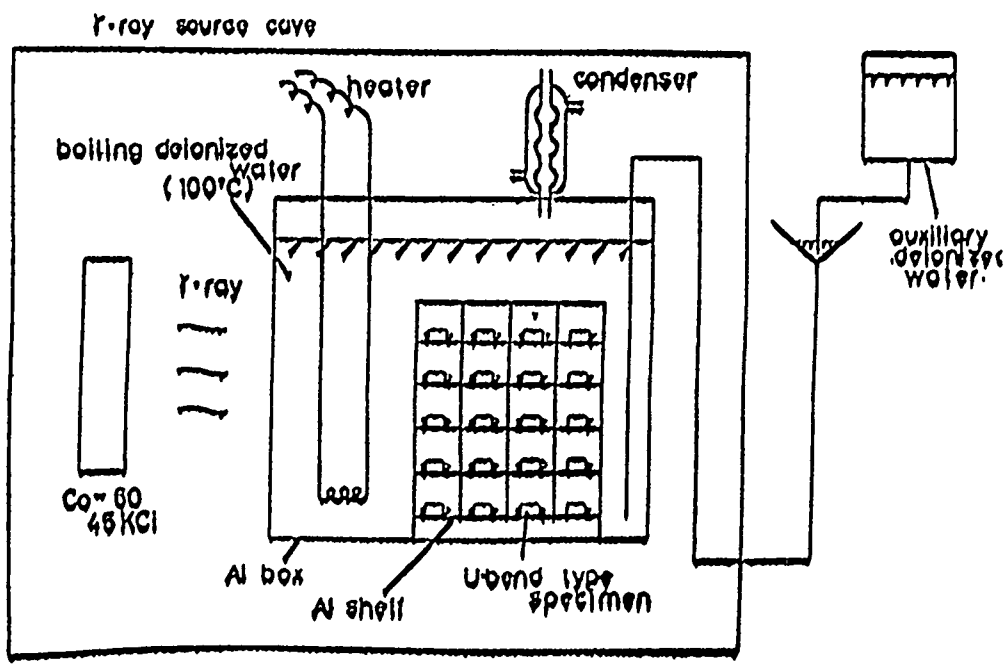

Figure 4.4(b). Schematic diagram of γ-ray irradiation (first test) (JAERI-M-82-145, 1983).

Table 4.1. SCC test in boiling deionized water (first test). (Dose rate: 1.1×10^5 R/h).

[Dose rate : 1.1×10^5 R/hr
Specimen numbers for each test : 2]

Alloy	Time (day)	γ-ray irradiation: Total dose (R)	γ-ray irradiation: Max. depth of SCC (mm) Plain	γ-ray irradiation: Max. depth of SCC (mm) V-notched	Non irradiation: Max. depth of SCC (mm) Plain	Non irradiation: Max. depth of SCC (mm) V-notched
Type 304 ss	7	2.0×10^7	1.5*1/0*2, 0.7/0	1.8/0, 1.8/0	1.3/0, 0.6/0	>1.5/0, 1.3/0
	14	4.0×10^7	>2/0, >2/0	>2*3/0, >2/0	>2/0, >2/0	>1.5/0, >1.5/0
	30	8.6×10^7	>2/0, >2/0	>2/0, >2/0	>2/0, >2/0	>2/0, >2/0
	60	1.7×10^8	>2/0, >2/0	>2/0, >2/>1.5*4	>2/0, >2/0	>2/0, >2/0
	90	2.6×10^8	>2/0, >2/0	>2/>1.5, >2/0	>2/0, >2/0	>1.5/>1.5, >1.5/>1.5
	180	5.2×10^8	>2/0, >2/0	>2/>1.5, >2/>1.5	>2/0, >2/0	>1.5/>1.5, >1.5/0
Type 304L ss	180	5.2×10^8	>2/0, >2/0	>2/>1.5, >2/>1.5	>2/0, >2/0	>1.5/>1.5, >1.5/0
Type 304EL ss	7	2.0×10^7	0/0, 0/0	0/0, 0/0	0/0, 0/0	0/0, 0/0
	14	4.0×10^7	0/0, 0/0	0/0, 0/0	0/0, 0/0	0/0, 0/0
	30	8.6×10^7	0/0, 0/0	0/0, 0/0	0/0, 0/0	0/0, 0/0
	60	1.7×10^8	0/0, 0/0	0/0, 0/0	0/0, 0/0	0/0, 0/0
	90	2.6×10^8	0/0, 0/0	0/0, 0/0	0/0, 0/0	0/0, 0/0
	180	5.2×10^8	0/0, 0/0	0/0, 0/0	0/0, 0/0	0/0, 0/0
Type 309S ss	180	5.2×10^8	>2/0, >2/0	—, —	>2/0, 0/0	—, —
Incoloy 825	180	5.2×10^8	0/0, 0/0	0/0, 0/0	0/0, 0/0	0/0, 0/0
Inconel 600	180	5.2×10^8	0/0, 0/0	0/0, 0/0	0/0, 0/0	0/0, 0/0
Inconel 625	180	5.2×10^8	0/0, 0/0	0/0, 0/0	0/0, 0/0	0/0, 0/0
SMA 50	180	5.2×10^8	0/0, 0/0*5	—, —	0/0, 0/0*5	—, —

*1 ; Max. depth of SCC on inner specimen
*2 ; Max. depth of SCC on outer specimen
*3 ; >2 : failed from other than V-notched root
*4 ; >1.5 : failed from V-notched root
*5 ; Pitting corrosion was observed

Preliminary work at LLNL using slow-strain-rate testing under tuff repository conditions indicates that stress-assisted failure is unlikely (UCRL-89988, 1983). However, these tests are accelerated tests and do not address the very long term exposures which may be needed to initiate cracks. This work also did not include the potentially adverse effects of gamma radiolysis of solutions which would be an added source of O_2 and H_2.

Clearly, the above data from the literature show that stressed Types 304, 304L and 321 stainless steel are very susceptible to failure in steam and liquid water environments containing very low levels of Cl^- and O_2. In fact, the tuff repository conditions which are likely to prevail during the steam and liquid water periods appear to be much more aggressive than those cited above. It is important, therefore, to examine the likelihood of failure of NNWSI candidate container materials. In the present BNL testing program the goal is to assess the stress corrosion cracking susceptibility of the four alloys being considered by NNWSI. The tests will last for a period of up to one year in an

environment consisting of simulated J-13 groundwater in equilibrium with crushed tuff at 100°C. Below are given the experimental details of this program along with results obtained to date.

4.3 Test Plan

C-ring stress corrosion cracking testing is planned on as-received and sensitized Types 304L, 316L and 321 stainless steel and Incoloy 825. Testing will be conducted in synthetic J-13 and ten-times concentrated J-13 water in equilibrium with crushed tuff. Specimens will be tested in the steam phase above the two solutions as well as in the solutions. The testing in the steam phase corresponds to the initial period of repository life, and that in the liquid phase corresponds to the later period when the waste package would have cooled down sufficiently to prevent boiling. In the present tests, steam will be present at approximately 100°C, although in a repository the steam temperature could be as high as the container temperature (≈300°C).

Tests will be conducted in parallel for three-, six- and twelve-month durations. Thus, there will be six independent test vessels, three for each solution. To obtain good statistics for the results, triplicate samples will be used for each test condition. A total of 288 specimens will be used in this test plan as described in the test matrix given in Table 4.2.

Table 4.2. Test matrix for stress corrosion of candidate stainless steels and Incoloy-825.[a]

Sample Condition	Exposure Medium[b]	Total Exposure Time and Number of Samples		
		3-Month	6-Month	12-Month
Solution Annealed (SA)	J-13 Steam	3	3	3
SA + Sensitized	J-13 Steam	3	3	3
SA	J-13 Water	3	3	3
SA + Sensitized	J-13 Water	3	3	3
SA	(J-13 Steam)X10[c]	3	3	3
SA + Sensitized	(J-13 Steam)X10	3	3	3
SA	(J-13 Water)X10	3	3	3
SA + Sensitized	(J-13 Water)X10	3	3	3

[a]This test matrix comprising 72 samples consitutes the tests on one of the four candidate materials. An identical matrix will be used for all eight materials and the total number of all specimens tested will be 288.
[b]All tests are conducted in the presence of crushed tuff.
[c]This environment is the steam/air phase above 10X concentrated J-13 well water.

4.4 Materials and Specimens

C-Rings:

Types 304L, 316L and 321 stainless steel and Incoloy 825 are the materials selected for the SCC tests. Seamless 0.75-inch o.d. x 0.125-inch wall tubing of stainless steel and 0.84-inch o.d. x 0.109-inch wall tubing for the Incoloy was purchased from Royce Aerospace Materials Corporation*. Chemical compositions and mechanical properties of these alloys, as supplied by the vendor, are given in Tables 4.3 and 4.4, respectively.

Table 4.3. Vendor supplied chemical analysis of test alloys (weight percent).

Alloy	C	Mn	Si	P	S	Cr	Ni	Mo	Ti	Al	Fe
Type 304L SS	0.016	1.95	0.48	0.038	0.025	18.54	10.55				Balance
Type 316L SS	0.016	1.94	0.37	0.035	0.010	16.66	12.80	2.02			Balance
Type 321 SS	0.028	1.03	0.74	0.026	0.002	17.41	10.75		0.24		Balance
Incoloy 825	0.02	0.44	0.27		0.001	22.34	44.14	2.78	0.84	0.07	27.26

Table 4.4. Mechanical properties of as-received test alloys (vendor supplied data).

Alloy	Ultimate Tensile Strength (MPa)	Ultimate Tensile Strength (ksi)	0.2% Offset Yield Strength (MPa)	0.2% Offset Yield Strength (ksi)	Elongation (%)	Rockwell Hardness (RB)
Type 304L SS	536	77.8	276	40.1	65.3	85.2
Type 316L SS	562	81.5	254	36.9	59.2	69.4
Type 321 SS	558	81.0	225	32.7	65	78
Incoloy 825	799	116.0	475	68.9	36	95

*West Babylon, New York.

C-ring test specimens were fabricated from the as-received (solution annealed) as well as from heat treated (sensitized) tubing for each alloy. During heat treatment the tubing was maintained at 600°C for 100 hours followed by furnace cooling. This treatment is expected to sensitize the specimens because of the formation of chromium-depleted zones adjacent to grain boundary carbides. This can lead to stress corrosion cracking along the grain boundaries. Sensitization of HLW containers can possibly occur during glass pouring or welding operations.

The procedure for testing C-ring samples is given elsewhere (ASTM, 1979). The surfaces of the as-received and heat treated tubing were rough so it was decided to obtain a consistent surface by polishing with 600-grit silicon carbide paper. Notched C-ring specimens were machined from the polished tubing according to the specifications given in Figure 4.5. Before stressing, each specimen was degreased in trichloroethane and then cleaned with Alconox soap, methanol and distilled water.

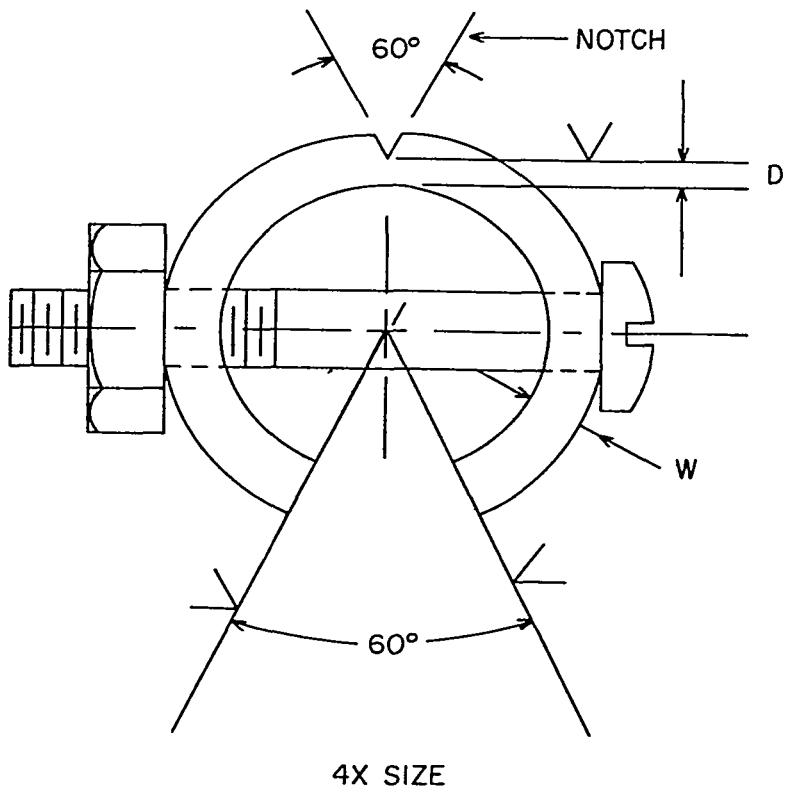

Figure 4.5. C-ring specimen design.

Tuff:

Topopah Spring tuff was supplied by Ward's Natural Science Establishment, Inc. from a surface outcrop of the Paintbrush tuff formation, southern Fran Ridge, between the J-13 well and eastern Yucca Mountain. The approximate geographical location of the site from where specimens were obtained is 116° 25' west and 36° 50' north.

The mineral composition of the rock specimens, as determined by Globo de Plomo Enterprises* using a Kevex energy-dispersive X-ray spectrometer is given in Table 4.5. Aluminum is the lightest element which could be determined quantitatively. The results are normalized to SiO_2 whose absolute concentration was not determined. As was clear from visible observation, the rock specimens had varying appearance and, hence, also varying composition from rock to rock. Results in Table 4.4 represent a typical composition. A brief geochemical description of the tuff given by Globo de Plomo Enterprises is presented below:

> "The rock is a welded vitric tuff of rhyolite composition composed of flattened glass fragments kneaded into a streaky fabric. Welding has not been sufficient to blur fragment boundaries. The fragments carry scattered phenocrysts of sanidine with less plagioclase and oxidized biotite. Traces of augite and oxyhornblende were observed in addition to accessory magnetite. Other accessories found near magnitite and mafites include zircon, allanite, and monazite.
>
> "All of the glass domains have just begun to devitrify, producing orthoclase, quartz, and iron oxides. Tridymite lines collapsed voids and has formed in certain frothy glasses instead of quartz. Some larger voids are lined with chalcedony, then tridymite, then iron oxides, and are infilled with caliche-like calcite.
>
> "A polished section reveals that accessory magnetite grains are penetrated and about half replaced by tablets of hematite. Rutile was also observed.
>
> "Phenocrysts comprise about 20% of the rock by volume and a breakdown is: plagioclase 30%, biotite 5%, augite 2%, magnetite 2%, oxyhornblende 1%, sanidine 60%. Matrix components are too fine grained and intimately intergrown to estimate."

The as-supplied tuff specimens were too large to be used in the corrosion tests. Therefore, they were crushed into small pieces which were then sieved to separate them into two sizes, viz. coarse (0.25 in.-0.50 in.) and fine (0.187 in.-0.250 in.). In a preliminary test to estimate the solution chemistry crushed tuff of a finer size (0.0165 in.-0.187 in.) was used.

*P. O. Box 872, Douglas, Arizona.

Table 4.5. Geochemical analysis of Topopah Spring tuff (values in ppm unless percent is specified).

Al_2O_3	13.1%
K_2O	4.52%
CaO	2.21%
TiO_2	0.38%
MnO	0.07%
Fe_2O_3	1.83%
Cu	17
Zn	35
As	22
Th	18
Rb	116
Sr	109
Y	17
Zr	482
Nb	13
Sb	15
Ba	314
La	62
Ce	83

Groundwater:

Although there is no information available on the composition of groundwater which would come in contact with the waste package in tuff, groundwater from the J-13 well (which is located below the repository horizon) has been designated as the reference test solution (UCRL-89988, 1983). A chemical analysis of reference J-13 groundwater as given in Table 4.6 has been specified by DOE subcontractors (UCRL-89988, 1983) but there is no procedure given for its preparation in the laboratory. The J-13 water used by NNWSI is obtained from the actual site rather than prepared artificially. Therefore, a solution preparation procedure was developed at BNL.

Table 4.6. Reference groundwater composition for tuff repositories (based on composition of Jackass Flats Well J-13 at the Nevada Test Site).

	Concentration (mg/liter)
Lithium	0.05
Sodium	51.0
Potassium	4.9
Magnesium	2.1
Calcium	14.0
Strontium	0.05
Barium	0.003
Iron	0.04
Aluminum	0.03
Silica	61.0
Fluoride	2.2
Chloride	7.5
Carbonate	0.0
Bicarbonate	120.0
Sulfate	22.0
Nitrate	5.6
Phosphate	0.12

pH - slightly basic (7.1).

Fourteen reagents were selected such that their solution in water would give ionic concentrations very close to that found in reference J-13 groundwater. The amount of chemical compounds added to distilled water to make 20 liters of synthetic J-13 water is given in Table 4.7. Initially, there was a problem in dissolving the required amount of silicic acid. With some trial and error and considering higher solubility of silica at higher temperature and pH, this problem was resolved by first adding $NaHCO_3$ to distilled water, heating it to near boiling and then adding silicic acid; other compounds were added subsequently.

Table 4.7. Amount of chemical compounds used in preparing 20 liters of synthetic J-13 water (mg).

1.	$NaHCO_3$	3292
2.	KOH	140
3.	$SiO_2 \cdot XH_2O$ (1.87% H_2O)	1243
4.	$CaCl_2$	232
5.	$CaSO_4$ (460 mg $CaCO_3$ + 440 mg H_2SO_4)	624
6.	$Ca(NO_3)_2$	48
7.	$Mg(NO_3)_2 \cdot 6H_2O$	256
8.	MgF_2 (46.6 mg MgO + 96.5 mg HF - 48%)	72
9.	$LiNO_3$	10
10.	$Sr(NO_3)_2$	2.4
11.	$BaCl_2 \cdot 2H_2O$	1.8
12.	$Fe(NO_3)_3 \cdot 9H_2O$	7.2
13.	H_3PO_4 (85%)	2.8
14.	$Al(NO_3)_3 \cdot 9H_2O$	13.9

As mentioned above, groundwater coming in contact with a HLW canister can have much higher ionic concentrations than in J-13 groundwater. This would happen when salts, precipitated during initial evaporation of groundwater, are redissolved as new cooler groundwater arrives at a later time. Since there are no estimates available for this groundwater concentration effect, we have arbitrarily assumed a concentration factor of ten. However, for a ten-times concentration solution some of the species (e.g. SiO_2, divalent cations) may be already past their saturation limit at room temperature. However, the solubility would be increased at the 100°C test temperature used. The equilibrium composition of ten-times concentrated J-13 water at 100°C is difficult to determine. Therefore, we have added ten times the quantity of salts needed for synthetic J-13 water and let the salts (including those insoluble at room temperature) equilibrate at 100°C. Such a liquid, which is not transparent at room temperature, provides ten times higher ionic concentration of the soluble species and saturation concentration of insoluble species of the corrosion specimen kept at 100°C. In the actual tests to be performed the solution composition will be further modified due to the interaction between water and crushed tuff. Thus, post-test analysis of the solutions were carried out.

4.5 Apparatus

The tests are conducted in six identical test vessels (corresponding to six different test conditions). One is shown in Figure 4.6. In each unit, C-ring specimens along with crushed rock and test solution are stacked in a 4-liter Pyrex vessel. Approximately 6/7 of the vessel height is enclosed within an electrical furnace. The lid of the vessel has space for four connections, two of which are kept closed. A thermometer and a cold water condenser are placed in the other two receptacles. Flowing cold water helps in condensing the steam approaching the condenser to water which drips back into the kettle. The top of the condenser is open to the atmosphere so that some air is present.

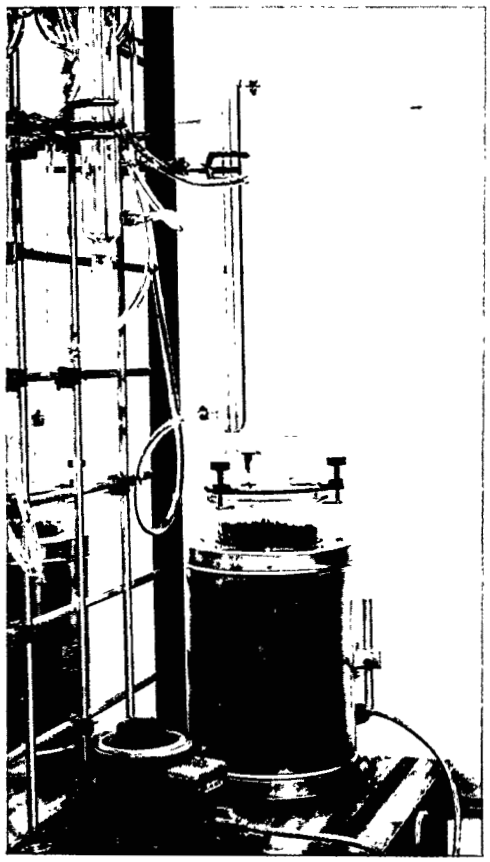

Figure 4.6. C-ring stress corrosion cracking test apparatus.

To measure the in situ pH of the solution during a test it becomes necessary to have easy access to the solution. For this purpose, a 15-mm o.d. quartz bube with many small holes along its length is placed in the center of the vessel. A microcombination pH probe (MI-410, Microelectrodes, Inc.) can be inserted in this tube from the top of the vessel and the solution pH measured with a standard pH meter.

4.6 Test Procedure

According to the test plan, a C-ring specimen is supposed to be stressed such that stress levels at the apex of an unnotched (smooth) specimen would be 90 percent of the elastic limit at room temperature. Therefore, one smooth C-ring specimen for each of the eight alloys (three stainless steels and Incoloy 825 in the as-received and sensitized conditions), identical in dimensions to notched test specimens, was tested in an Instron machine to obtain stress-strain characteristics. A typical load vs deflection curve is shown in Figure 4.7 for as-received Type 304L sensitized stainless steel; the C-ring was stressed in the same orientation as expected from the usual nut and bolt arrangement. The load and deflection at the elastic limit (shown by arrow) obtained from such curves are given in Table 4.8. The notched C-ring test specimens

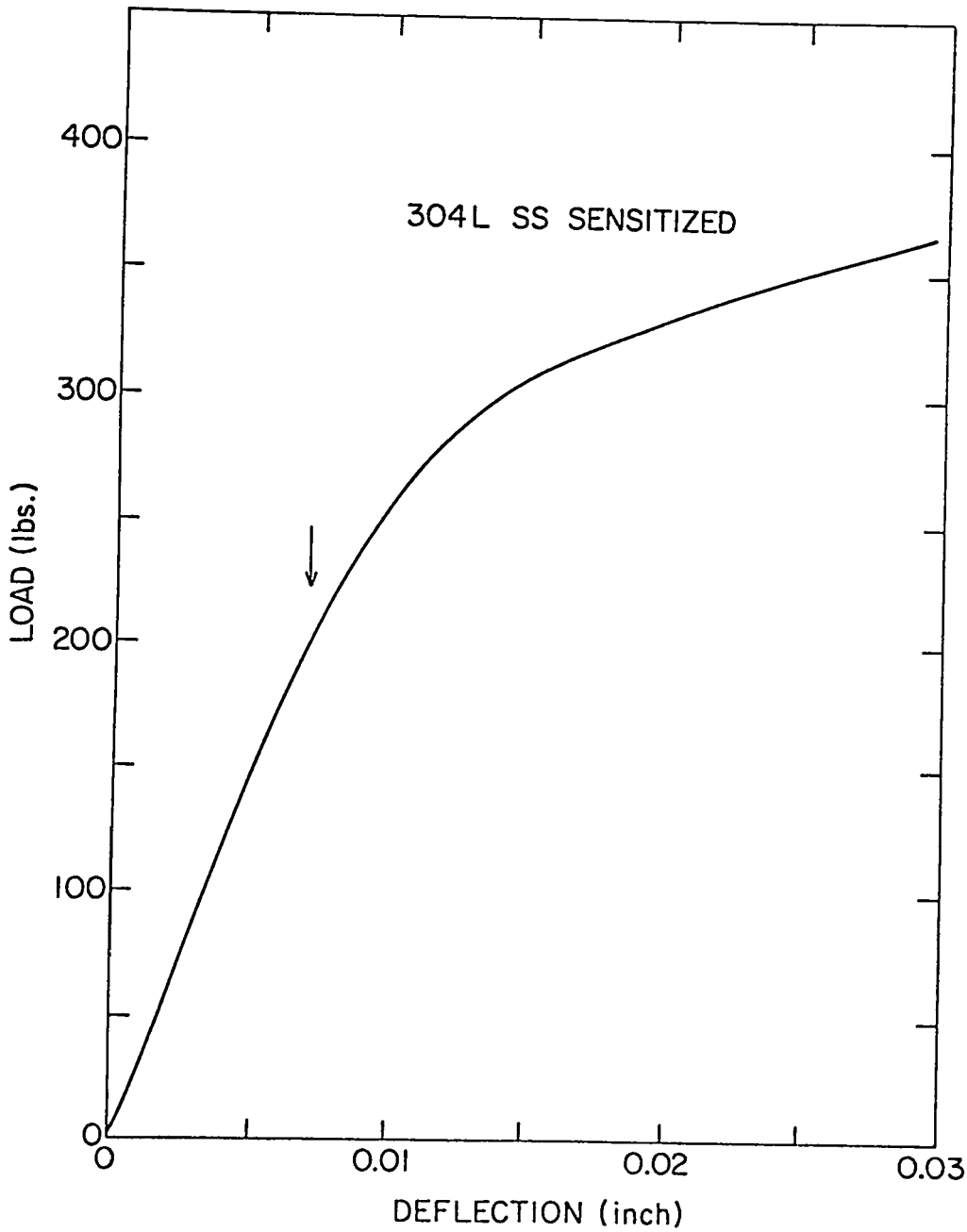

Figure 4.7 Load vs deflection of Type 304L stainless steel sensitized C-ring test specimen under compression.

were stressed with the help of commercial stainless steel nuts and bolts such that the change in o.d. was 90% of the deflection at the elastic limit (Table 4.8).

In the present procedure the applied tensile stress in most of the volume of a specimen will be within the elastic limit, which corresponds to those expected in a normal waste container. However, the actual stress in the cross section of test specimen through the notch will be higher than the "90% of elastic limit" value because of stress concentration effects. This will probably cause some plastic deformation. The rationale of having plastic stresses near the notch is that in a realistic situation, similar plastic deformation is possible at dents, flaws or inclusions in the container surface. Inadvertant mishandling during transportation or disposal of waste can also cause plastic deformation in a container.

Table 4.8. Stress-strain properties of eight alloys as obtained from Instron machine tests on smooth C-ring specimens.

Alloy	Load at 100% Elastic Limit (kg)	Deflection at 100% Elastic Limit (cm)	Deflection at 90% Elastic Limit (cm)	Longitudinal Strain at Elastic Limit (10^{-6})
Type 304L SS (as-received)	102.0	0.0254	0.0229	1564
Type 304L SS (sensitized)	90.7	0.0178	0.0160	1339
Type 316L SS (as-received)	124.5	0.0356	0.0320	1730
Type 316L SS (sensitized)	113.4	0.0267	0.0241	1517
Type 321 SS (as-received)	79.4	0.0163	0.0147	1200
Type 321 SS (sensitized)	90.7	0.0178	0.0160	1198
Incoloy 825 (as-received)	170.1	0.0394	0.0356	2770
Incoloy 825 (sensitized)	283.5	0.0610	0.0549	3707

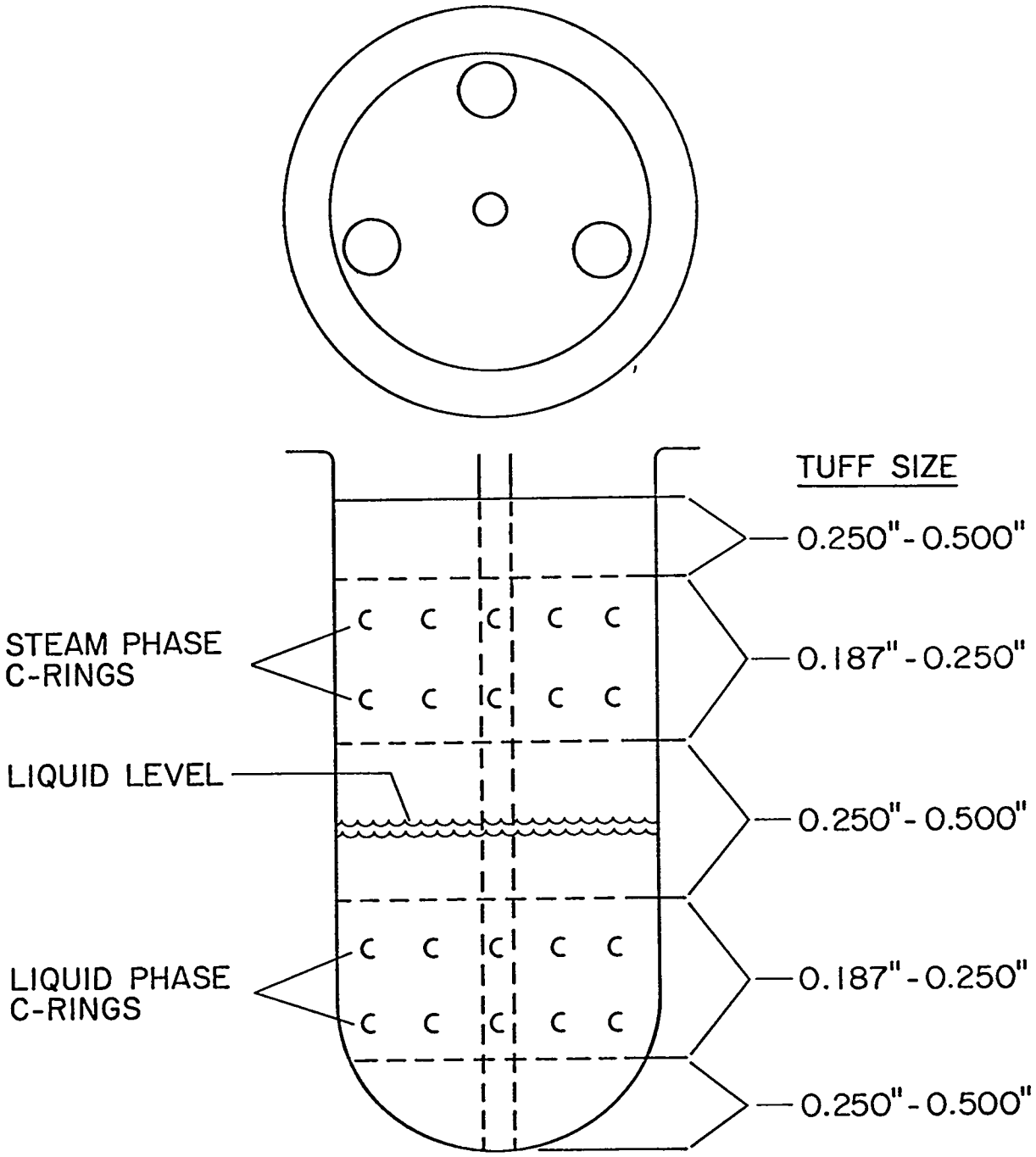

Figure 4.8. Schematic of the specimen arrangement in a test vessel.

A specific mark was indented on the side of a specimen to identify the alloy. Triplicate samples of each alloy were stacked within the crushed tuff in two layers at two levels in a test vessel (Figure 4.8). The samples at the lower level were submerged in solution whereas those at the upper level were surrounded by crushed tuff, air and steam. Note that the C-ring specimens were surrounded only by fine size crushed tuff. Before filling the vessel with tuff, the pH tube was placed in the center of the vessel. Care was exercised so that no specimens touched.

Crushed rock surrounding the specimens filled nearly to the top and approximately 1100 cc of test solution was added to bring the liquid level to half the depth of the vessel. After some time the liquid became slightly lower presumably due to soaking by the rocks but the lower level specimens were always well submerged in solution as confirmed by checking the water level every week. After putting the lid with thermometer and condenser in place, the vessel was slowly heated to bring the solution to boiling. The furnace power was adjusted so that the water from the condenser dripped at a rate of 5-10 drops per minute.

4.7 Results to Date

The notched C-ring specimens used in the present study were stressed to 90% of the elastic limit measured at the apex of smooth specimens. The notches in the specimens would result in local deformation. This was confirmed by the observation that when the stress on selected specimens was removed, the deflection was only partially recovered. Such stress concentration effects could occur on the surface of a HLW container when, for example, scratches or dents are inadvertently produced during handling.

An attempt was made to determine the strain present on the surface of a smooth C-ring specimen. Three longitudinal and one transverse strain gauges were attached on the outer surface of the specimen which was then compressed in an Instron machine. A typical load vs strain curve from these measurements is shown in Figure 4.9 for as-received Type 316L stainless steel. The average value of three longitudinal strains corresponding to elastic limit is given in Table 4.8.

The metallographic examination of Types 304L, 316L and 321 stainless steel and Incoloy 825 have been completed. A comparison of microstructures for the as-received (annealed) and heat treated condition shows that the heat treatment (100 hours at 600°C, followed by furnace cooling) has sensitized the stainless steels by precipitating carbides at the grain boundaries. Such an observation is much less evident in the case of Incoloy 825, for which the heat treatment has resulted in the precipitation of second-phase particles (probably TiC).

It is interesting to note that sensitization in the stainless steels is stronger near the surfaces of the C-ring specimens. These surfaces are the inner and outer diameters of the tubing from which the samples were fabricated. Figure 4.10 shows this effect for Type 304L stainless steel for which the microstructure near the outer diameter is more heavily etched. This preferential sensitization is most likely due to unavoidable contamination from lubricants, coupled with higher residual stresses at the tubing surfaces during manufacturing processes. The extra surface strain energy enhances carbide

nucleation and growth processes. For a HLW stainless steel container, this observation suggests that any stresses introduced on the container surface during its production or handling would enhance its susceptibility to sensitization and, therefore, to stress corrosion cracking.

A few days after starting each test, small white precipitates appeared on some of the tuff pieces near the top of the vessel and also on the inside of the vessel. These are presumably due to vapor phase transport of some compound in solution. We plan to characterize the white compound at the end of each test and hope to evaluate its effect on metal corrosion.

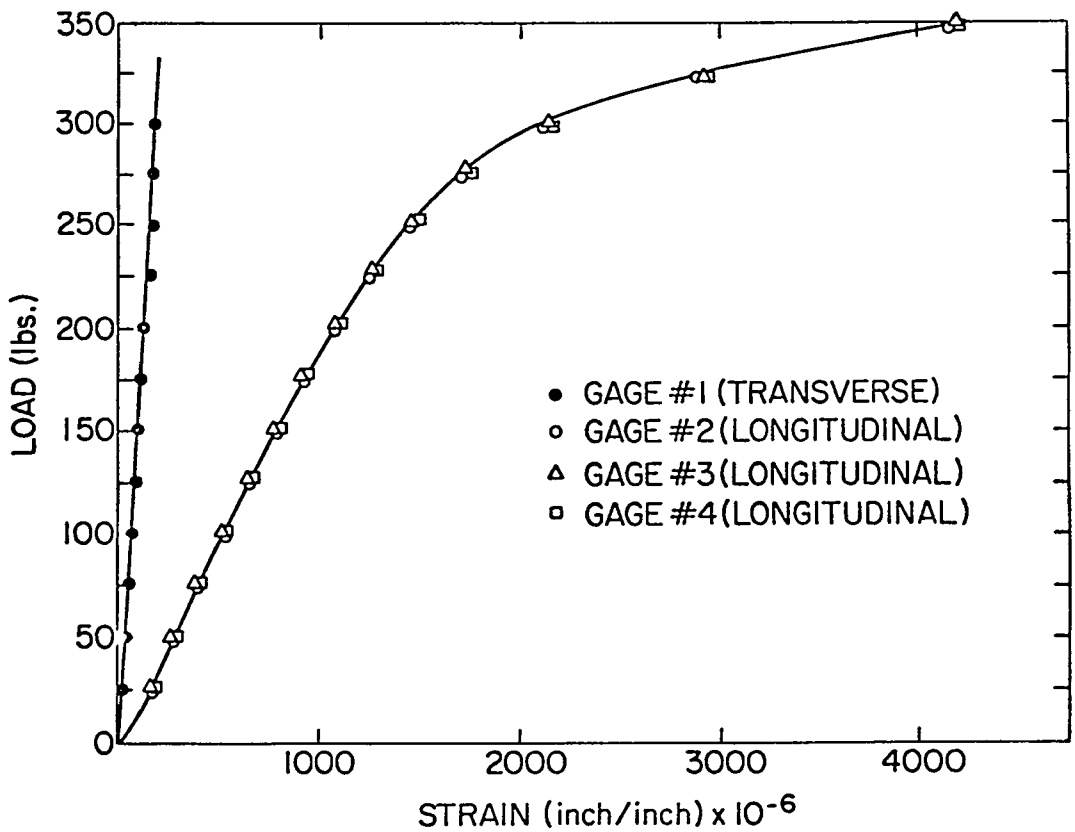

Figure 4.9. Load vs in situ strain at the apex of a Type 316L stainless steel C-ring specimen.

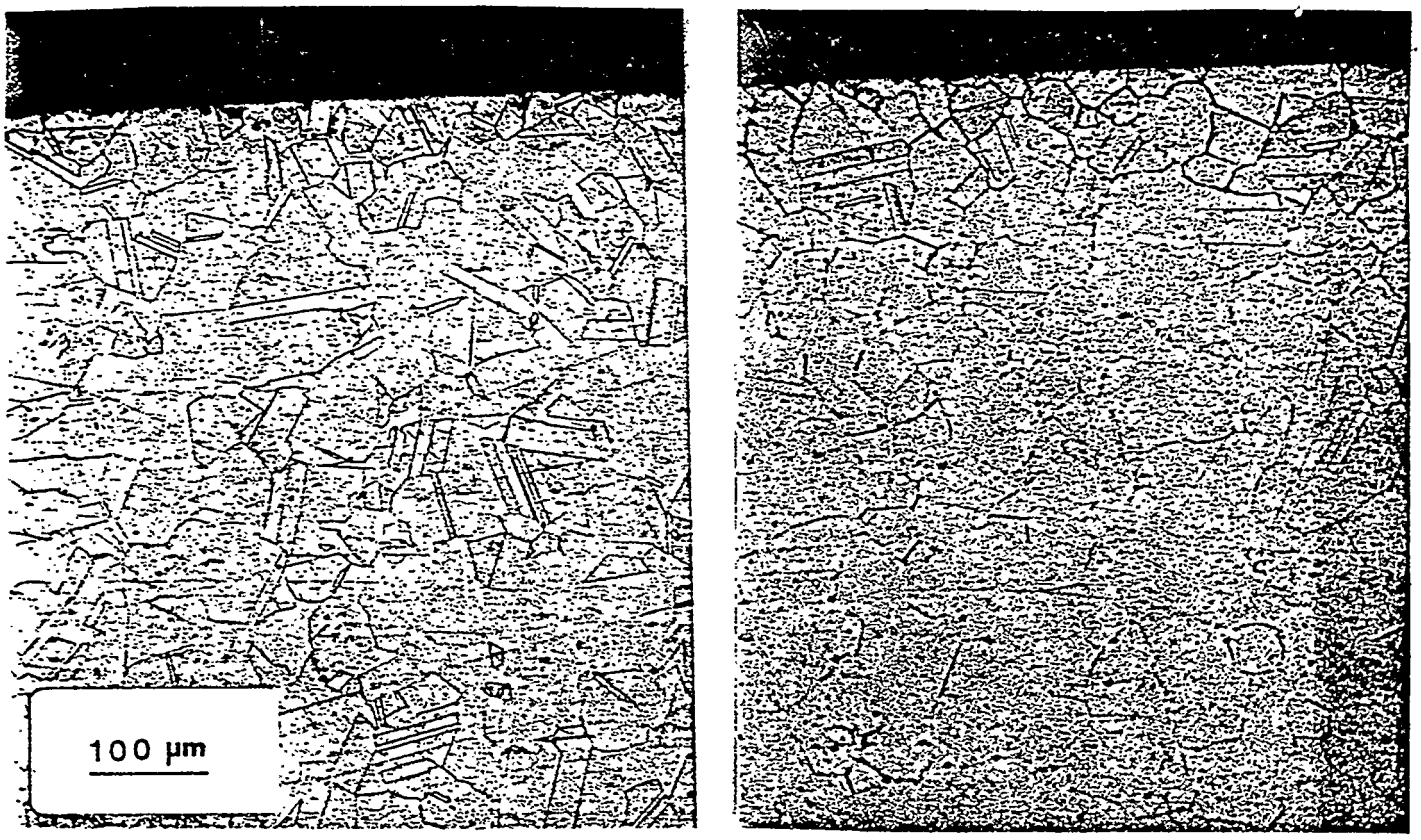

(a) (b)

Figure 4.10. Microstructure of Type 304L stainless steel.
(a) As-received, etched in glyceregia.
(b) Sensitized at 600°C for 100 hours, etched in oxalic acid.

The pH of as-prepared J-13 and ten-times concentrated J-13 water at room temperature was determined to be 8.4 and 8.3, respectively. When these solutions were heated to boiling, the pH decreased to 6.9 and 7.9, respectively. Subsequent changes during tests are shown in Figure 4.11. After an initial sharp increase, the solution pH appears to be decreasing slowly with time. However, there is a large amount of scatter from vessel to vessel, and additional long-term results are needed to confirm this trend.

The six- and twelve-month tests are continuing and the three-month test has been just terminated. The pH of the solution at the end of the three-month test has been measured. The value increased with decreasing temperature as shown in Table 4.9. Nearly equal values of pH were measured for both the test solutions suggesting that the crushed tuff may be buffering the water by steam.

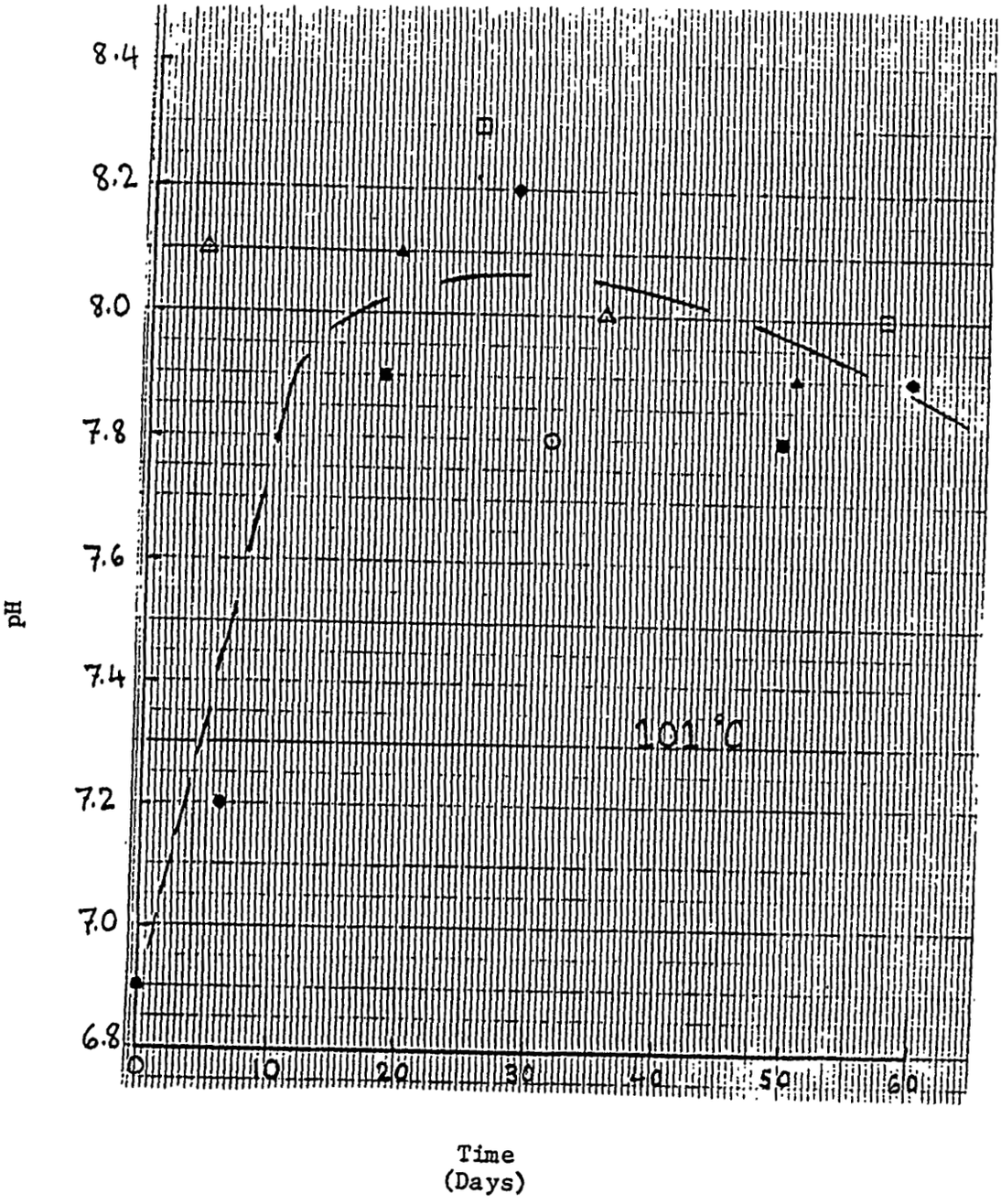

Figure 4.11. pH of the six test solutions at 101°C as a function of time. Each symbol represents the solution in one test vessel.

Table 4.9. pH of test solutions at the end of the three-month tests.

J-13 Solution		Concentrated J-13 Solution	
Temperature (°C)	pH	Temperature (°C)	pH
101.4	7.7	101.7	7.6
68.0	8.1	50.0	8.1
60.0	8.1	44.0	8.2
35.0	8.3	33.0	8.3
27.0	8.4	26.5	8.4

The C-ring specimens from the three-month tests have been only briefly examined. No macroscopic cracks have been found on these samples. A complete examination will be conducted in the near future which would show whether or not any microcracks are present. All C-ring specimens placed in solution have a generally uniform coating of salt and corrosion scale, whereas stainless steel specimens in the steam phase show patches of unreacted metal surrounded by a brown, rust-colored scale (Figure 4.12). Incoloy specimens in steam do not show any corrosion scale. It appears that stainless steel specimens did not corrode in the areas touching tuff pieces. Such areas apparently had a film of relatively pure condensed water whereas the rest of the sample was exposed to steam and air.

The chemical analyses of the solution obtained from the central tube at the end of the three-month tests are given in Table 4.10; results for Na^+, K^+ and NO_3^- will become available in the near future. Note that ionic concentrations are much higher than J-13 groundwater (Table 4.6). Part of the increased ionic concentration may be from dissolution of salts present in the tuff (see below results from preliminary groundwater chemistry test). To estimate solution chemistry at 100°C, 100 mL specimens of the hot test solution were mixed with boiling distilled water and filtered through Whatman 42 paper (specimens No. 6 and No. 9). The dilution was expected to prevent precipitation on cooling. Solution No. 7 and No. 10 were not diluted but filtered as before. To determine the concentration of any particles suspended in solution, Sample No. 7 was also analyzed without filtering (called No. 8). A comparison of the two (Table 4.10) indicates that there is no significant amount of suspended solid material which could be filtered through a Whatman 42 paper. A comparison of results for undiluted and diluted solutions suggests that dilution by a factor of two reduces the concentrations approximately by a factor of two for all species. Therefore, no significant precipitation appears to occur during the cooling of undiluted solution.

To estimate the possible range of solution chemistry a parallel test was conducted in a vessel similar to the ones used in the C-ring tests. It was filled with crushed tuff of relatively fine size (0.165 to 0.187 inch) and distilled water and then equilibrated under boiling water conditions. Crushed tuff was used in the as-received condition. The chemical analysis of the water after a test period of one month (Table 4.11) suggests that major cations and

anions can be present in concentrations much larger than assumed in J-13 reference groundwater. Apparently, large ionic concentrations were found in the as-received tuff equilibrated water due to the dissolution of salts present in tuff outcrop material. To determine the extent of such contributions to the chemical composition of groundwater, the test was continued, first by draining all the existing solution, and then adding 1150 mL of distilled water. The test vessel was heated to and maintained under boiling water conditions for a period of one month just as in the C-ring tests. The chemical analysis of a water sample obtained at the end of this test is given in the last column of Table 4.11. We note that although the ionic concentration in the second test is lower by a factor of two to four than in the first test, it is still much higher than in the reference J-13 groundwater. Thus, high anion concentrations (e.g. Cl^-) in the second water sample suggests that the use of J-13 groundwater composition in container corrosion studies may not correspond to the most severe possible conditions in a tuff repository.

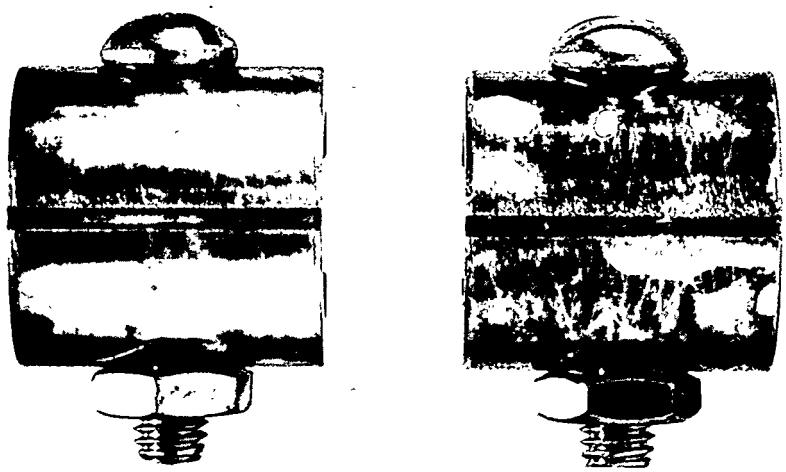

Figure 4.12. C-ring specimens of Type 321 sensitized stainless steel after three-month test in "synthetic J-13 water." The specimen on left was exposed to liquid phase and the one on the right was exposed to steam phase (X2.2).

Table 4.10. Chemical composition of test solutions obtained at the end of three-month tests (μg/mL).

	Starting Solution: Synthetic J-13 Water		Starting Solution: Ten-Times Concentrated J-13 Water		
	Sample No. 7 (Undiluted, Filtered)	Sample No. 6 (Diluted, Filtered)	Sample No. 10 (Undiluted, Filtered)	Sample No. 9 (Diluted, Filtered)	Sample No. 11 (Undiluted, Unfiltered)
Mg	<0.05	<0.05	<0.05	<0.05	<0.05
Ca	308	151	301	161	332
Fe	<0.1	<0.1	<0.1	<0.1	<0.1
Ni	<0.1	<0.1	<0.1	<0.1	<0.1
Sr	3.35	1.97	4.38	2.18	4.24
Al	<2.0	<2.0	<2.0	<2.0	<2.0
Cu	<0.1	<0.1	<0.1	<0.1	<0.1
F^-	12.1	7.1	14	8.9	15
Cl^-	130	72	330	160	330
SO_4^{2-}	820	420	1300	660	1300
PO_4^{3-}	<1	<1	<1	<1	<1
SiO_2	414	219	408	205	421

Table 4.11. Room temperature chemical composition of filtered solutions obtained from the reaction of distilled water with crushed tuff. Composition of reference J-13 groundwater is included for the purpose of comparison (μg/mL).

	J-13 Groundwater	Test Solution Following One-Month Equilibration of Crushed Tuff With Distilled Water	Test Solution Following the Subsequent One-Month Equilibration of the Same Crushed Tuff With Fresh Distilled Water
Na^+	45	308	190
K^+	4.9	50.5	21
Mg^+	2.1	Not determined	<0.1
Ca^{2+}	14	930	298
F^-	2.2	8.5	<4
Cl^-	7.5	160	43.7
HCO_3^-	120	Not determined	Not determined
SO_4^{2-}	22	343	530
NO_3^-	5.6	460	188
PO_4^{3-}	0.12	Not determined	Not detected
Silica	61	95.1	142
pH (at room temperature)	8.5	8.4	8.5 7.0 (at 100°C)

4.8 References

ASTM, Annual Book of Standards, Part 10, Making and Using C-Ring Stress Corrosion Test Specimens, Designation G38-73, 1979.

Birchon, D. and G. G. Boothe, "Stress Corrosion Cracking of Some Austenitic Stainless Steels as Affected by Surface Treatment and Water Composition," in Proceedings of 2nd International Congress on Metallic Corrosion, NACE, 1964, p. 33.

JAERI-M-82-145, "Progress Report on Safety Research of High Level Waste Management for the Period April 1981 to March 1982," S. Tashiro, JAERI, 1982.

Russell, E. W. and others, "Selection of Barrier Metals for a Waste Package in Tuff," in Scientific Basis for Nuclear Waste Management, VII, G. L. McVay, Editor, New York, North Holland, 1984, p. 763.

UCRL-89988, "Selection of Candidate Canister Materials for High Level Nuclear Waste Containment in a Tuff Repository," R. D. McCright and others, University of California Radiation Laboratory, November 1983.

Warren, D., "Chloride-Bearing Cooling Water and the Stress Corrosion Cracking of Iron-Nickel-Chromium Alloys," in Proceedings of the 15th Industrial Waste Conference, 1960, p. 420.

Williams, W. L., "Chloride and Caustic Stress Corrosion of Austenitic Stainless Steel in Hot Water and Steam," Corrosion 13, 539A, 1957.

NRC FORM 335 (2-84) NRCM 1102, 3201, 3202

U.S. NUCLEAR REGULATORY COMMISSION

BIBLIOGRAPHIC DATA SHEET

SEE INSTRUCTIONS ON THE REVERSE

1 REPORT NUMBER (Assigned by TIDC, add Vol No., if any)

NUREG/CR-3091
BNL-NUREG-51630.
Vol. 6

2. TITLE AND SUBTITLE

Review of Waste Package Verification Tests
Semiannual Report Covering the Period
October 1984 - March 1985

3. LEAVE BLANK

4 DATE REPORT COMPLETED

MONTH	YEAR
March	1985

5. AUTHOR(S)

P. Soo, Ed.

6 DATE REPORT ISSUED

MONTH	YEAR
July	1985

7. PERFORMING ORGANIZATION NAME AND MAILING ADDRESS (Include Zip Code)

Brookhaven National Laboratory
Upton, NY 11973

8 PROJECT/TASK/WORK UNIT NUMBER

9 FIN OR GRANT NUMBER

A3167

10. SPONSORING ORGANIZATION NAME AND MAILING ADDRESS (Include Zip Code)

Division of Waste Management
Office of Nuclear Material Safety and Safeguards
U.S. Nuclear Regulatory Commission
Washington, DC 20555

11a TYPE OF REPORT

Technical

b PERIOD COVERED (Inclusive dates)

12 SUPPLEMENTARY NOTES

13. ABSTRACT (200 words or less)

The potential of WAPPA, a second-generation waste package system code, to meet the needs of the regulatory community are analyzed. The analysis includes an indepth review of WAPPA's individual process models and a review of WAPPA's operation. It is concluded that the code is of limited use of the NRC in the present form. Recommendations for future improvement, usage, and implementation of the code are given. This report also describes the results of a testing program undertaken to determine the chemical environment that will be present near a high-level waste package emplaced in a basalt repository. For this purpose, low carbon 1020 steel (a current BWIP reference container material), synthetic basaltic groundwater and a mixture of bentonite and basalt were exposed, in an autoclave, to expected conditions some period after repository sealing (150°C, ≈10.4 MPa). Parameters measured include changes in gas pressure with time and gas composition, variation in dissolved oxygen (DO), pH and certain ionic concentrations of water in the packing material across an imposed thermal gradient, mineralogic alteration of the basalt/bentonite mixture, and carbon steel corrosion behavior. A second testing program was also initiated to check the likelihood of stress corrosion cracking of austenitic stainless steels and Incoloy 825 which are being considered for use as waste container materials in the tuff repository program.

14. DOCUMENT ANALYSIS – a KEYWORDS/DESCRIPTORS

waste package

b IDENTIFIERS/OPEN-ENDED TERMS

15 AVAILABILITY STATEMENT

Unlimited

16 SECURITY CLASSIFICATION

(This page)
Unclassified

(This report)
Unclassified

17 NUMBER OF PAGES

18 PRICE